Université de Montréal

Carboxydothermus hydrogenoformans comme catalyseur biologique pour la conversion du monoxyde de carbone en hydrogène simultanément à la minéralisation de calcium et phosphate

Carboxydothermus hydrogenoformans as a biological catalyst for carbon monoxide conversion to hydrogen simultaneously to mineralization of calcium phosphate

par

Mathieu Haddad

Département de microbiologie, infectiologie et immunologie

Faculté de Médecine

Thèse présentée à la Faculté des Études Supérieurs

en vue de l'obtention du grade de Philosophiæ Doctor (Ph.D.)

en Microbiologie et Immunologie

Février, 2014

Université de Montréal
Faculté des études supérieures et postdoctorales

Cette thèse intitulée:

Carboxydothermus hydrogenoformans comme catalyseur biologique pour la conversion du monoxyde de carbone en hydrogène simultanément à la minéralisation de phosphate de calcium

Carboxydothermus hydrogenoformans as a biological catalyst for carbon monoxide conversion to hydrogen simultaneously to mineralization of calcium phosphate

Présentée par :
Mathieu Haddad

a été évaluée par un jury composé des personnes suivantes :

George Szatmari, Ph.D., président-rapporteur
Serge R. Guiot, Ph.D., directeur de recherche
Patrick Hallenbeck, Ph.D., membre du jury
Satinder Kaur Brar, Ph.D., examinateur externe
Gertraud Burger, Ph.D., représentant du doyen de la FES

Résumé

La gazéification est aujourd'hui l'une des stratégies les plus prometteuses pour valoriser les déchets en énergie. Cette technologie thermo-chimique permet une réduction de 95 % de la masse des intrants et génère des cendres inertes ainsi que du gaz de synthèse (syngaz). Le syngaz est un combustible gazeux composé principalement de monoxyde de carbone (CO), d'hydrogène (H_2) et de dioxyde de carbone (CO_2). Le syngaz peut être utilisé pour produire de la chaleur et de l'électricité. Il est également la pierre angulaire d'un grand nombre de produits à haute valeur ajoutée, allant de l'éthanol à l'ammoniac et l'hydrogène pur. Les applications en aval de la production de syngaz sont dictées par son pouvoir calorifique, lui-même dépendant de la teneur du gaz en H_2. L'augmentation du contenu du syngaz en H_2 est rendu possible par la conversion catalytique à la vapeur d'eau, largement répandu dans le cadre du reformage du méthane pour la production d'hydrogène. Au cours de cette réaction, le CO est converti en H_2 et CO_2 selon : $CO + H_2O \rightarrow CO_2 + H_2$. Ce processus est possible grâce à des catalyseurs métalliques mis en contact avec le CO et de la vapeur.

La conversion catalytique à la vapeur d'eau a jusqu'ici été réservé pour de grandes installations industrielles car elle nécessite un capital et des charges d'exploitations très importantes. Par conséquent, les installations de plus petite échelle et traitant des intrants de faible qualité (biomasse, déchets, boues ...), n'ont pas accès à cette technologie. Ainsi, la seule utilisation de leur syngaz à faible pouvoir calorifique, est limitée à la génération de chaleur ou, tout au plus, d'électricité. Afin de permettre à ces installations une gamme d'application plus vaste de leurs syngaz, une alternative économique à base de catalyseur biologique est proposée par l'utilisation de bactéries hyperthermophiles hydrogénogènes.

L'objectif de cette thèse est d'utiliser *Carboxydothermus hydrogenoformans*, une bactérie thermophile carboxydotrophe hydrogénogène comme catalyseur biologique pour la conversion du monoxyde de carbone en hydrogène. Pour cela, l'impact d'un phénomène de biominéralisation sur la production d'H_2 a été étudié. Ensuite, la faisabilité et les limites de l'utilisation de la souche dans un bioréacteur ont été évaluées.

Tout d'abord, la caractérisation de la phase inorganique prédominante lorsque *C. hydrogenoformans* est inoculé dans le milieu DSMZ, a révélé une biominéralisation de phosphate de calcium (CaP) cristallin en deux phases. L'analyse par diffraction des rayons X et spectrométrie infrarouge à transformée de Fourier de ce matériau biphasique indique une signature caractéristique de la Mg-whitlockite, alors que les images obtenues par microscopie électronique à transmission ont montré l'existence de nanotiges cristallines s'apparentant à de l'hydroxyapatite. Dans les deux cas, le mode de biominéralisation semble être biologiquement induit plutôt que contrôlé. L'impact du précipité de CaP endogène sur le transfert de masse du CO et la production d'H_2 a ensuite été étudié. Les résultats ont été comparés aux valeurs obtenues dans un milieu où aucune précipitation n'est observée. Dans le milieu DSMZ, le K_La apparent (0.22 ± 0.005 min^{-1}) et le rendement de production d'H_2 (89.11 ± 6.69 %) étaient plus élevés que ceux obtenus avec le milieu modifié (0.19 ± 0.015 min^{-1} et 82.60 ± 3.62% respectivement). La présence du précipité n'a eu aucune incidence sur l'activité microbienne. En somme, le précipité de CaP offre une nouvelle stratégie pour améliorer les performances de transfert de masse du CO en utilisant les propriétés hydrophobes de gaz.

En second lieu, la conversion du CO en H_2 par la souche *Carboxydothermus hydrogenoformans* fut étudiée et optimisée dans un réacteur gazosiphon de 35 L. Parmi toutes les conditions opérationnelles, le paramètre majeur fut le ratio du débit de recirculation du gaz sur le débit d'alimentation en CO (Q_R:Q_{in}). Ce ratio impacte à la fois l'activité biologique et le taux de transfert de masse gaz-liquide. En effet, au dessus d'un ratio de 40, les performances de conversion du CO en H_2 sont limitées par l'activité biologique alors qu'en dessous, elles sont limitées par le transfert de masse. Cela se concrétise par une efficacité de conversion maximale de 90.4 ± 0.3 % et une activité spécifique de 2.7 ± 0.4 $mol_{CO} \cdot g^{-1}{}_{VSS} \cdot d^{-1}$. Malgré des résultats prometteurs, les performances du bioréacteur ont été limitées par une faible densité cellulaire, typique de la croissance planctonique de *C. hydrogenoformans*. Cette limite est le facteur le plus contraignant pour des taux de charge de CO plus élevés. Ces performances ont été comparées à celles obtenues dans un réacteur à fibres creuses (BRFC) inoculé par la souche. En dépit d'une densité cellulaire et d'une activité volumétrique plus élevées, les

performances du BRFC à tout le moins cinétiquement limitées quand elles n'étaient pas impactées par le transfert de masse, l'encrassement et le vieillissement de la membrane. Afin de parer à la dégénérescence de *C. hydrogenoformans* en cas de pénurie de CO, la croissance de la bactérie sur pyruvate en tant que seule source de carbone a été également caractérisée. Fait intéressant, en présence simultanée de pyruvate et de CO, *C. hydrogenoformans* n'a amorcé la consommation de pyruvate qu'une fois le CO épuisé. Cela a été attribué à un mécanisme d'inhibition du métabolisme du pyruvate par le CO, faisant ainsi du pyruvate le candidat idéal pour un système *in situ* de secours.

Mots-clés : Adsorption, Biominéralisation, CaP, *Carboxydothermus hydrogenoformans*, Hydrogène, Hydroxyapatite, Monoxyde de Carbone, Pyruvate, Conversion catalytique à la vapeur d'eau, Transfert de masse, Whitlockite.

Abstract

Gasification is today one of the most promising strategies to recover energy from waste. This thermo-chemical technology allows a 95% weight reduction of the input and generates inorganic inert ashes as well as a synthesis gas (syngas). Syngas is a gaseous fuel mainly composed of carbon monoxide (CO), hydrogen (H_2) and carbon dioxide (CO_2). Syngas can be burned to produce heat and electricity. It is also the building block of many high added-value products ranging from ethanol to ammonia and pure hydrogen. Downstream applications of syngas production will depend on its heating value, which is determined by its content in H_2. Upgrading the H_2 content in syngas is performed by the water-gas shift (WGS) reaction, widely utilized during methane reforming for hydrogen production. During the WGS reaction CO is converted to H_2 and CO_2 according to: $CO + H_2O \rightarrow CO_2 + H_2$. This process is achieved using a metallic catalyst in a heterogeneous gas-phase reaction with CO and steam.

The WGS reaction has so far been reserved for large-scale gasification plants and requires high capital and operational expenditures. Hence, smaller scale plants that process low-grade materials (biomass, waste, sludge…), would not have access to such technology. The only possible outcome with the synthesis gas (syngas) produced and which generally has a poor heating value, is to generate heat or at best, electricity. In order to offer small plants access to the WGS reaction and to a higher range of products from their syngas, an alternative to the expensive and energy-intensive established catalyst-based WGS is here considered, such as extreme-thermophilic microbial processes carried out by hydrogenogens.

The goal of this thesis was to use *Carboxydothermus hydrogenoformans*, a thermophilic carboxydotrophic hydrogenogenic bacterium as a biological catalyst for the WGS reaction. This was done by characterizing the impact of a growth-associated biomineralization phenomenon on H_2 production and assessing the feasibility and limitations of using the strain in a bioreactor.

First, characterization of the predominant inorganic phase when *Carboxydothermus hydrogenoformans* was inoculated in the DSMZ medium revealed the biomineralization of two crystalline CaP phases. The X-ray diffractometry peaks and Fourier transform infrared spectroscopy spectrum of this biphasic material consistently showed features characteristic of Mg-whitlockite, whereas transmission electron microscopy analysis showed the existence of hydroxyapatite-like nanorods crystals. In both cases, the mode of biomineralization appears to be biologically induced rather than biologically controlled. The impact of the endogenous CaP precipitate on CO mass transfer and H_2 production was thus assessed and compared to a medium where no precipitation was observed. In the DSMZ medium, the apparent K_La (0.22 ±0.005 min^{-1}) and H_2 production yield (89.11 ±6.69%) were higher than the ones obtained in the modified medium (0.19 ±0.015 min^{-1} and 82.60 ±3.62% respectively). The presence of the precipitate had no impact on *C. hydrogenoformans* CO uptake. Overall, the CaP precipitate offers a novel strategy for gas-liquid mass transfer enhancement using CO hydrophobic properties.

Second, the conversion of CO into H_2 by *C. hydrogenoformans* was investigated and optimized in a 35 L gas-lift reactor. Upon all operational conditions, the ratio of gas recirculation over CO feed flow rates (Q_R:Q_{in}) was the major parameter that impacted both biological activity and volumetric gas-liquid mass transfer. The CO conversion performance of the gas lift reactor was kinetically limited over a Q_R:Q_{in} ratio of 40, and mass transfer limited below that ratio, resulting in a maximum conversion efficiency of 90.4±0.3% and a biological activity of 2.7±0.4 $mol_{CO}\cdot g^{-1}{}_{VSS}\cdot day^{-1}$. Despite very promising results, CO conversion performance was limited by a low cell density, typical of *C. hydrogenoformans* planktonic growth. This limitation was found to be the most restrictive factor for higher CO loading rates. Results were compared to the performance of the strain inoculated in a hollow fiber membrane bioreactor where performance, despite the higher cell density and volumetric activity, was biokinetically limited, when not limited by gas–liquid mass transfer, membrane fouling and aging.

To avoid any *C. hydrogenoformans* decay during potential CO shortages, growth of the bacterium on pyruvate as a sole carbon source was characterized. Interestingly, when grown

simultaneously on pyruvate and CO, pyruvate consumption was initiated upon CO depletion. This was attributed to the inhibition of pyruvate oxidation by CO, making pyruvate the ideal candidate for an in-situ back-up system.

Keywords : Adsorption, Biomineralization, CaP, Carbon Monoxide, Hydrogen, *Carboxydothermus hydrogenoformans*, Hydroxyapatite, Mass transfer, Pyruvate, Water-Gas shift reaction, Whitlockite.

Table des matières

Liste des tableaux

Liste des figures

Liste des abréviations

°C	Degrees Celsius
β-TCP	β-Tri-Calcium Phosphate
ΔG°'	Gibbs free energy
µmol	Micromole
A	Biological specific activity
BCM	Biologically controlled mineralization
BIM	Biologically induced mineralization
bp	Base Pair
ca	Approximately
CaP	Calcium Phosphate
CO	Carbon Monoxide
CO_2	Carbon dioxide
CoA	Coenzyme-A
COD	Chemical oxygen demand
CODH	Carbon monoxide dehydrogenase
CSTR	Continuous stirred tank reactor
d_{CO}	dissolved CO
DNA	Deoxyribonucleic acid
e-	Electron
E_{CO}	CO conversion efficiency
EDX	Energy dispersive spectrometer
EDS	Energy dispersive spectrometer

EPS	Extracellular polymeric substance
FTIR	Fourier transform infrared spectroscopy
GC	Gas chromatograph
GLR	Gas-lift reactor
h	Hour
H_2	Hydrogen
HA	Hydroxyapatite
HFMBR	Hollow fiber membrane bioreactor
HRT	Hydraulic retention time
JCPDS	Joint-Committee on Powder Diffraction Standards
K_La	Mass transfer coefficient
mg	Milligram
mmol	Millimole
mol	Mole
OD	Optical density
PFL	Pyruvate formate lyase
POR	Pyruvate-ferredoxin oxidoreductase
Q_{CO}	CO feeding rate
Q_R	Gas recirculation rate
SEM	Scanning electron microscopy
SS	Suspended solids
TEM	Transmission electron microscopy
UASB	Up flow anaerobic sludge blanket

VFA	Volatile fatty acid
VSS	Volatile suspended solid
WGS	Water-gas shift
XRD	X-ray diffractometry

À mes parents, À mon frère Alain.

Remerciements

Après plus de trois années passées sur ce projet, il m'est très difficile de comparer la thèse doctorale avec toute autre expérience professionnelle ou académique. Il est vrai que c'est une traversée en solitaire. Un long cheminement parsemé de nombreuses embuches et épreuves qui testent en permanence notre patience, motivation, détermination et rigueur scientifique. Le plus difficile n'aura pourtant pas été les échecs techniques mais ces terribles moments de solitude où l'on est envahi par le doute. Le doute d'avoir choisi le bon projet, le doute d'avoir pris le bon chemin dans la vie et finalement le doute au plus profond de nous : notre estime de soi. Fort heureusement, j'ai eu la chance d'être entouré, tout au long de cette expédition, par des êtres formidables, sans qui tout cela n'aurait pas été possible et que je souhaite remercier.

Papa, Maman, et Alain. Ma famille. Ma fondation. Vous avez toujours été la pour me soutenir dans mes rêves et mes projets et rien de tout cela n'aurait été possible sans votre amour, encouragement et votre confiance. Merci. J'espère que nous nous retrouverons sous peu dans un lieu où les peuples ne se déchirent pas pour des questions d'appartenance religieuse, identitaire ou politique et où l'on pourra savourer paisiblement chaque instant de la vie.

Je voudrais exprimer toute ma gratitude à mon Directeur de Thèse, le Professeur Serge R. Guiot pour m'avoir donné l'opportunité de bâtir mon propre sujet de thèse, de m'avoir accordé les moyens techniques et financiers pour le mener à bien et son aide ainsi son soutien financier pour présenter mes résultats à deux conférences internationales : Bioenergy Australia 2013 (Hunter Valley, NSW, Australia) et BIO Pacific Rim Summit on Industrial Biotechnology and Bioenergy 2013 (San Diego, CA, USA).

Toute ma reconnaissance va également aux Dr. Jeanne Paquette et Hojatollah Vali (Université McGill) pour leur soutien, leur patience, aide et conseils scientifiques dans un domaine tout à fait nouveau pour moi : la biominéralisation.

Tout cela n'aurait pas non plus été possible sans ma deuxième famille : mes amis. Clairsemés à travers les continents mais jamais loin du cœur, ils m'ont accompagné dans différentes étapes de ma thèse et de ma vie. Une page entière à chacun d'entre vous ne suffirait même pas pour vous exprimer ma reconnaissance. Ainsi je m'excuse par avance de l'énumération sommaire de vos noms, dont la position n'est que purement aléatoire. Merci à vous tous pour avoir été là durant les bons moments et de m'avoir soutenu lors des moments plus difficiles. Du fond du cœur, merci à : Aram Karagueuzian, Laura Desrosiers et Tante Arek (ma famille arménienne adoptive), Emmanuelle Sana, Rania Awad, Danielle Bacon et Patricia Prazeres (mes grandes sœurs), May Shawi (mon mentor), Prabhdeep Singh (mon grand frère) et sa famille, Jessica Plucain et Irina Mouilleron (mes âmes sœurs), Christine et Pierre Calise (ma famille grenobloise adoptive) et Laurent Dallongeville (mon camarade de route).

Je suis grandement reconnaissant de l'amitié, aide, conseils, présence et des grandes discussions socio-polico-historico-anthropologiques de mes collègues du groupe de bioingénierie (NRC-CNRC, Montréal). Je souhaite remercier tout particulièrement Ruxandra Cimpoia (ma mère roumaine adoptive), Michelle-France Manuel, Punita Mehta et Jérôme Breton.

Introduction

1. Contexte

Avec le développement économique des populations et l'exode rural qu'a connu le siècle dernier, la production de déchets a été multipliée par dix. En effet, en 1900, la terre comptait 220 millions de citadins, soit 13% de la population mondiale, responsables d'une production quotidienne de 300.000 tonnes de déchets. En 2012, les 2,9 milliards de citadins représentaient 49 % de la population mondiale et généraient plus de 3.6 millions de tonnes de déchets solides par jour soit 1. 2 kg / habitant / jour. En 2025, cette quantité de déchets est supposée doubler, et cela malgré les efforts de réduction et de dématérialisation dans les pays de l'OCDE (**Figure 1**). La stagnation de la production de déchets dans ces pays, est contrée par les tendances en Asie ; plus particulièrement en Chine où une augmentation de génération des déchets solides de 520 550 tonnes par jour en 2005 à 1.4 million de tonnes par jour en 2025 est prévue (Hoornweg et al. 2013). En plus des problèmes sanitaires et sociaux, les émissions de gaz à effet de serre (GES) des ces sous-produits urbains représentent une préoccupation majeure puisqu'ils constituent près de 5% (1.460 Mt CO_2 équivalent) des émissions mondiales de GES.

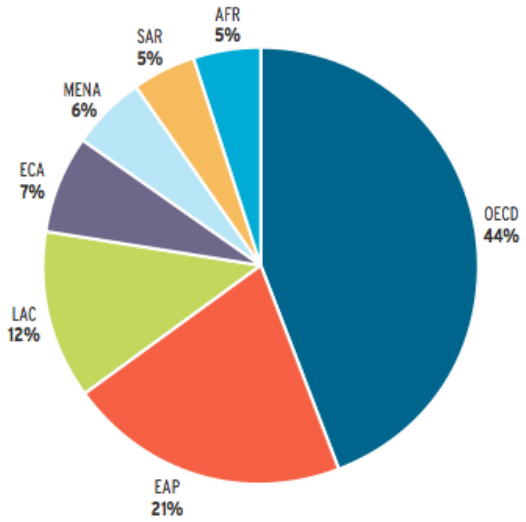

Figure 1 : La génération des déchets par région. (OECD) Pays membres de l'OECD; (EAP) Asie de l'Est et Pacifique, (LAC) Amérique Latine et Caraïbes, (EAC) Europe et Asie Centrale, (MENA) Moyen Orient et Afrique du Nord, (SAR) Asie du Sud, (AFR) Afrique (Hoornweg & Bhada-Tata 2012).

Mise à part la réduction à la source, il existe aujourd'hui quatre voies d'élimination des déchets: le recyclage, le compostage ou la digestion anaérobie, l'incinération (avec ou sans récupération d'énergie) et la décharge en site d'enfouissement sanitaire. Afin d'éviter l'enfouissement et permettre la récupération de l'énergie résiduelle, une valorisation des déchets utilisant une voie thermochimique (la gazéification) commence à s'implanter dans le monde du déchet à travers plusieurs compagnies comme, entre autres, AlterNRG Inc., Dynamis Energy Inc., Enerkem Inc, InEnTec Inc. et Plasco Energy Group Inc.

1.1. Une voie de valorisation énergétique des déchets : la gazéification

Au sens large, la gazéification est une conversion à haute température (800 - 1800°C) sous pression atmosphérique ou élevée (jusqu'à 33 bars) de tout combustible carboné en un

gaz possédant un certain pouvoir calorifique. Cette conversion est réalisée en deux étapes : une pyrolyse, un processus anaérobie dans lequel du goudron est produit, suivie de la gazéification à proprement parler, où ce goudron est converti en un mélange d'hydrogène (H_2) et de monoxyde de carbone (CO) à des températures élevées avec une quantité contrôlée d'oxygène ou de vapeur. Le mélange gazeux résultant de ce procédé est appelé gaz de synthèse (syngaz) (Rezaiyan & Cheremisinoff 2005).

La première production de syngaz aurait eu lieu en 1792 lorsque Murdoch, un ingénieur écossais, effectua la pyrolyse du charbon dans une cornue de fer. Il utilisa ensuite le gaz produit pour éclairer sa maison. Il faudra attendre le début du 19^{e} siècle avec la fondation de la *Gas Light and Coke Company* à Westminster, pour voir l'implantation à grande échelle de la pyrolyse du charbon, dont le syngaz était utilisé pour éclairer le pont de Westminster. Les États-Unis emboitèrent le pas au Royaume-Uni avec, en 1816, la construction de la première usine de production de gaz de synthèse à partir du charbon pour éclairer les rues de la ville de Baltimore. En 1826, la plupart des grandes villes dans le monde possédaient leurs usines à gaz de houille ainsi que les réseaux de distribution permettant l'éclairage des rues (Higman & Van der Burgt 2008).

Cependant, le procédé n'allant pas jusqu'au stade de la gazéification, les produits de pyrolyse, le goudron et les fumées non traitées, ont commencé à polluer de nombreux sites, impactant négativement l'opinion publique. La découverte, après la Seconde Guerre mondiale, de grandes quantités de gaz naturel disponibles à faible coût et à haut pouvoir calorifique (≈37 $MJ.m^{-3}$), conduira à la disparition de l'industrie du gaz de houille. Il faudra attendre la première crise pétrolière au début des années 1970, agitant le spectre d'un risque de pénurie de gaz naturel, pour relancer l'intérêt pour la gazéification. La production d'électricité a émergé comme un nouveau grand marché pour ce procédé, utilisé depuis comme un moyen de renforcer l'acceptabilité environnementale du charbon ainsi que d'accroître l'efficacité globale de la conversation de l'énergie chimique du charbon en électricité (Higman & Van der Burgt 2008).

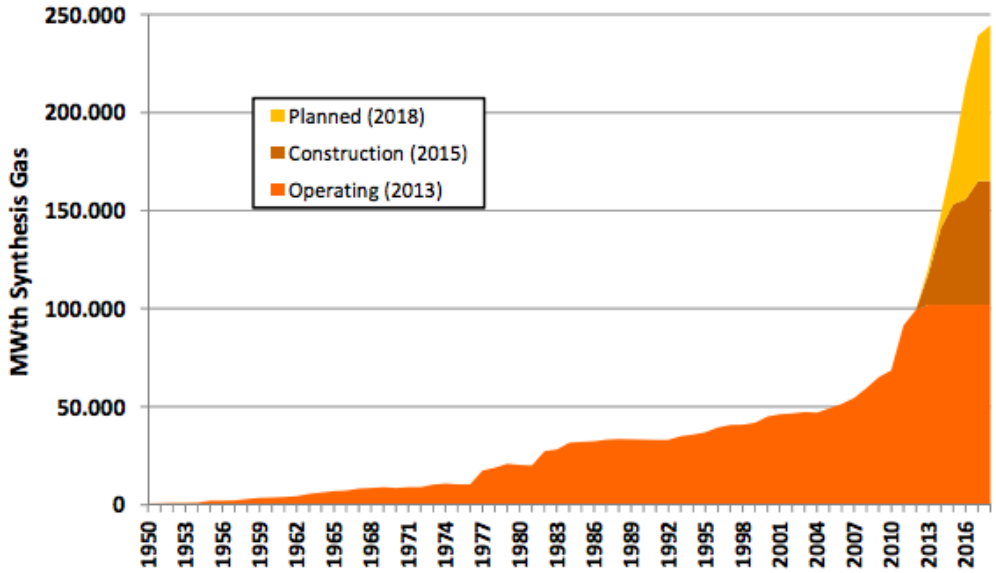

Figure 2 : Capacité cumulative de gazéification dans le monde et prédiction de croissance (Higman 2013 avec permission)

La capacité de gazéification mondiale est aujourd'hui de 104.7 GW_{th} avec 63.4 et 84.0 GW_{th} en construction et planification respectivement (**Figure 2**). Cela équivaut à 234 sites d'exploitation et 618 gazogènes (Higman 2013). Le charbon reste cependant la matière première prédominante (51%) suivi par le pétrole (25%) et le gaz naturel (22%), avec peu de développement sur la gazéification de la biomasse et des déchets (Kirkels & Verbong 2011; DoE-NETL 2010) (**Table 1**).

Feedstock		Operating 2010	Construction 2010	Planned 2011-2016	Totals
Coal	Syngas Capacity (MW_{th})	36,315	10,857	28,376	75,548
	Gasifiers	201	17	58	276
	Plants	53	11	29	93
Petroleum	Syngas Capacity (MW_{th})	17,938			17,938
	Gasifiers	138			138
	Plants	56			56
Gas	Syngas Capacity (MW_{th})	15,281			15,281
	Gasifiers	59			59
	Plants	23			23
Petcoke	Syngas Capacity (MW_{th})	911		12,027	12,938
	Gasifiers	5		16	21
	Plants	3		6	9
Biomass/Waste	Syngas Capacity (MW_{th})	373		29	402
	Gasifiers	9		2	11
	Plants	9		2	11
Total Syngas Capacity (MW_{th})		70,817	10,857	40,432	122,106
Total Gasifiers		412	17	76	505
Total Plants		144	11	37	192

Table 1 : Aperçu de l'industrie de la gazéification (DoE-NETL 2010)

1.2. Les applications du gaz de synthèse ; l'importance du ratio H_2 : CO

Historiquement, le syngaz est produit pour la génération de chaleur ou d'électricité. Cependant, de part sa composition en CO et H_2, le syngaz est aussi le bloc constitutif pour la production de divers combustibles tels que le gaz naturel de synthèse, des produits chimiques tels que l'ammoniac, le méthanol, éthanol et autre carburant ou encore de l'H_2 (Belgiorno et al. 2003). Pour la génération de ces derniers, les normes du syngaz varient en terme de pouvoir calorifique inférieur, du ratio H_2 : CO (**Figure 3**) ainsi que de la concentration des impuretés (NH_3, H_2S, Cl_2, goudrons et poussières) (Torres et al. 2007; Littlewood 1977).

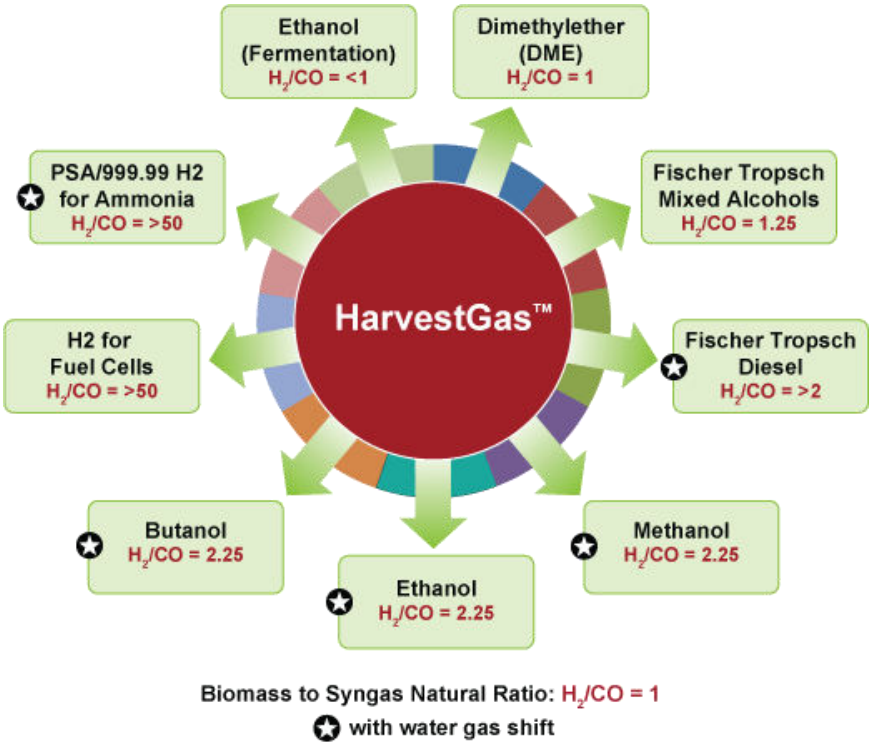

Figure 3 : Ratio H_2 : CO requis pour la conversion du syngaz carburants et autre produits à haute valeur ajoutée (Syngest Inc., 2009)

La composition finale du gaz de synthèse varie en fonction des intrants (biomasse agricole, déchets municipaux, boues d'épuration, etc.) ainsi que de la réalité socio-économique des populations. En effet, il a été démontré que la gazéification du même type de déchets dans des pays à haut revenus génère un syngaz de composition et de pouvoir calorifique supérieur à celui obtenu dans les pays à faibles revenus (De Filippis et al. 2004). Afin d'augmenter la teneur en hydrogène dans le gaz de synthèse et ainsi améliorer son pouvoir calorifique, une solution, aujourd'hui largement répandue dans l'industrie pétrolière, est utilisée : La conversion catalytique à la vapeur d'eau.

2. La conversion catalytique à la vapeur d'eau : Augmenter la teneur en hydrogène dans le gaz de synthèse

La production mondiale annuelle en hydrogène s'élève à environ 55 millions de tonnes qui sont principalement utilisées comme matière première dans l'industrie chimique, en particulier pour les activités de raffinage et la production d'ammoniac (Bičáková & Straka 2012) .

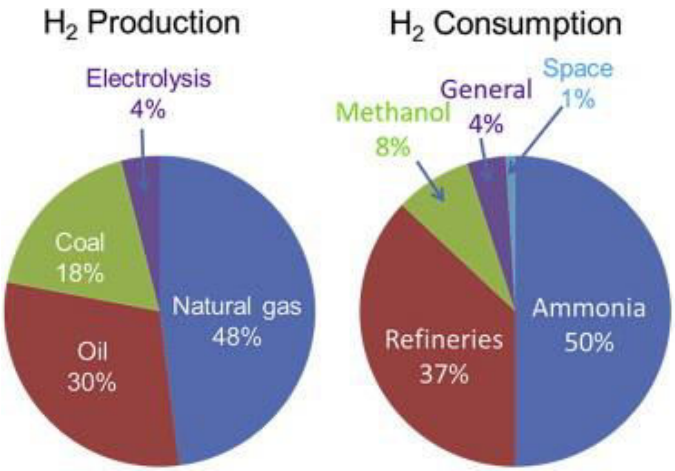

Figure 4 : Production et consommation mondiale d'hydrogène (Lan et al. 2012 avec permission)

Le reformage à la vapeur reste le principal processus de production d'hydrogène comptant pour 48% de la production totale (**Figure 4**) (B. E. Logan 2004). Il s'agit d'une étape de reformage à la vapeur suivie de la conversion catalytique à la vapeur d'eau selon Padro & Putsche (1999) (**Figure 5**). La conversion catalytique à la vapeur d'eau un procédé dans lequel de la vapeur d'eau réagit avec du CO afin de produire du CO_2 et de l'H_2 et ainsi augmenter la teneur du syngaz en H_2 selon la réaction suivante:

$$CO + H_2O \rightarrow CO_2 + H_2 \qquad (\Delta H = -41 \text{ kJ. mol}^{-1})$$

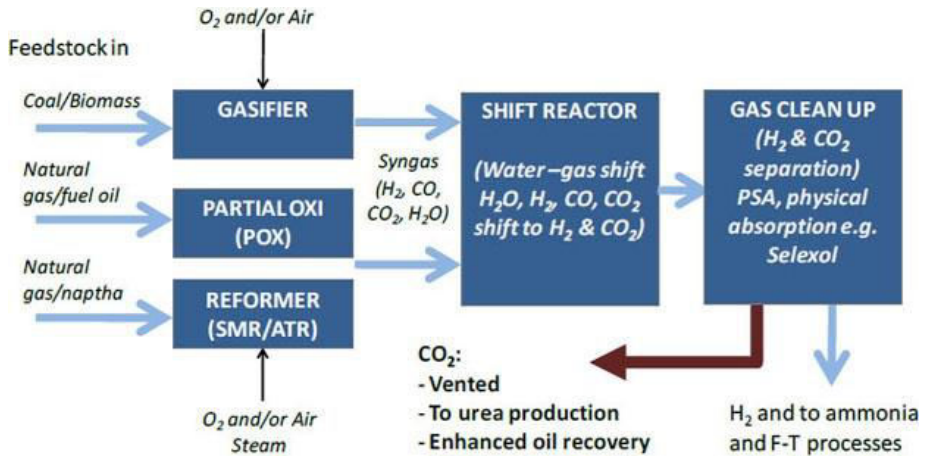

Figure 5 : Schéma général des procédés de production industriel d'hydrogène et de syngaz. (SMR), reformage du méthane à la vapeur; (ATR) Reformage auto-thermique du méthane à la vapeur; (POX), oxydation partielle (Zakkour & Cook 2010)

2.1. L'approche conventionnelle : catalyseurs chimiques

Le procédé conventionnel de la conversion catalytique à la vapeur d'eau se déroule en deux étapes. Durant la première étape, la vapeur d'eau réagit avec des catalyseurs Cr_2O_3 - Fe_2O_3 à température élevée (350 - 370°C). A la fin de la réaction, 90% du CO ont été convertis en H_2 et CO_2. Il s'en suit alors une seconde étape à basse température (200 - 220°C) avec un catalyseur à base de CuO, qui permet de convertir le CO résiduel. A la fin de la réaction, la teneur en CO se situe entre 0.5 et 1 mol % (Smith R J et al. 2010; Bičáková & Straka 2012).

Une limite du procédé catalytique réside dans le fait que le catalyseur à base de cuivre est hautement intolérant au soufre. En effet, seule une concentration en dessous de 0.1 ppm de soufre dans le gaz est toléré afin de garantir le fonctionnement et la longévité des catalyseurs, d'où la nécessité d'avoir des lits adsorbants en amonts du réacteur de la conversion catalytique à la vapeur d'eau (Torres et al. 2007; Newsome 1980). D'autre part,

du fait de la variabilité de la composition des catalyseurs, de la surface active, l'âge, la structure et la pression et composition des gaz, il n'existe pas une expression universelle pour déterminer la vitesse de réaction et les mécanismes d'adsorption. Cela se traduit donc par la nécessité d'une étude préliminaire pour chaque type de catalyseur pour déterminer les conditions expérimentales de son utilisation (Smith R J et al. 2010). Finalement, le procédé catalytique est très énergivore, notamment à cause de la production de vapeur et de la nécessité de fonctionner à haute température (Newsome 1980).

2.2. L'approche biologique

Le CO et H_2 présents dans le gaz de synthèse peuvent être les substrats pour une grande variété de microorganismes anaérobes dont les bactéries hydrogénogènes, photosynthétiques, acétogènes, et methanogènes. Ces bactéries métabolisent le syngas en produits divers tels que: l'hydrogène, l'éthanol, le butanol, l'acide acétique, l'acide butyrique, le méthane, des biopolymères et protéines (Mohammadi et al. 2011; Henstra et al. 2007).

Les bactéries hydrogénogènes carboxydotrophes sont capables d'une croissance lithotrophique en utilisant le CO comme seul source de carbone et d'énergie, en le convertissant par réaction avec l'eau, en H_2 et CO_2 en quantité équimolaire. Parmi ces hydrogénogènes, on retrouve trois groupes distincts de procaryotes, à savoir les mésophiles à Gram négatif, les thermophiles à Gram positif et les archées thermophiles (Svetlitchnyi et al. 2001) (**Table 2**). La découverte des carboxydotrophes hydrogénogènes thermophiles capables d'une croissance rapide est une alternative biologique intéressante aux catalyseurs chimiques de la conversion catalytique à la vapeur d'eau (Svetlichny et al. 1991).

Organism	T_{opt} (°C)	pH_{opt}	T_d (h)

Bactéries mésophiles			
Citrobacter amalonaticus Y19	30 – 40	5.5 – 7.5	8.3
Rhodopseudomonas palustris P4	30	nd	23
Rhodospirillum rubrum	30	6.8	8.4
Rubrivivax gelatinosus	34	6.7 – 6.9	6.7
Bactéries thermophiles			
Caldanaerobacter subterraneus ssp. Pacificus	70	6.8 – 7.1	7.1
Carboxydibrachium pacificus	70	6.8 – 7.1	7.1
Carboxydocella sporoproducens	60	6.8	1
Carboxydocella thermoautotrophica	58	7.0	1.1
Carboxydothermus hydrogenoformans	70 - 72	6.8 – 7.0	2
Carboxydothermus siderophilus	70	7.0	9.0
Dictyoglomus carboxydivorans	75	nd	nd
Moorella strain AMP	60 – 65	6.9	nd
Thermincola carboxydiphila	55	8.0	1.3
Thermincola ferriacetica	57 - 60	7.0 – 7.1	1.5

Thermolithobacter carboxydivorans	70	7.0	8.3
Thermosinus carboxydivorans	60	6.8 – 7.0	1.5
Archées thermophiles			
Thermococcus strain AM4	82	6.8	nd
Thermofilum carboxyditrophus	92	nd	nd

Table 2 : Microorganismes caboxydotrophes hydrogénogènes (Henstra et al. 2007; Sokolova et al. 2009; Sipma 2006). nd : non disponible

Jusqu'à présent, toutes les bactéries carboxydotrophes hydrogénogènes ont été isolées dans des environnements chauds (sources hydrothermales) avec un pH variant entre 5.5 et 10 et des températures entre 50 et 90°C (Sokolova et al. 2009). Du point de vu des types trophiques, on retrouve parmi les hydrogénogènes des chimiolithoautotrophes et des organohétérotrophes sans pour autant noter la production de composés organiques à partir du CO (Henstra et al. 2007).

La croissance de ces carboxydotrophes hydrogénogènes est rapide sous une atmosphère composée de 100% CO, exceptée pour les souches *Dictyoglomus carboxydivorans* and *Thermofilum carboxyditrophus* qui ne sont pas capables de croître à des concentrations en CO supérieures à 15% et 45% respectivement (Sokolova et al. 2009).

2.2.1. Le rôle des déshydrogénases du monoxyde de carbone (CODH)

La conservation de l'énergie par les carboxydotrophes hydrogénogènes se fait à travers l'oxydation du CO en CO_2, catalysée par la CODH et la réduction subséquente de protons en H_2, effectuée par l'hydrogénase selon:

$$CO + H_2O \rightarrow CO_2 + 2H^+ + 2e^-$$
$$2H^+ + 2e^- \rightarrow H_2$$

Les CODH chez les microorganismes anaérobies sont des enzymes intolérantes à l'oxygène dont le site actif est structuré autour d'un atome de nickel. Les CODH peuvent être monofonctionnelles ou bifonctionnelles (Lindahl 2002).

Les CODH monofonctionnelles catalysent l'oxydation du CO. Elle existent par exemple chez *Rhodospirillum rubram* et *Carboxydothermus hydrogenoformans* (Wu et al. 2005), où elles forment un complexe enzymatique membranaire avec une hydrogénase (ECH), une protéine fer-soufre contenant du nickel qui effectue la réduction des protons en hydrogène (**Figure 6**). L'ECH couple la formation d'H_2 à la translocation de protons ou d'ions sodium à travers la membrane bactérienne ce qui génère un gradient électrochimique. Ce dernier entraine la formation d'une force proton motrice qui génère à son tour la synthèse de l'ATP au travers d'une ATP synthase (Sapra et al. 2003; Oelgeschläger & Rother 2008).

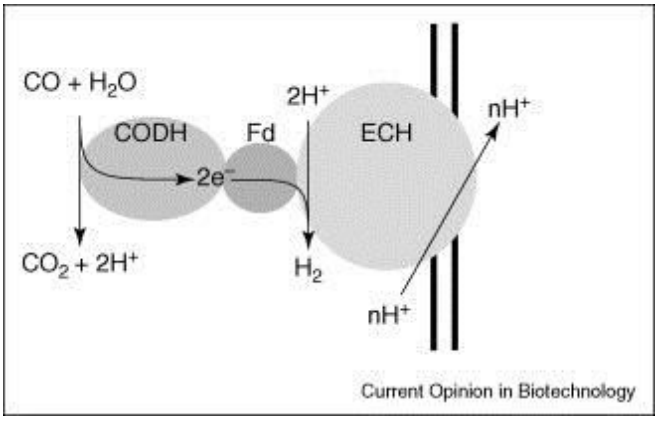

Figure 6 : Représentation schématique du couplage CODH et ECH chez *Carboxydothermus hydrogenoformans* lors de l'oxydation du CO en CO_2 et de la réduction des proton en H_2 (Henstra et al. 2007 avec permission)

Les CODH bifonctionnelles, forment un ensemble avec l'acétylCoA synthase (ACS) et catalysent la production d'acétylCoA. Ces complexes, notés CODH/ACS, sont la voie d'entrée pour la fixation du carbone chez les microorganismes anaérobies autotrophes et la formation de l'acétate par les homoacétogènes, les bactéries sulfato-réductrices et les méthanogènes. (Ragsdale 2004).

2.2.2. *Carboxydothermus hydrogenoformans :* une solution biologique aux catalyseurs chimiques de la conversion catalytique à la vapeur d'eau

Carboxydothermus hydrogenoformans est une bactérie carboxydotrophe hydrogénogène qui a été isolée dans une source thermale dans l'île Kounachir en Russie en 1991 (Svetlichny et al. 1991). Prokaryote anaérobie strict à Gram positif, *C. hydrogenoformans* se développe de manière optimale aux alentour de 70°C à pH neutre. L'intérêt pour cette espèce est multiple.

Premièrement, contrairement aux autres espèces d'hydrogénogènes, *C. hydrogenoformans* peut croître sans présence de CO sur du substrat organique tel que le pyruvate. Aussi, le microorganisme accepte divers donneurs (formate, lactate, glycérol) et accepteurs d'électrons (9,10-anthraquinone-none-2,6-disulfonate, sulfite, thiosulfate, soufre, nitrate, fumarate) (Henstra & Stams 2004).

De plus, le séquençage du génome de *C. hydrogenoformans* a permis de démontrer que ce dernier contient cinq familles de gènes codant pour différentes CODH (Wu et al. 2005) (**Figure 7**). D'après la littérature ce carboxydotrophe est le seul à posséder autant de CODH. Cela expliquerait les valeurs élevées des taux de croissance de 2 h^{-1} et de production d'hydrogène de ca. 3 $mol.g^{-1}_{VSS}.j^{-1}$en présence de CO mais aussi sa résistance à 2 atm de CO dans la phase gazeuse (Zhao et al. 2011; Oelgeschläger & Rother 2008; Sokolova et al. 2009). De plus, ces multiples CODH confèrent à *C. hydrogenoformans* la capacité à éliminer le CO présent dans la phase gazeuse à hauteur de 117 ppm ou 2 ppm si le CO2 est éliminé (Henstra & Stams 2011).

Finalement, contrairement au catalyseurs chimique, *C. hydrogenoformans* n'est pas intolérant au souffre, qui compose son milieu de culture. En effet, le soufre est utilisé afin de réduire le potentiel d'oxydo-réduction du milieu (Svetlichny et al. 1991; Gerhardt et al. 1991; Mohammadi et al. 2011).

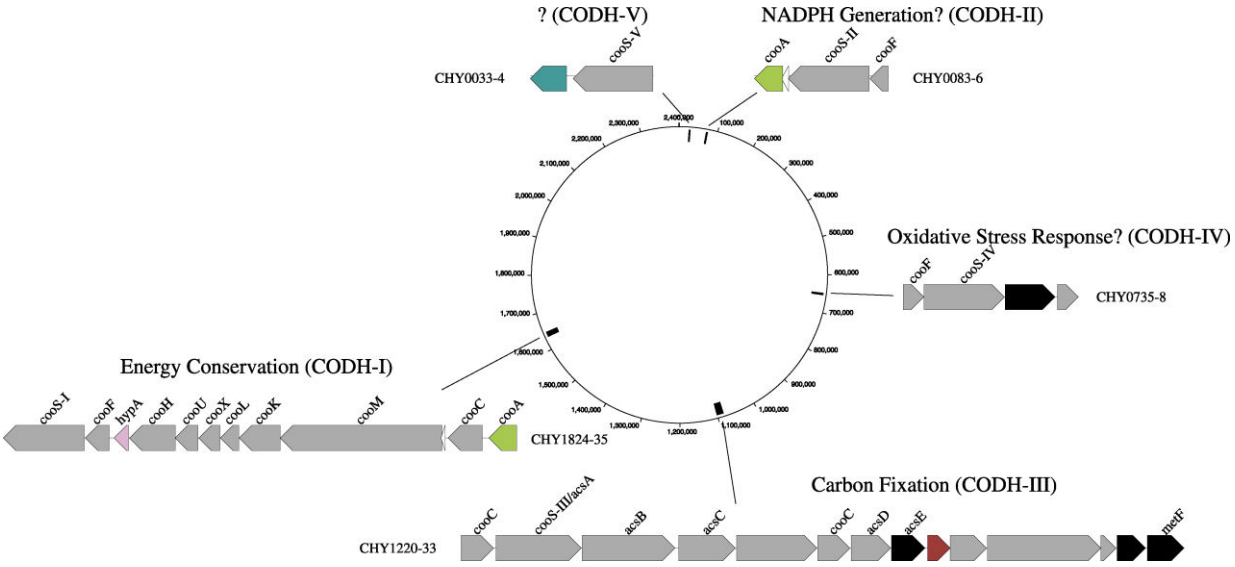

Figure 7 : Schéma et emplacement des familles multigéniques codant pour les 5 différentes CODH de *C. hydrogenoformans* (Wu et al. 2005 avec permission)

Ces multiples avantages lui attribuent donc un solide potentiel pour des petites et moyennes installations de gazéification ne pouvant se doter d'un système onéreux de traitement du gaz et de réacteur à catalyseur chimique permettant d'enrichir le syngaz en hydrogène.

3. Objectifs de l'étude

Malgré les avantages cités plus haut, l'utilisation de *C. hydrogenoformans* dans un procédé en continu de bioaugmentation du syngaz en H_2 doit d'abord contourner deux limitations majeurs : la faible concentration cellulaire et le transfert de masse du CO dans la phase liquide.

En effet, le microorganisme est connu pour sa faible densité microbienne en culture planctonique (Gerhardt et al. 1991). Cela pose un problème dans un système continu où l'activité volumique, dont dépend le dimensionnement des installations, est directement liée à la densité cellulaire de la souche.

Aussi, le CO étant hautement hydrophobe, sa biodisponibilité dans la phase liquide est d'autant plus limité à haute température. Ajoutons à cela que le transfert de masse de CO de la phase gazeuse à la phase liquide devient limitant, en bouteille, au dessus d'une concentration de 25 $mg_{VSS}.L^{-1}$ (Zhao et al. 2011). Ainsi, la technologie du bioréacteur devra remédier à ces deux limitations tout en étant simple à intégrer dans un système existant, non énergivore et à faibles charges d'exploitations et d'investissements.

L'objectif de la présente étude est double. Premièrement, nous caractérisons un phénomène de biominéralisation d'un précipité abiotique de phosphate de calcium, préalablement observé en présence de *C. hydrogenoformans* dans le milieu de culture riche en calcium et phosphate (Zhao et al. 2011) (**Chapitre 1**). Ensuite, l'impact de ce précipité sur le transfert de masse du CO, les performances de la production d'hydrogène et l'activité microbienne est quantifié (**Chapitre 2**). L'emphase est ensuite portée sur l'utilisation d'un fermenteur gazosiphon inoculé avec *C. hydrogenoformans* et alimenté en continue avec du CO (100%) pendant 3 mois pour évaluer la faisabilité de la technologie. Une attention toute particulière est consacrée au phénomène de transfert de masse, à la croissance cellulaire et aux performances du fermenteur (**Chapitre 3**). Les résultats sont comparés à ceux obtenus avec un réacteur à fibres creuses inoculé avec *C. hydrogenoformans* (**Annexe 1, 2**). Finalement, la croissance sur une source de carbone alternative, le pyruvate, est caractérisée (**Chapitre 4**). Peu documenté, la croissance de *C.*

hydrogenoformans sur pyruvate est importante dans un système en continu dans la mesure où, le substrat (CO) venant à manquer lors d'une interruption en amont du procédé, la biomasse ne serait pas amenée à décroitre.

Chapter 1: The role of *Carboxydothermus hydrogenoformans* in the conversion of calcium phosphate from amorphous to crystalline state

Mathieu Haddad[a,b], Hojatollah Vali[c,d], Jeanne Paquette[c], Serge R. Guiot[a,b]

[a] Bioengineering Group, Energy, Mining and Environment, National Research Council Canada, 6100 Royalmount Avenue, Montreal, Canada H4P 2R2

[b] Department of Microbiology, Infectiology and Immunology, Université de Montréal, Montreal, Canada H3C 3J7

[c] Department of Earth and Planetary Sciences, McGill University, Montreal, Canada H3A 3A1

[d] Facility for Electron Microscopy Research, McGill University, Montreal, Canada H3A 2B2

Author contribution: MH and HV designed the experiment, MH carried out the experimental work, MH, HV and JP interpreted the results; MH, HV, JP and SRG wrote the manuscript.

Article status: This article was submitted for publication to PLOS ONE on 19 November 2013 and accepted, 21 January 2014 and published 26 February 2014.

Keywords: *Carboxydothermus hydrogenoformans*; Mg-whitlockite; nano-HAP; biologically induced mineralization; calcium phosphate; biofilm.

ABSTRACT

Two previously unknown modes of biomineralization observed in the presence of *Carboxydothermus hydrogenoformans* are presented. Following the addition of $NaHCO_3$ and the formation of an amorphous calcium phosphate precipitate in an inoculated DSMZ medium, two distinct crystalline solids were recovered after 15 and 30 days of incubation in the presence of an active culture. The first of these solids occurred as micrometric clusters of blocky, angular crystals, which were associated with bacterial biofilm. The second solid occurred as 30 - 50 nm nanorods that were found scattered among the organic products of bacterial lysis. The biphasic mixture of solids was clearly dominated by the first phase. The X-ray diffractometry (XRD) peaks and Fourier transform infrared spectroscopy (FTIR) spectrum of this biphasic material consistently showed features characteristic of Mg-whitlockite. No organic content or protein could be identified by dissolving the solids. In both cases, the mode of biomineralization appears to be biologically induced rather than biologically controlled. Since Mg is known to be a strong inhibitor of the nucleation and growth of CaP, *C. hydrogenoformans* may act by providing sites that chelate Mg or form complexes with it, thus decreasing its activity as nucleation and crystal growth inhibitor. The synthesis of whitlockite and nano-HAP-like material by *C. hydrogenoformans* demonstrates the versatility of this organism also known for its ability to perform the water-gas shift reaction, and may have applications in bacterially mediated synthesis of CaP materials, as an environmentally friendly alternative process.

INTRODUCTION

Biomineralization as described by Lowenstam (Lowenstam 1981) is the ability of living organisms to form minerals as well as materials composed of an organic and inorganic phase (Bäuerlein 2008; Weiner et al. 2001). Among more than 60 biominerals formed by bacteria

discovered so far, 25% are amorphous and 75% crystalline (Weiner et al. 2001; Cölfen & Qi 2001; Berman et al. 1993) have investigated the mechanism of biomineralization and found that organisms across different phyla control biomineralization in a distinct manner and that biominerals have different functions. According to Mann (Mann 1993) biomineralization occurs at the organic-inorganic interface where a molecular recognition system is involved in the control of crystal nucleation and growth.

Biomineralization processes fall in two categories: Biologically Induced Mineralization (BIM) and Biologically Controlled Mineralization (BCM) (Lowenstam 1981). In BIM, biomineralization occurs outside the cell and none of the cell components are serving as a template for nucleation and growth of the precipitate. In this case, cellular activity results in changes in the microenvironment and anionic and cationic precipitation (Weiner et al. 2001). Biominerals produced by BIM are characterized by poor crystallinity and high variations in morphology, water content, structure, particle size as well as the presence of trace elements (Frankel & Bazylinski 2003). In BCM, also known as inorganic matrix-mediated mineralization (Lowenstam 1981), the cell controls all of the above described stages of mineralization from nucleation to crystal-formation, leading to a highly specie-specific product (Bazylinski 2003). BCM is based on a site-specific matrix (cytoplasm or on the cell wall) that enables the formation of a compartmentalized environment with its own chemical composition. Nucleation is then made possible by sequestering specific ions leading to supersaturation and precipitation in the matrix (Bazylinski et al. 2007).

Bacteria living under high temperature conditions are known as thermophiles (40 – 69°C) and hyperthermophiles (70 – 110°C). Biomineralization processes in this latter group of bacteria have not been extensively explored yet. Indeed, known processes describe magnetite and realgar formation (Huber et al. 2000) as well as reductive precipitation of uranium, manganese and other toxic metals (Kashefi & Lovley 2000).

In this study, we report that *C. hydrogenoformans* a carboxydotrophic hydrogenogenic hyperthermophilic bacterium (Svetlichny 1991) converts an amorphous calcium phosphate phase into a fully crystalline whitlockite mineral and spherulitic clusters that we interpret to be

hydroxyapatite-like nanocrystals. In addition to conventional microbiological analysis, Fourier transform infrared spectroscopy (FTIR), X-ray diffractometry (XRD) and electron microscopy techniques were applied. We demonstrate that an abiotic soluble CaP precursor is converted, in the present of an active culture of *C. hydrogenoformans*, to a biphasic mixture of granular aggregates of whitlockite and spherulitic hydroxyapatite. This phase is then converted in the crystalline whitlockite by *C. hydrogenoformans* activity.

Microbial calcification is a widespread phenomenon that biomineralizes calcium phosphates (CaP) (Sidaway 1978). CaP display high biocompatibility and biodegradability due to their chemical similarity to calcified tissue (Dorozhkin & Epple 2002; Chevalier & Gremillard 2009; Yuan et al. 1998). A large range of CaP, which differ in origin, composition and form, are currently used in medicine for regeneration of hard tissues (LeGeros 2002). Depending on the required characteristic (bioactive or resorbable material) for CaP applications (bone replacement, filling or coating, functionalized nanoparticle), different phases of CaP ceramics are used (β-TCP, Hydroxyapatite or biphasic CaP) (Chevalier & Gremillard 2009; Epple & Kovtun 2010). The chemical synthesis of CaP and CaP-based materials, while being very effective on one hand, are relatively expensive and eco-hazardous, requiring extremes of temperature and pH (Dorozhkin & Epple 2002). Thus, the present work offers an alternative biological approach with a more environmentally friendly process making *C. hydrogenoformans* a possible ecofriendly nanofactory for CaP synthesis.

MATERIALS AND METHODS

Bacterial strain and growth conditions

C. hydrogenoformans (DSM 6008) was obtained from the German Collection of Microorganisms and Cell Cultures (DSMZ, Braunschweig, Germany). Microorganisms were cultivated under strictly anaerobic conditions in basal mineral bicarbonate-phosphate buffered medium that contained (in g/L of demineralized water): KCl (0.33), $MgCl_2 \cdot 6H_2O$ (0.52),

$CaCl_2 \cdot 2H_2O$ (0.29), NH_4Cl (0.33), KH_2PO_4 (0.33) and 10 mL of trace metals solution. The medium was boiled and then introduced anaerobically in sterilized serum bottles under N_2 air flush. After autoclaving, it was then supplemented with (in $mL \cdot L^{-1}$ of medium): 5% $NaHCO_3$ stock solution (20), 2.5% $Na_2S \cdot 9H_2O$ stock solution (10), 0.5% yeast extract solution (10) and vitamin solution (1). The trace metals and vitamin stock solutions were prepared as described by Stams and coll. (Stams et al. 1993) All stock solutions were autoclaved, except the vitamin solution, which was sterilized by filtration through 0.22 µm filter membranes. After supplementation, the pH was between 6.8 and 7.0. All experiments were performed at 70°C, 150 rpm in 500 mL bottles. Bottles contained 200 mL of medium inoculated with the same amount of biomass under a 300 mL headspace. Initial headspace composition was set at 100% CO and 1 atm.

Control experiments

In control experiments, the bacterial biomass was resuspended in a modified medium described by Zhao and coll. (Zhao et al. 2011) in which no precipitation of amorphous calcium phosphate was observed. The modified medium differed from the DSMZ one only in $MgCl_2 \cdot 6H_2O$, $CaCl_2 \cdot 2H_2O$, KH_2PO_4 and $NaHCO_3$ concentrations, which were (in $g \cdot L^{-1}$ of demineralized water): 0.102, 0.015, 0.136, 0.401, respectively. In this medium, no amorphous CaP was observed to form abiotically over a period of 30 days, and the addition of a live bacterial culture did not induce detectable precipitation of CaP. The modified medium was also used to determine the proteomic profile of *C. hydrogenoformans* when no biomineralization took place (see biomolecular techniques).

Another control experiment was conducted to verify if proteins or amino acids released in the medium by the bacteria had a direct or indirect role in the crystallization of the precipitate. Dry amorphous precipitate obtained in the sterile DSMZ medium was incubated for 15 days at 70°C in the filtered (0.33µm) inoculated DSMZ medium from which crystalline phases had been recovered. The result of this control experiment was also negative as XRD analysis showed that the CaP precipitate remained amorphous.

In order to exclude the precipitation of an amorphous calcium carbonate in the DSMZ medium, the third abiotic control experiment was carried out using NH_3OH as buffer instead of $NaHCO_3$. A similar precipitate appeared and its energy dispersive X-ray spectrometry (EDX) patterns showed Ca and P peaks identical to those of the solid produced by $NaHCO_3$ addition. This confirmed that the amorphous precipitate formed in the DSMZ medium was dominantly a calcium phosphate phase.

Sampling procedures

All measurements that were carried out on the DSMZ medium were processed immediately after sampling in order to avoid any time related alteration. For precipitate characterization, samples were first concentrated by centrifugation during 10 min at 15000 rpm. Supernatant was removed and the pellet washed 3 times in MilliQ water to remove any remaining medium. Since the abiotic precipitate obtained in the absence of *C. hydrogenoformans* was highly soluble in water, the pellet obtained by centrifuging the control samples was washed only once in MilliQ water prior to any characterization.

Experimental parameters

Dissolved total phosphate

The dissolved phosphate ions concentration was measured in aliquots sampled from bottles inoculated with active cultures of *C. hydrogenoformans*. Sterile control series were also conducted on DSMZ medium. 2 mL of medium was sampled every 24 hours and centrifuged. The supernatant was analyzed on a Hamilton PRP-X100 (Hamilton Company, Reno, NV, USA) polymer-based chromatography column (250x41mm O.D.) in a high-performance liquid chromatograph TSP model P4000 & AS 3000 (TSP, San Jose, CA, USA). Conductivity data were obtained by using a Waters Millipore detector model 432. The mobile phase was p-Hydroxybenzoic Acid at pH 8.5 with 2.5% methanol at a flow rate of 1.8 $mL.min^{-1}$ at 40 °C.

Organics and Inorganics

The suspended solids (SS) and volatile suspended solids (VSS) were determined according to Standard Methods (Eaton et al. 2005). The sample was dried at 105°C overnight, weighed then placed in a muffle furnace at 600°C for two hours. VSS is determined from the weight loss from ignition.

Volatile fatty acids (VFA)

VFAs (i.e. acetic, propionic and butyric acids) were measured on an Agilent 6890 (Wilmington, DE) gas chromatograph (GC) equipped with a flame ionization detector (FID) on 0.2 µl samples diluted 1:1 (vol./vol.) with an internal standard of iso-butyric acid in 6% formic acid, directly injected on a glass column of 1 m × 2 mm Carbopack C (60-80 mesh) coated with 0.3 % Carbowax 20M and 0.1% H_3PO_4. The column was held at 130°C for 4 min. Helium was the carrier gas fed at a rate of 20 $mL \cdot min^{-1}$. Both injector and detector were maintained at 200°C.

Solvents

For measurement of solvents (methanol, ethanol, acetone, 2-propanol, tert-butanol, n-propanol, sec-butanol, n-butanol) 100 µL of liquid was transferred into a vial that had 20 mL of headspace and was crimp sealed with a Teflon-coated septum. The vial was heated at 80ºC for 2 min, then 1000 µl of headspace gas was injected onto a DB-ACL2 capillary column of 30 m x 530 mm x 2 µm using a Combipal autosampler (CTC Analytics AG, Zwingen, Swizerland). The column was held at 40ºC for 10 min. Helium was the carrier gas at a head pressure of 5 psi. The injector and the detector were maintained at 200ºC and 250ºC, respectively.

Mono and disaccharides

Mono and disaccharides were measured using an HPLC from Waters Corporation (Milford, MA) consisting of a pump (model 600, Waters Corporation) and an auto sampler model 717 Plus equipped with a refractive index detector (model 2414, Waters Corporation).

Organics acids were monitored using a PDA detector (model 2996, Waters Corporation). The column used for the separation was a Transgenomic ICSep IC-ION-300 (300 mm x 7.8 mm OD) (Transgenomics, San Jose, CA, USA). The mobile phase was 0.01N H_2SO_4 at 0.4 mL min^{-1}. Analysis was carried out at 35°C.

Sample characterization

The goal of sample characterization was to compare the solid precipitate obtained from experiments carried out in inoculated and sterile DSMZ media. The characterized solid was obtained by centrifugation of the sampled medium and could not be physically separated from the biomass. In some cases, the bacterial biomass was eliminated by calcination (heating to 600°C for 2 hours) but most observations were carried out on a dried (105°C overnight) composite material made of bacterial biomass intimately mixed with the CaP precipitate. Precipitate from inoculated medium (dried and calcinated to remove all organic matter) and from sterile medium (dried only) were analyzed by XRD. Number and positions of XRD peaks were unchanged from dried-only to dried and calcinated precipitates. Also, XRD patterns of dried precipitate from the sterile medium consistently showed broad humps of an amorphous material, showing that drying did not induce crystallinity. To eliminate the signature of the biomass, FTIR and scanning electron microscopy (SEM) analysis were conducted on the calcinated and dried sample from inoculated media, and compared to those of dried-only samples from sterile media.

Elemental analysis of the biotic precipitate

Elemental analysis was performed on a dry sample of a 30-day culture of *C. hydrogenoformans* in DSMZ medium. standard Methods were used for determination of elemental carbon, hydrogen, nitrogen, oxygen and sulfur (ASTM Standard D5373 2008)·(ASTM Standard D5291 2010). The sample was combusted at 1030°C. The combustion gases produced were then passed in on a gas chromatograph (ECS 4010, Costech Analytical Technologies, Valencia, CA) using ultra high purity helium as the carrier gas and equipped

with a TCD, which analyzes the concentrations of CO_2, N_2, H_2O and SO_2 from which percentages of carbon, hydrogen, nitrogen and sulfur are derived. The same procedure was utilized for oxygen analysis using a combustion elemental analyzer EA 1108 (Fisons/Carlo Erba, Milan, Italy). Similar samples were analyzed at two different analytical facilities (Dept. of Chemistry, Université de Montréal, Montreal, QC and Chemisar Inc., Guelph, ON) and resulted in the same elemental content.

Metals and phosphorus content of the biotic precipitate

A centrifuged sample from a 39 day *C. hydrogenoformans* culture was washed twice and resuspended in milliQ water. Phosphorus was determined using colorimetric methods (method 365.1, (USEPA 1993)). Calcium and metals were determined by Agatlabs Inc. (Montreal, QC) using inductively coupled plasma mass spectrometry (Elan 9000, Perkin-Elmer, Überlingen, Germany) (CEAEQ 2004).

X-ray diffractometry of the abiotic and biotic precipitate

Phase analysis was performed on a Bruker D8 Advance X-ray diffractometer (Bruker, Germany) using Cu Kα radiation (1.5417Å) at 40kV and 40mA. The scanning range (2θ) was from 5° to 80° at a scan speed of 0.15° min^{-1} (for the dried sample) and 0.075° min^{-1} (for the calcinated sample) with a step size of 0.025°.

Phases were identified by matching the peaks to the JCPDS (Joint Committee on Powder Diffraction Standards) database. As β-TCP and whitlockite have similar XRD profiles (Gopal & Calvo 1972; Calvo & Gopal 1975; Frondel 1943) diffractograms were compared to one obtained from a commercial 100% crystalline (based on the manufacturer's description) β-tri-Calcium phosphate (β-TCP, ≥98% β-phase basis, Sigma-Aldrich Co., St Louis, MO, USA). The relative crystallinity (Cr) of the magnesium whitlockite powder was determined as described elsewhere (Kweh et al. 2000). In short, the most intense peak (31.4º at 2θ) of the powders, was compared to the same peak of the reference β-TCP according to:

$$Cr\ (\%) = A_{(31.4\ 2\theta)}/A_{s(31.4\ 2\theta)}*100\%$$

where Cr is the relative crystallinity of the measured magnesium whitlockite powder, and $A_{s(31.4\theta)}$ and $A_{(31.4\theta)}$ are the integrated area intensity of the 31.4 2θ peak of the β-TCP standard and the biomass powder respectively. TOPAS® software (Bruker AXS) was used for profile fitting and crystallite size calculations.

Fourier transform infrared spectroscopy (FTIR)

Attenuated Total Reflectance (ATR) Fourier transform infrared (FT-IR) spectra of pure powdered solids were obtained using a Bruker Tensor Series FT-IR (Bruker, Germany) spectrometer equipped with a zinc selenide crystal. Each Spectrum (sum of 64 scans) was collected from 4000 to 500 cm^{-1} at a spectral resolution of 4 cm^{-1}. An air spectrum was also obtained at the beginning of the analysis to measure the water and carbon dioxide content in the air and these were subtracted from the sample spectra. The spectra obtained from both biotic and abiotic precipitates were compared with that of the commercial reference material β-tricalcium phosphate (β-TCP, ≥98% β-phase basis, Sigma-Aldrich Co., St Louis, MO, USA).

Scanning Electron Microscopy (SEM)

SEM imaging was carried on two 30 day aged samples in order to compare: (1) the precipitate obtained from the sterile medium and (2) the precipitate that aged in the presence of *C. hydrogenoformans*. In both cases, a 40 mL sample was centrifuged, washed and dried, but the precipitate from the inoculated medium was also calcinated. Specimens were then mounted on SEM stubs with double side carbon tape. In order to avoid any interference during elemental analysis, no coating was applied. Examination and elemental analysis was done using a S-4700 Hitachi FE-SEM (Tokyo, Japan) working under vacuum at an acceleration voltage of 2.0 kV coupled to an Oxford INCA energy dispersive spectrometer (EDX) detector.

Backscattering electron (BSE) imaging was performed on an environmental SEM (ESEM, Quanta 200 FEG, FEI Company Hillsboro, OR) equipped with an energy dispersive X-ray (EDX) spectrometer (Genesis 2000, XMS System 60 with a Sapphire Si/Li Detector from EDAX Inc., Mahwah, NJ). Imaging was also done under the high vacuum mode of the ESEM microscope at an accelerating voltage of 20 kV and a working distance of 5 - 10 mm.

Transmission Electron Microscopy (TEM)

Whole mounts were prepared from 1 mL sample of an active 30 day bacterial culture of *C. hydrogenoformans* suspended in distilled water. They were imaged using a CM200 TEM (Philips, Netherlands), operating at an accelerating voltage of 200 kV. It was equipped with an AMT 2k x 2k CCD Camera and an EDAX Genesis (EDAX Inc, Mahwah, NJ) energy dispersive spectrometer (EDS).

To document the evolution of the solids in the presence of the bacterial culture, a time course experiment was carried on a 27 day culture. Every 3 days, a 50 mL aliquot of medium was sampled and centrifuged. The resulting pellet was washed in a 0.1M sodium cacodylate buffer and then fixed in 1 mL of fixative solution (2.5% glutaraldehyde in 0.1M sodium cacodylate buffer). Samples were then centrifuged for 5 minutes at 5000 rpm and post-fixed with 1% aqueous OsO_4 + 1.5% aqueous potassium ferrocyanide for 2 h, and washed 3 times with washing buffer. Samples were then dehydrated in a graded acetone series, infiltrated with graded Epon:acetone and embedded in Epon. Sections were polymerized for at least 120 h at 58ºC. Sections that were 90 – 100 nm thick were cut using a diamond knife on a Reichert Ultracut II microtome, collected on 200-mesh copper grids, and stained with uranyl acetate and Reynold's lead for 6 and 5 min, respectively. Samples were imaged with a FEI Tecnai 12 transmission electron microscope (FEI Company, Hillsboro, OR) operating at an accelerating voltage of 120 kV equipped with an AMT XR-80C 8 megapixel CCD camera (Advanced Microscopy Techniques, Corp. Woburn, MA).

Biomolecular techniques

To assess the potential role of proteins in the biomineralization process, protein extraction within and adsorbed to the precipitate was carried out on four independent cultures (200 mL each) after 21 days of *C. hydrogenoformans* growth. Each culture was centrifuged at 10000 rpm during 10 min at 4°C. The pellet was washed in 20 mL of sterile PBS buffer to remove any residual medium and then centrifuged. After its resuspension in a 10 mL crystal dissolving solution (151 U/mg trypsin in in 0.2M EDTA), it was sonicated 5 times for 20 seconds at 40 Watts on ice using a Vibra-Cell Ultrasonic Processor (Sonics & Materials Inc., Danbury, CT, USA). This solution was then decanted for 1 hour and centrifuged. Potentially adsorbed proteins released in the supernatant were then analyzed by SDS-PAGE using a Criterion XT Precast Gel, 4-12% Bis-Tris (Bio-Rad, Hercules, CA, USA). SDS-PAGE was run at 200 V for 60 min in a Bio-Rad Criterion Cell. The running buffer was XT MOPS (Bio-Rad) and the gel was stained with the Bio-Rad Silver Stain Plus Kit according to the manufacturer's procedure. The same steps were also applied to samples drawn from the control experiments in the sterile DSMZ and inoculated modified DSMZ media.

RESULTS AND DISCUSSION

A white precipitate appeared immediately after addition of $NaHCO_3$ to the inoculated DSMZ medium. Its appearance coincided with a sharp decrease in the total phosphate concentration of the solution (Figure 1). The same phenomenon was noted following an addition of $NaHCO_3$ to the same DSMZ medium without bacterial inoculation (hereafter referred to as the sterile DSMZ medium).

The centrifuged reaction product from 30-day culture in the DSMZ medium showed a 5.0 wt. % VSS/SS ratio, suggesting 95% inorganic precipitate and 5% biomass. This is inconsistent with the usual composition of microbial biomass where the inorganic portion represents typically less than 10% of dry weight (Rouf 1964). Chemical analysis of the organic and inorganic components obtained from bacterial culture confirmed that 6.33% was

organic (Table 1). This SS, expressed as absolute concentration, was 0.31+/-0.03 g_{SS}.L-1 after 30 days, and was identical to what was measured within 2 hours following the initial addition of $NaHCO_3$ in either sterile or inoculated media. The most abundant elements (in weight) were calcium and phosphorus (27 and 18 % dry wt) while the total of other metals did not exceed 4% (Table 2). The metals detected were Mg, Mn, Cu, Ba and Al, with respective abundances of 3.81, 0.15, 0.13, 0.01, 0.01 % dry wt. Converted to molar ratios, these relative abundances fall in the compositional range of the Ca-phosphate (CaP) phases listed in Table 2.

The identical initial decrease, following medium complementation with $NaHCO_3$, in phosphate concentration and the similarly steady pH maintained in sterile and inoculated media suggest that bacterial growth did not influence these parameters to induce the initial precipitation of the solid detected in our experiments. Within 25 hours of the initial formation of this precipitate, the dissolved phosphate concentration dropped slightly below 100 mg/L and varied very little for the remaining 29 days, in the sterile DSMZ medium. In contrast, measurements from several experiments on inoculated bottles showed a large scatter in values at 25 hours (resulting in the large error bar shown on Figure 1, at 25 hours) before a subsequent decline to a level comparable to the concentrations observed in the sterile medium after 48 hours.

Following repeated washing and recentrifugation, the precipitate in the sterile medium was invariably dissolved. This was not the case for the precipitate recovered from the inoculated DSMZ medium. The precipitate formed in the sterile DSMZ medium was therefore consistently more soluble in water.

The XRD pattern (Figure 2) of solids recovered after 30 days in the inoculated DSMZ medium showed sharp peaks at the same angles as the one of whitlockite XRD pattern from the JCPDS database (file number 01-070-1786). Lattice parameters of these solids were determined as a = 10,330 A˚ and c = 37,103 A˚, in agreement with those reported from natural whitlockite (Gopal & Calvo 1972). The calculated value of crystallite size was 30 nm compared to the crystallite size of 102 nm for the commercial β-TCP. The calculated

crystallinity of the dried-only solid was 91.7%. After calcination (600°C) in air for 1 h, the solid showed 100% crystallinity (Figure 3). By comparison, the XRD spectrum (Figure 4) of the solid recovered after 30 days of aging in the sterile DSMZ medium showed a broad hump around 30º and no sharp peaks, suggesting either a total lack of crystallinity or barely incipient nanocrystallinity.

The FTIR spectrum of the calcinated solids recovered from a 30 days experiment in inoculated DSMZ medium showed multiple split bands (Figure 5) associated with distinct absorption domains assigned to phosphate groups. Two groups of bands were observed: P–O stretching in HPO_4 and PO_4 groups at 1110, 1075, 1058, 1023, 962 603 cm^{-1} and the whitlockite specific bands at 990 and 555 cm^{-1}. According to literature, these latter bands correspond to the phosphate groups with different structural environments present in whitlockite (Mandel & Tas 2010; Rey et al. 1991; Rey et al. 1990).

The FTIR spectra of the sample recovered from a sterile DSMZ medium (Figure 5) showed two broad and unsplit phosphate absorption bands between 1250 and 900 cm^{-1} and 650 and 500 cm^{-1}. No bands related to carbonate groups were detected. Similar broad bands have been reported from FTIR spectra of amorphous calcium phosphate in previous studies where FTIR spectrum without any well-defined absorption bands, which indicated a disordered environment (Layrolle et al. 1998).

SEM imaging of solids from the 30-day inoculated DSMZ medium showed granules of 1-2 µm diameter consisting of angular particles approximately 50 nm across (Figure 6), which is a size consistent with the one determined from XRD spectra. Five EDS analyses from different granules revealed constant proportions of Ca (41), P (22), O (32), Mg (2) (% dry wt) without detectable spatial variation.

In contrast SEM imaging of the solid recovered from the sterile DSMZ medium revealed the presence of smooth spherical aggregates of 1-2 µm diameter (Figure 7). Their EDS analysis showed considerable variation in elemental composition within the following ranges: Ca (30 - 42), O (28 - 44) and Mg (4 – 5) while phosphorus remained constant around 24 dry wt.%.

To document the evolution of CaP phases with time, from an amorphous precursor phase

to crystalline phases, samples incubated in the presence of *C. hydrogenoformans* were analysed using analytical TEM and biochemical techniques. An unstained whole-mount (see TEM analysis in methods) of a sample from the 30-day inoculated DSMZ medium showed granules made of angular particles similar in size and shape to those imaged by SEM. EDX confirmed their uniform concentrations of P, Ca and Mg (Figure 8, A, B). The granules were covered with a biofilm (Figure 8, C). Lattice fringes (Figure 8, E, F) were observed at the edges of the granules, confirming the crystalline character of their constituent particles.

Ultrathin sections of samples obtained from the time course experiment shed additional light on the evolution of the amorphous precipitate. Because of its high solubility, the only evidence of the solid granules produced in the sterile DSMZ medium were holes left in the epoxy matrix (Figure 9, A). The granules were dissolved during the sectioning process, which exposed them to low-pH water. After 3 days of *C. hydrogenoformans* growth, a nanocrystalline phase composed of 30-50 nm rod-like crystals, distinct from the previously characterized whitlockite, was observed (Figure 10, D). These nanorods resembled hydroxyapatite produced by bacteria and mammalian cells such as bone and calcified tissue (Azari et al. 2008). In this sample, well-preserved bacteria were observed (Figure 9, B).

Backscatter analysis was carried out on the cutting face of the epoxy blocks used for the sectioning. Distribution and chemical composition of the amorphous CaP precursor confirmed the results previously obtained with TEM and SEM analysis (Figure 11, A, B). No traces of CaP material were detected in the epoxy matrix for the sample recovered after 15 days from the sterile DSMZ medium (Figure 11, C). The backscatter analysis of the blocks containing the sample recovered after 15 days of incubation in an inoculated DSMZ medium (Figure 11, D) revealed a presence both larger crystals and the chemical signature of a CaP material dispersed throughout the matrix, which could be mixture of disaggregated granular whitlockite and nanorods (Figure 11, E, F). With time, there was increasing visible evidence for bacterial lysis (Figure 10) and the nanorods were always associated with those degraded bacterial remnants (Figure 10, C, D). Disruption of cytoplasmic membrane led to the formation of vesicles that could have served as nucleation site for the precipitation of hydroxyapatite

(Figure 10, A, B).

In summary, we report the formation of two distinct CaP crystalline solids in the presence of *C. hydrogenoformans* grown in a phosphate and calcium rich medium under a near-steady pH and at a controlled temperature. For both CaP phases, the path of biomineralization appears to follow biologically induced mineralization (BIM) (Frankel & Bazylinski 2003) in contrast to biologically controlled mineralization (BCM) (Bazylinski 2003). Both phases only appeared in the inoculated DSMZ medium.

One mode of mineralization involves conversion of a granular amorphous CaP precipitate to polycrystalline granules of whitlockite. The presence in the whole mount of a microbial biofilm that covers and binds the granules suggests that the biofilm creates the conditions for a dissolution-reprecipitation mechanism. This is strongly supported by the phosphate resolubilization (Figure 1) observed during the first 25 hours following DSMZ medium inoculation with *C. hydrogenoformans*. Lagier and Baud (2003) report that whitlockite formation was caused by the binding of the amorphous CaP precursor with phospholipids, with the magnesium content in the precursor inhibiting apatite to the benefit of whitlockite formation. In our system, the bacterial biofilm could have played a similar role in the conversion of amorphous CaP to whitlockite.

A number of biochemical analysis were conducted on the precipitate (see Biomolecular techniques in methods section) to look for evidence of biomolecules occluded or strongly adsorbed to its surface. The analyses of metabolic by-products of bacteria (mono or disaccharides, VFAs and alcohols) and protein content in the crystalline material dissolved to detect them were negative. Since this precipitate, according to XRD, is dominantly whitlockite (or a Mg-stabilized beta-TCP), we conclude to a conversion by a biologically induced mechanism rather than a biologically controlled one. The inhibiting effect of Mg on a conversion from an amorphous CaP precursor to hydroxyapatite is widely documented (Blumenthal 1989; Boskey & Posner 1974). It is therefore plausible that the biofilm

counteracts this by chelating Mg and decreasing its capacity to inhibit either dissolution of the amorphous CaP or nucleation of other crystalline CaP phases.

The second mode of mineralization involves formation of nanorods interpreted to be hydroxyapatite-like (HA). The bacterial cells were lysed and fragmented leading to formation of vesicles, and there was a direct association between the HA nanorods and the fragmented membrane material (Figure 9, B, C, D; Figure 10; Figure 11, F). According to Mann (Mann 1993), a cellular membrane can serve as a template for the nucleation of HA. Our nanorods resemble closely those obtained in other cases of induced biomineralization described in *Serratia* species, where presence of high concentration of calcium and phosphate in the growth medium coupled to the presence of an organic matrix (EPS), triggered hydroxyapatite nucleation (Medina Ledo et al. 2008).

Bioresorption or biodegradation of the CaP ceramics is a biological mechanism during which part of (or all) grafted CaP disappear partially (or completely) over a period of time in vivo (Blokhuis et al. 2000). The major factor accelerating CaP resorption is local pH diminution, which can be caused either chemically or biologically (Hench 1991). This feature allows avoiding lifetime implants of foreign bodies and stronger newly formed bone (Blokhuis et al. 2000). All synthetic calcium phosphate ceramics are bioresorbable to a certain extent, from most to least: amorphous calcium phosphate, tetracalcium phosphate, α-TCP, β-TCP, Hydroxyapatite (HA) (LeGeros 2002). Resorption rate increases with surface area increase and decreases with an increase of crystallinity, grain size and ionic substitutions of CO_3^{2-}, Mg^{2+} and Sr^{2+} in HA (Hench 1991). Little is known about bioresorption of whitlockite. Ramselaar (Ramselaar et al. 1991) concluded that, in vivo, whitlockite was biodegraded at a faster rate than HA - because of differences in density and pore diameter - but at a slower rate than β-TCP, due probably to the presence of metal oxides that may make the material less resorbable. Magnesium incorporation was also shown to stimulate human osteoblast proliferation (Sader et al. 2009) making whitlockite less quickly resorbable than β-TCP but more osteoinductive, thus with an interesting range of application in bone engineering.

CONCLUSION

C. hydrogenoformans is a carboxydotrophic bacteria that was first isolated from a hot spring in Kunashir Island, Russia (Svetlichny et al. 1991). This bacteria has been subject to an extensive investigation with respect to its genomic and metabolic activities (Svetlichny et al. 1991; Wu et al. 2005; Henstra & Stams 2004; Henstra & Stams 2011). The main interest in this organism has been its ability to produce hydrogen from carbon monoxide, which is a potential biological based alternative to the currently conventional chemical catalysed water-gas shift reaction (Newsome 1980; Henstra et al. 2007; Zhao et al. 2013). So far, there has not been any report on biomineralization activities associated with *C. hydrogenoformans*. The results presented here show two previously unknown modes of biomineralization carried out in the presence of *C. hydrogenoformans*.

The suggested BIM pathway for HAP nanorods follows a typical pattern, widely documented in the literature (Frankel & Bazylinski 2003), but the association of nanorods with cellular components resulting from *C. hydrogenoformans* lysis is unusual. The whitlockite, however, is a novel aspect where a biofilm is involved but acts on an amorphous precipitate, by a different mechanism possibly neutralizing the inhibiting effect of Mg on the dissolution of the amorphous CaP and the nucleation of whitlockite. The result is a biphasic crystalline product induced by the bacterial activity and decay. Further investigation of the mechanisms by which this biomineralization proceeds could lead to interesting applications in the field of CaP bioceramics.

ACKNOWLDGMENTS

The authors wish to thank R. Cimpoia, J. Mui, L. Mongeon, X.D. Liu, A. Corriveau and S. Deschamps for their assistance and discussions. One of the authors (M.H.) was supported by the Natural Sciences and Engineering Research Council of Canada (grant 185778-2009).

REFERENCES

ASTM Standard D5291, 2010. *Instrumental determination of carbon, hydrogen, and nitrogen in petroleum products and lubricants.*, West Conshohocken, PA.

ASTM Standard D5373, 2008. *Instrumental Determination of Carbon, Hydrogen, and Nitrogen in Laboratory Samples of Coal.*, West Conshohocken, PA.

Azari, F. et al., 2008. Intracellular precipitation of hydroxyapatite mineral and implications for pathologic calcification. *Journal of Structural Biology*, 162(3), pp.468–479.

Bäuerlein, E., 2008. Growth and Form: What is the Aim of Biomineralization? In *Handbook of Biomineralization*. Wiley-VCH Verlag GmbH, pp. 1–20.

Bazylinski, D. a., 2003. Biologically Controlled Mineralization in Prokaryotes. *Reviews in Mineralogy and Geochemistry*, 54(1), pp.217–247.

Bazylinski, D. a., Frankel, R.B. & Konhauser, K.O., 2007. Modes of Biomineralization of Magnetite by Microbes. *Geomicrobiology Journal*, 24(6), pp.465–475.

Berman, A. et al., 1993. Biological control of crystal texture: a widespread strategy for adapting crystal properties to function. *Science*, 259(5096), pp.776–779.

Blokhuis, T.J. et al., 2000. Properties of calcium phosphate ceramics in relation to their in vivo behavior. *The Journal of Trauma*, 48(1), pp.179–86.

Blumenthal, N.C., 1989. Mechanisms of inhibition of calcification. *Clinical Orthopaedics and Related Research*, (247), pp.279–89.

Boskey, A.L. & Posner, A.S., 1974. Magnesium stabilization of amorphous calcium phosphate: A kinetic study. *Materials Research Bulletin*, 9(7), pp.907–916.

Calvo, C. & Gopal, R., 1975. The crystal structure of whitlockite from the Palermo Quarry. *American Mineralogist*, 60, pp.120–133.

CEAEQ, 2004. *Metal determination using inductively coupled plasma spectrometry (In French).*,

Chevalier, J. & Gremillard, L., 2009. Ceramics for medical applications: A picture for the next 20 years. *Journal of the European Ceramic Society*, 29(7), pp.1245–1255.

Cölfen, H. & Qi, L., 2001. A Systematic Examination of the Morphogenesis of Calcium Carbonate in the Presence of a Double-Hydrophilic Block Copolymer. *Chemistry – A European Journal*, 7(1), pp.106–116.

Dorozhkin, S. V & Epple, M., 2002. Biological and medical significance of calcium phosphates. *Angewandte Chemie (International ed. in English)*, 41(17), pp.3130–46.

Eaton, A. et al., 2005. *Standard methods for the examination of water and wastewater* 21st ed., Washington, D.C.: American Public Health Association, American Water Works Association, Water Environment Federation.

Emsley, J., 1991. *The elements* 2d ed., Oxford, UK.: Clarendon Press.

Epple, M. & Kovtun, A., 2010. Functionalized Calcium Phosphate Nanoparticles for Biomedical Application. *Key Engineering Materials*, 441, pp.299–305.

Frankel, R.B. & Bazylinski, D.A., 2003. Biologically Induced Mineralization by Bacteria. *Reviews in Mineralogy and Geochemistry* , 54 (1), pp.95–114.

Frondel, C., 1943. *Mineralogy of the calcium phosphates in insular phosphate rock*, Washington, D.C.: s.n.,].

Gopal, R. & Calvo, C., 1972. Structural Relationship of Whitlockite and βCa3(PO4)2. *Nature Physical Science*, 237, pp.30–32.

Hammes, F. & Verstraete, W., 2002. Key roles of pH and calcium metabolism in microbial carbonate precipitation. *Reviews in Environmental Science and Biotechnology*, 1(1), pp.3–7.

Heijnen, J.J. et al., 1999. in: Encyclopedia of bioprocess technology: Fermentation, biocatalysis & bioseparation. ed: Flickinger MC, Drew SW. Wiley-Interscience, New York, Vol 1, pp 267–291 (1999). , 1(May 1998).

Hench, L.L., 1991. Bioceramics: From Concept to Clinic. *Journal of the American Ceramic Society*, 74(7), pp.1487–1510.

Henstra, A.M. et al., 2007. Microbiology of synthesis gas fermentation for biofuel production. *Current Opinion in Biotechnology*, 18(3), pp.200–6.

Henstra, A.M. & Stams, A.J.M., 2011. Deep Conversion of Carbon Monoxide to Hydrogen and Formation of Acetate by the Anaerobic Thermophile *Carboxydothermus hydrogenoformans*. *International Journal of Microbiology*, 2011, p.641582.

Henstra, A.M. & Stams, A.J.M., 2004. Novel physiological features of *Carboxydothermus hydrogenoformans* and Thermoterrabacterium ferrireducens. *Applied and Environmental Microbiology*, 70(12), pp.7236–40.

Huber, R., Huber, H. & Stetter, K.O., 2000. Towards the ecology of hyperthermophiles: biotopes, new isolation strategies and novel metabolic properties. *FEMS Microbiology Reviews*, 24(5), pp.615–23.

Kaneko, K., 1994. Determination of pore size and pore size distribution: 1. Adsorbents and catalysts. *Journal of Membrane Science*, 96(1–2), pp.59–89.

Kashefi, K. & Lovley, D.R., 2000. Reduction of Fe(III), Mn(IV), and toxic metals at 100 degrees C by Pyrobaculum islandicum. *Applied and Environmental Microbiology*, 66(3), pp.1050–6.

Klasson, K.T. et al., 1992. Biological conversion of synthesis gas into fuels. *International Journal of Hydrogen Energy*, 17(4), pp.281–288.

Kweh, S.W., Khor, K. a & Cheang, P., 2000. Plasma-sprayed hydroxyapatite (HA) coatings with flame-spheroidized feedstock: microstructure and mechanical properties. *Biomaterials*, 21(12), pp.1223–34.

Lagier, R. & Baud, C.-A., 2003. Magnesium Whitlockite, a Calcium Phosphate Crystal of Special Interest in Pathology. *Pathology - Research and Practice*, 199(5), pp.329–335.

Layrolle, P., Ito, A. & Tateishi, T., 1998. Sol-Gel Synthesis of Amorphous Calcium Phosphate and Sintering into Microporous Hydroxyapatite Bioceramics. *Journal of the American Ceramic Society*, 81(6), pp.1421–1428.

LeGeros, R.Z., 2002. Properties of osteoconductive biomaterials: calcium phosphates. *Clinical Orthopaedics and Related Research*, (395), pp.81–98.

Logan, B., 2004. Peer reviewed: extracting hydrogen and electricity from renewable resources. *Environmental Science & Technology*, 38(9), p.160A – 167A.

Lowenstam, H. a, 1981. Minerals formed by organisms. *Science (New York, N.Y.)*, 211(4487), pp.1126–31.

Mandel, S. & Tas, a. C., 2010. Brushite ($CaHPO_4 \cdot 2H_2O$) to octacalcium phosphate ($Ca_8(HPO_4)_2(PO_4)_4 \cdot 5H_2O$) transformation in DMEM solutions at 36.5°C. *Materials Science and Engineering: C*, 30(2), pp.245–254.

Mann, S., 1993. Molecular tectonics in biomineralization and biomimetic materials chemistry. *Nature*, 365(6446), pp.499–505.

Medina Ledo, H. et al., 2008. Microstructure and composition of biosynthetically synthesised hydroxyapatite. *Journal of Materials Science. Materials in medicine*, 19(11), pp.3419–27.

Merchuk, J.C. & Gluz, M., 2002. Bioreactors, Air-lift Reactors. In *Encyclopedia of Bioprocess Technology*. John Wiley & Sons, Inc.

Munasinghe, P.C. & Khanal, S.K., 2010. Syngas fermentation to biofuel: evaluation of carbon monoxide mass transfer coefficient (kLa) in different reactor configurations. *Biotechnology progress*, 26(6), pp.1616–21.

Newsome, D.S., 1980. The Water-Gas Shift Reaction. *Catalysis Reviews*, 21(2), pp.275–318.

Norris, V. et al., 1996. Calcium signalling in bacteria. *Journal of Bacteriology*, 178(13), pp.3677–3682.

Oura, K. et al., 2010. *Surface Science: An Introduction*, Springer.

Padro, C.E.G. & Putsche, V., 1999. Survey of the Economics of Hydrogen Technologies. *National Renewable Energy Laboratory*, (September).

Ramselaar, M.M.A. et al., 1991. Biodegradation of four calcium phosphate ceramics;in vivo rates and tissue interactions. *Journal of Materials Science: Materials in Medicine*, 2(2), pp.63–70.

Rey, C. et al., 1991. Resolution-enhanced Fourier transform infrared spectroscopy study of the environment of phosphate ion in the early deposits of a solid phase of calcium phosphate in bone and enamel and their evolution with age: 2. Investigations in the nu3PO4 domain. *Calcified tissue international*, 49(6), pp.383–8.

Rey, C. et al., 1990. Resolution-enhanced Fourier transform infrared spectroscopy study of the environment of phosphate ions in the early deposits of a solid phase of calcium-phosphate in bone and enamel, and their evolution with age. I: Investigations in the upsilon 4 PO4 dom. *Calcified Tissue International*, 46(6), pp.384–94.

Roadmap, E., 2002. National Hydrogen Energy Roadmap. *(US Department of Energy (DOE), 2002. National Hydrogen Energy Roadmap. Washington, DC.)*, (November).

Roels, J.A., 1983. *Energetics and kinetics in biotechnology*, Elsevier Biomedical Press.

Rouf, M. a, 1964. Spectrochemical Analysis of Inorganic Elements in Bacteria. *Journal of Bacteriology*, 88, pp.1545–9.

Sader, M.S., Legeros, R.Z. & Soares, G. a, 2009. Human osteoblasts adhesion and proliferation on magnesium-substituted tricalcium phosphate dense tablets. *Journal of Materials Science. Materials in Medicine*, 20(2), pp.521–7.

Sidaway, D.A., 1978. A microbiological study of dental calculus. *Journal of Periodontal Research*, 13(4), pp.349–359.

SING, K.S.W. et al., 1985. Reporting physisorption data for gas/solid systems, with special reference to the determination of surface area and porosity. *Pure and Applied Chemistry*, 57(4), pp.603–619.

Solomon, B.D. & Banerjee, A., 2006. A global survey of hydrogen energy research, development and policy. *Energy Policy*, 34(7), pp.781–792.

Stams, A.J. et al., 1993. Growth of syntrophic propionate-oxidizing bacteria with fumarate in the absence of methanogenic bacteria. *Applied and Environmental Microbiology*, 59(4), pp.1114–1119.

Svetlichny, V., 1991. Bacterial CO utilization with H 2 production by the strictly anaerobic lithoautotrophic thermophilic bacterium *Carboxydothermus hydrogenus* DSM 6008 isolated from a hot swamp. , 83, pp.267–271.

Svetlichny, V.A. et al., 1991. Anaerobic Extremely Thermophilic Carboxydotrophic Bacteria in Hydrotherms of Kuril Islands Light Microscopy. , pp.1–10.

Techtmann, S., Colman, A. & Murphy, M., 2011. Regulation of multiple carbon monoxide consumption pathways in anaerobic bacteria. *Frontiers in Microbiology*, 2(July), p.12.

Thommes, M., 2010. Physical Adsorption Characterization of Nanoporous Materials. *Chemie Ingenieur Technik*, 82(7), pp.1059–1073.

Torres, W., Pansare, S.S. & Goodwin, J.G., 2007. Hot Gas Removal of Tars, Ammonia, and Hydrogen Sulfide from Biomass Gasification Gas. *Catalysis Reviews*, 49(4), pp.407–456.

Tung, M.S., 1998. Calcium phosphates: structure, composition, solubility and stability. In Z. Amjad, ed. *Biological and Industrial Systems*. Norwell, MA.: Kluwer Academic Publishers, pp. 1–19.

Ungerman, A.J. & Heindel, T.J., 2007. Carbon Monoxide Mass Transfer for Syngas Fermentation in a Stirred Tank Reactor with Dual Impeller Configurations. *Biotechnology Progress*, 23(3), pp.613–620.

USEPA, 1993. *Methods for the determination of inorganic substances in environmental samples.*,

Weiner, S. et al., 2001. An Overview of Biomineralization Processes and the Problem of the Vital Effect.

Wu, M. et al., 2005. Life in hot carbon monoxide: the complete genome sequence of *Carboxydothermus hydrogenoformans* Z-2901. *PLoS Genetics*, 1(5), p.e65.

Yang, J.D. & Wang, N.S., 1992. Oxygen mass transfer enhancement via fermentor headspace pressurization. *Biotechnology Progress*, 8(3), pp.244–251.

Yuan, H. et al., 1998. Osteoinduction by calcium phosphate biomaterials. *Journal of Materials Science. Materials in Medicine*, 9(12), pp.723–6.

Zhao, Y., Cimpoia, R., Liu, Z. & Guiot, S., 2011. Kinetics of CO conversion into H_2 by *Carboxydothermus hydrogenoformans*. *Applied Microbiology and Biotechnology*, 91(6), pp.1677–1684.

Zhao, Y., Cimpoia, R., Liu, Z. & Guiot, S.R., 2011. Orthogonal optimization of *Carboxydothermus hydrogenoformans* culture medium for hydrogen production from carbon monoxide by biological water-gas shift reaction. *International Journal of Hydrogen Energy*, 36(17), pp.10655–10665.

Zhao, Y. et al., 2013. Performance of a *Carboxydothermus hydrogenoformans*-immobilizing membrane reactor for syngas upgrading into hydrogen. *International Journal of Hydrogen Energy*, 38(5), pp.2167 – 2175.

FIGURES

Chemical element	Proportion (% wt)		Atomic fraction	
	This study	Literature	This study	Literature
C	2.81 ±0.09	48	1	1
H	0.85 ±0.03	7.3	3.62	1.8
N	0.49 ±0.02	11.3	0.15	0.2
O	2.18 ±0.14	32.5	0.58	0.5
S	0	0.01	0	0
Total	6.33 ±0.27	99.1		
Molecular weight ($g \cdot mol^{-1}$)			27	24.6

Table 1: Elemental analysis of a washed sample of *C. hydrogenoformans culture* grown on DSMZ medium compared to biomass elemental composition from literature (Heijnen et al. 1999)

Chemical element	Proportion (% wt)			
	Suspended Solids	whitlockite	hydroxyapatite	octacalcium phosphate
Calcium (Ca)	27.30 ±1.70	33.91	39.9	32.63
Phosphorus (P)	17.95 ±1.16	20.38	18.5	18.91
Hydrogen (H)	N.D.	0.076	0.2	1.23
Oxygen (O)	N.D.	42.11	41.4	40.71
Metals	4.10 ±0.45	N.D.	N.D.	N.D.
Ca/P ratio (weight)	1.52 ±0.01	1.66	2.15	1.72

Ca/P ratio (molar)	1.17 ±0.01	1.28	1.66	1.33
Formula		$Ca_9(Mg, Fe^{2+})(PO_4)_6(PO_3OH)$	$Ca_5(PO_4)_3(OH)$	$Ca_8H_2(PO_4)_6.5H_2O$

Table 2: Comparison of the elemental chemical composition of whitlockite (Calvo & Gopal 1975), hydroxyapatite (Emsley 1991), octacalcium (Tung 1998) to the elemental composition of suspended solids obtained after 39 days of *C. hydrogenoformans* growth on DSMZ medium. N.D. not determined

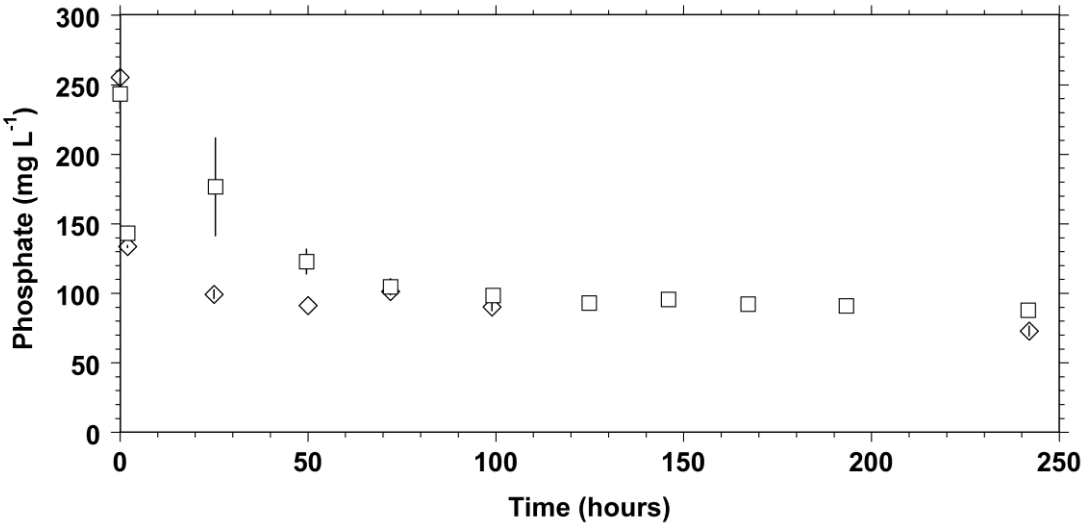

Figure 1: Change with time of dissolved total phosphate concentration in the sterile (dash) and inoculated (triangle) DSMZ medium after complementation with $NaHCO_3$ (at time 0).

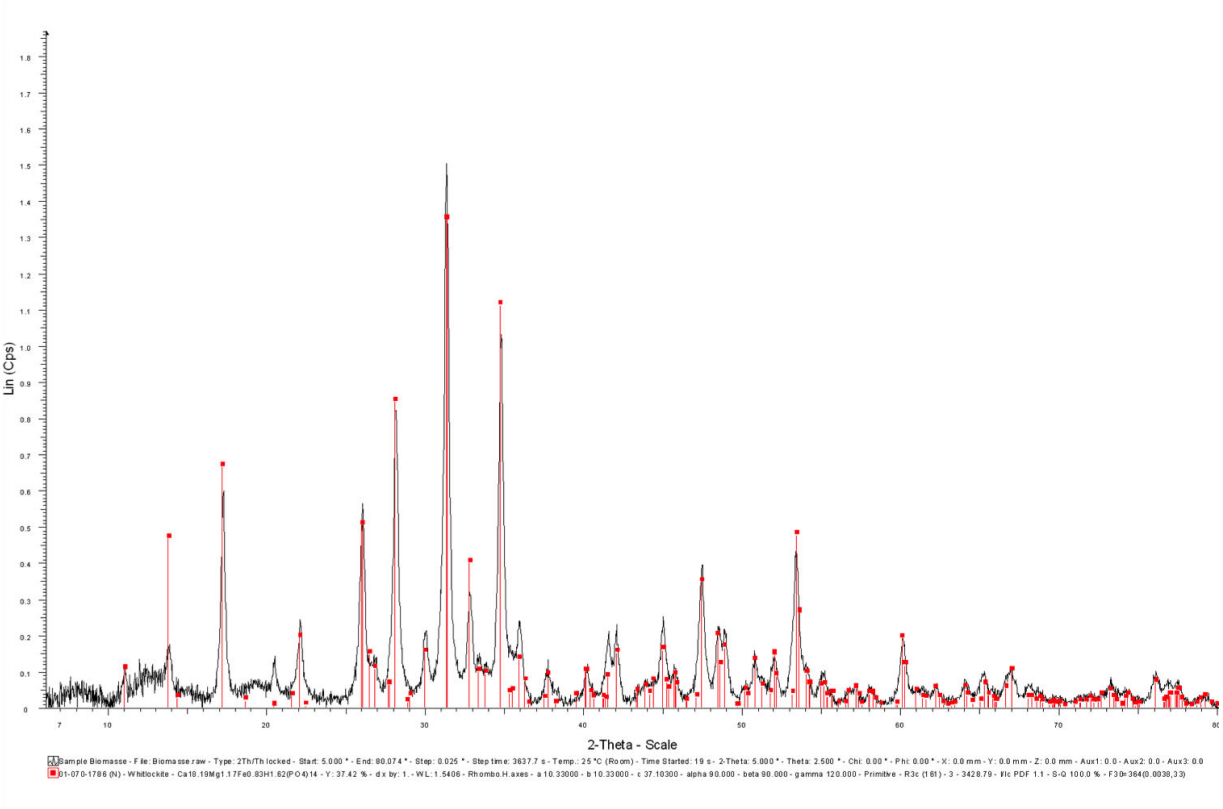

Figure 2: XRD spectra. Black: dried precipitate formed and aged during 30 days in the inoculated DSMZ medium. Red: whitlockite from the JCPDS (Joint Committee on Powder Diffraction Standards) database (number 01-070-1786).

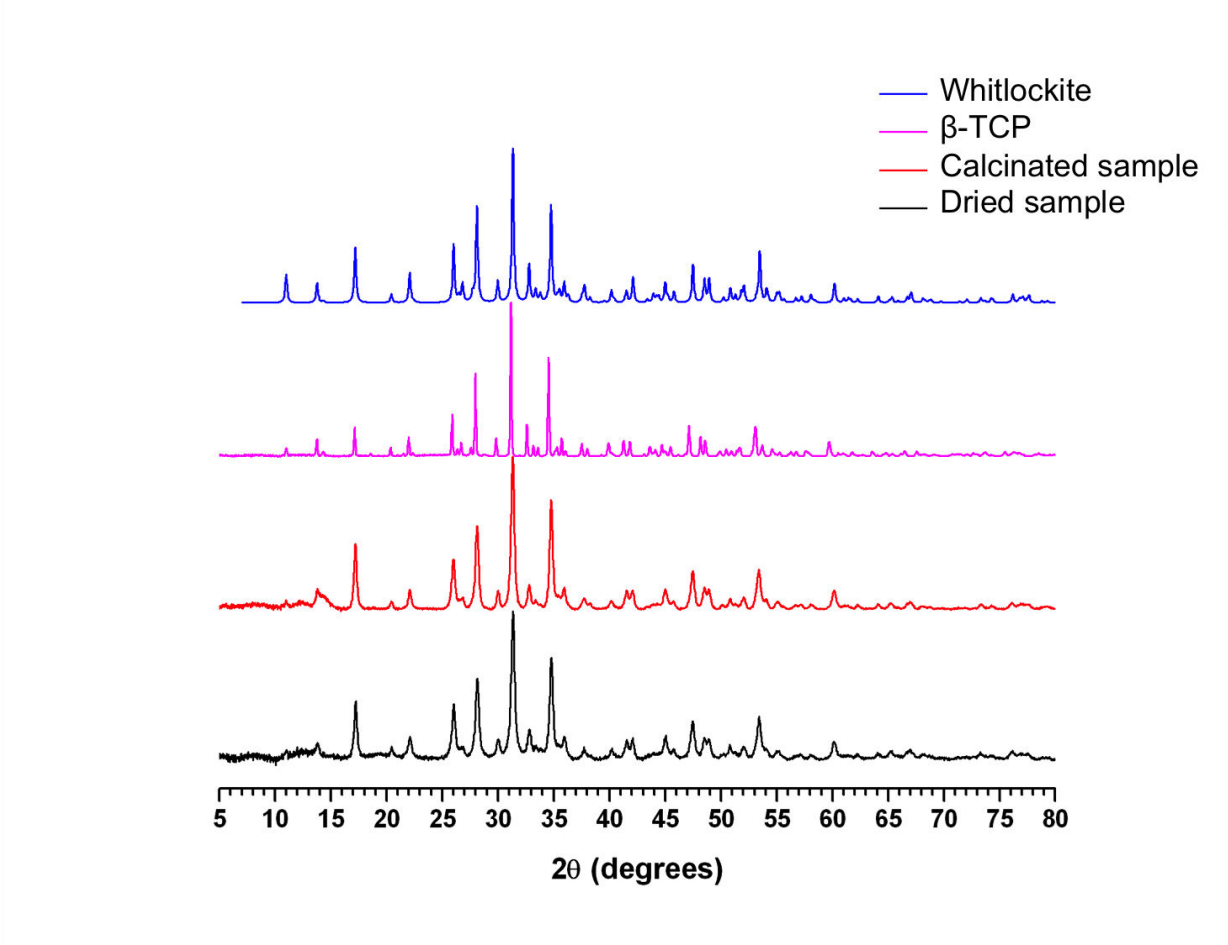

Figure 3: XRD spectra of (Dried sample) the dried precipitate recovered after 30 days of aging. in the inoculated DSMZ medium, (Calcinated sample) the "Dried sample" sample calcinated, (β-TCP) commercial sintered β-TCP and (Whitlockite) calculated whitlockite profile according to the JCPDS (Joint Committee on Powder Diffraction Standards) database (number 01-070-1786).

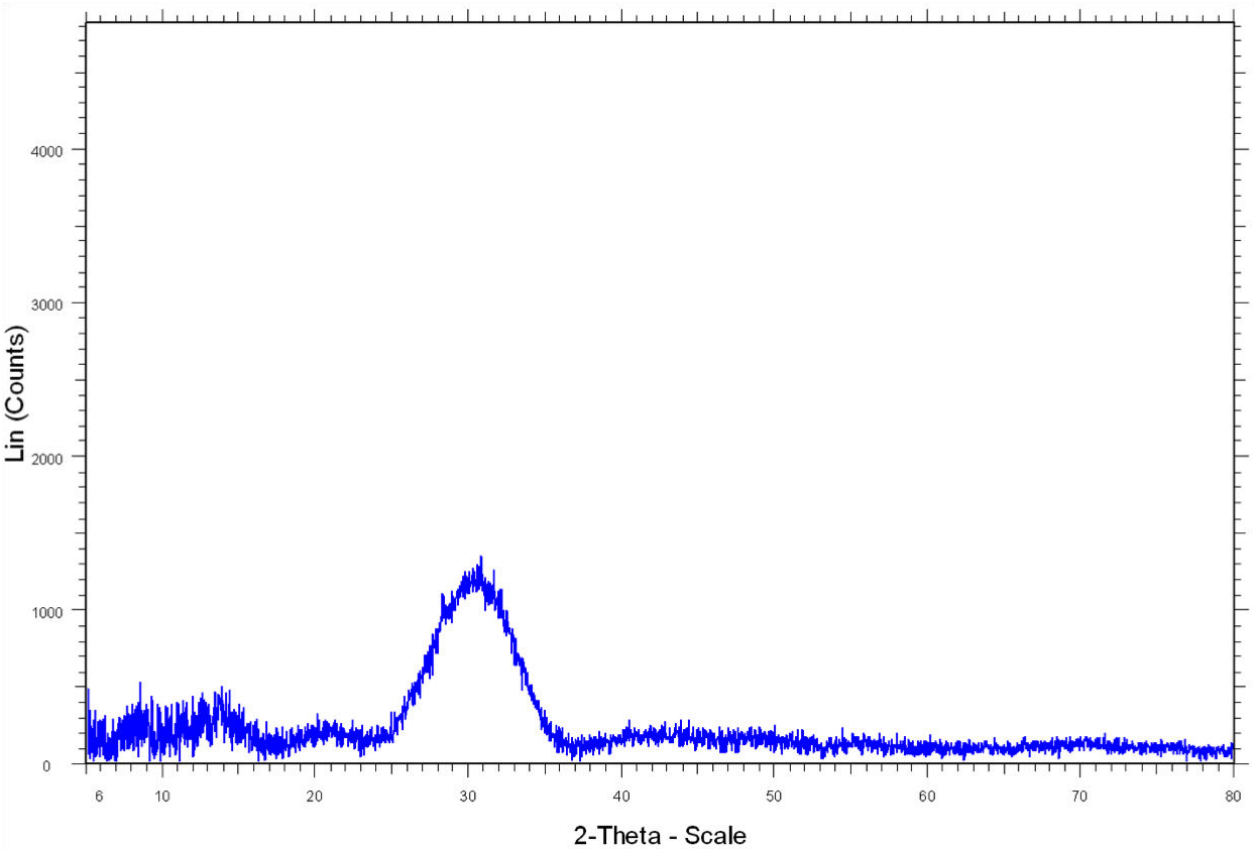

Figure 4: XRD pattern of the dried precipitate formed and sampled after 30 days of aging in the sterile DSMZ medium.

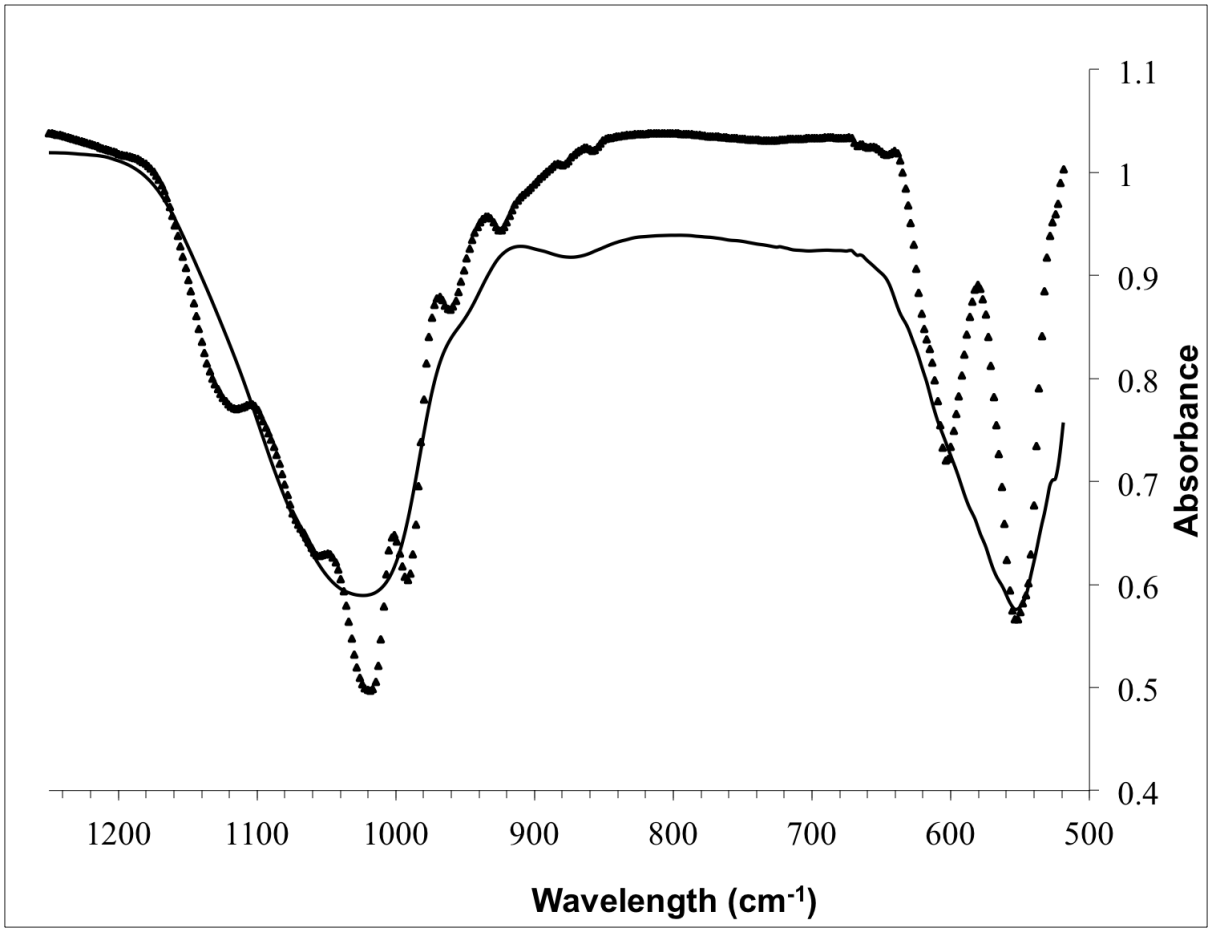

Figure 5: FTIR analysis of precipitate after 30 days of aging. Dried precipitate from sterile DSMZ medium (continuous line) and calcinated precipitate cultured in the DSMZ medium (triangles).

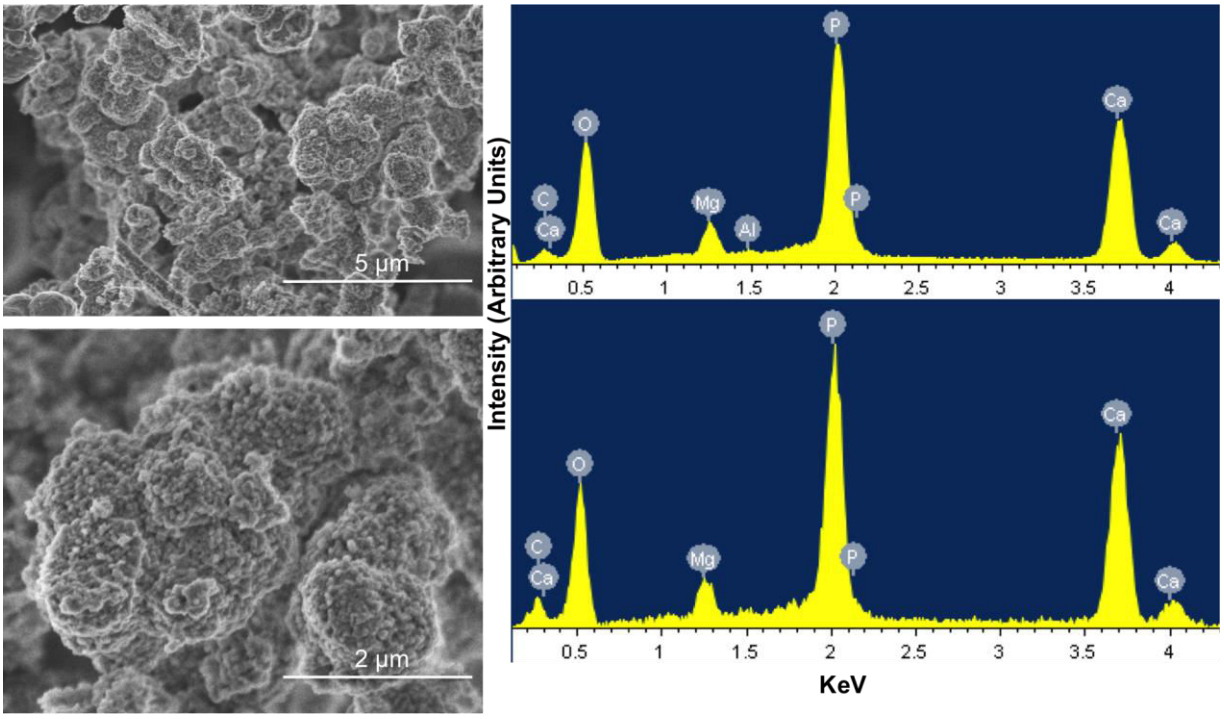

Figure 6: SEM-EDX analysis of two areas from a calcinated precipitate isolated after 30 days of aging in the inoculated DSMZ medium. Images on the left show two levels of magnification of same area. Images on the right show EDX spectrum of two distinct areas of the sample.

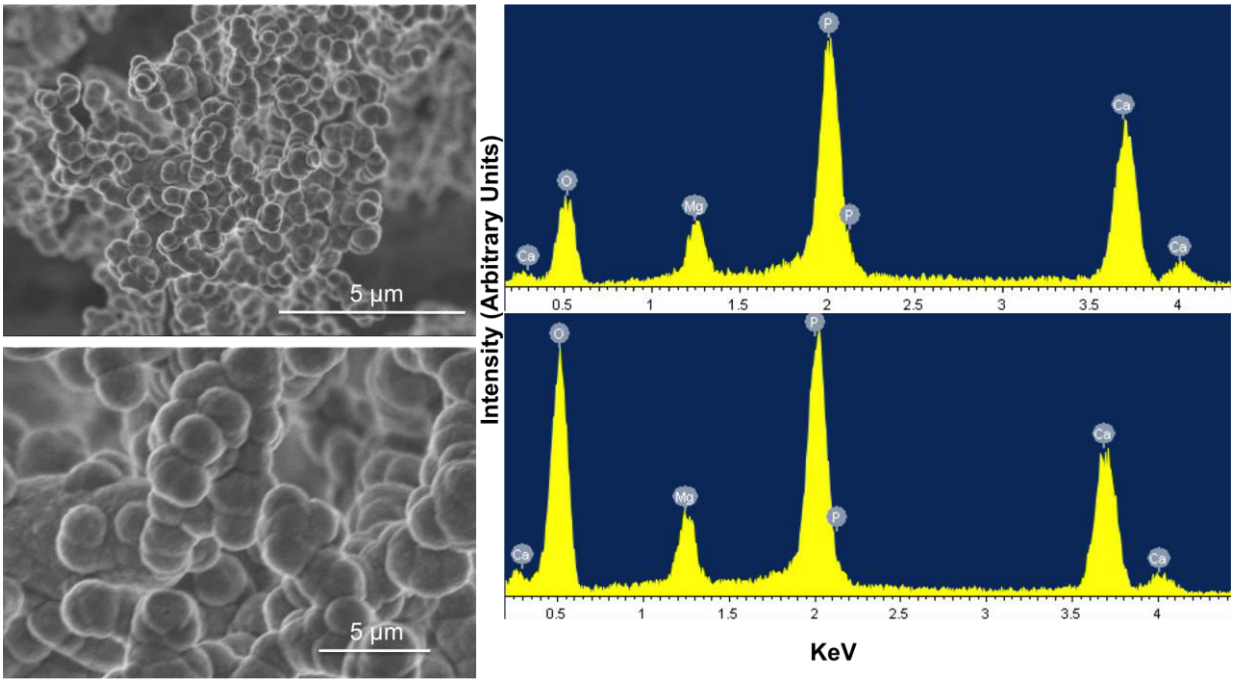

Figure 7: SEM-EDX analysis of two areas from a precipitate recovered and dried after 30 days of aging in the sterile DSMZ medium. Images on the left show two levels of magnification of same area. Images on the right show EDX spectrum of two distinct areas of the sample.

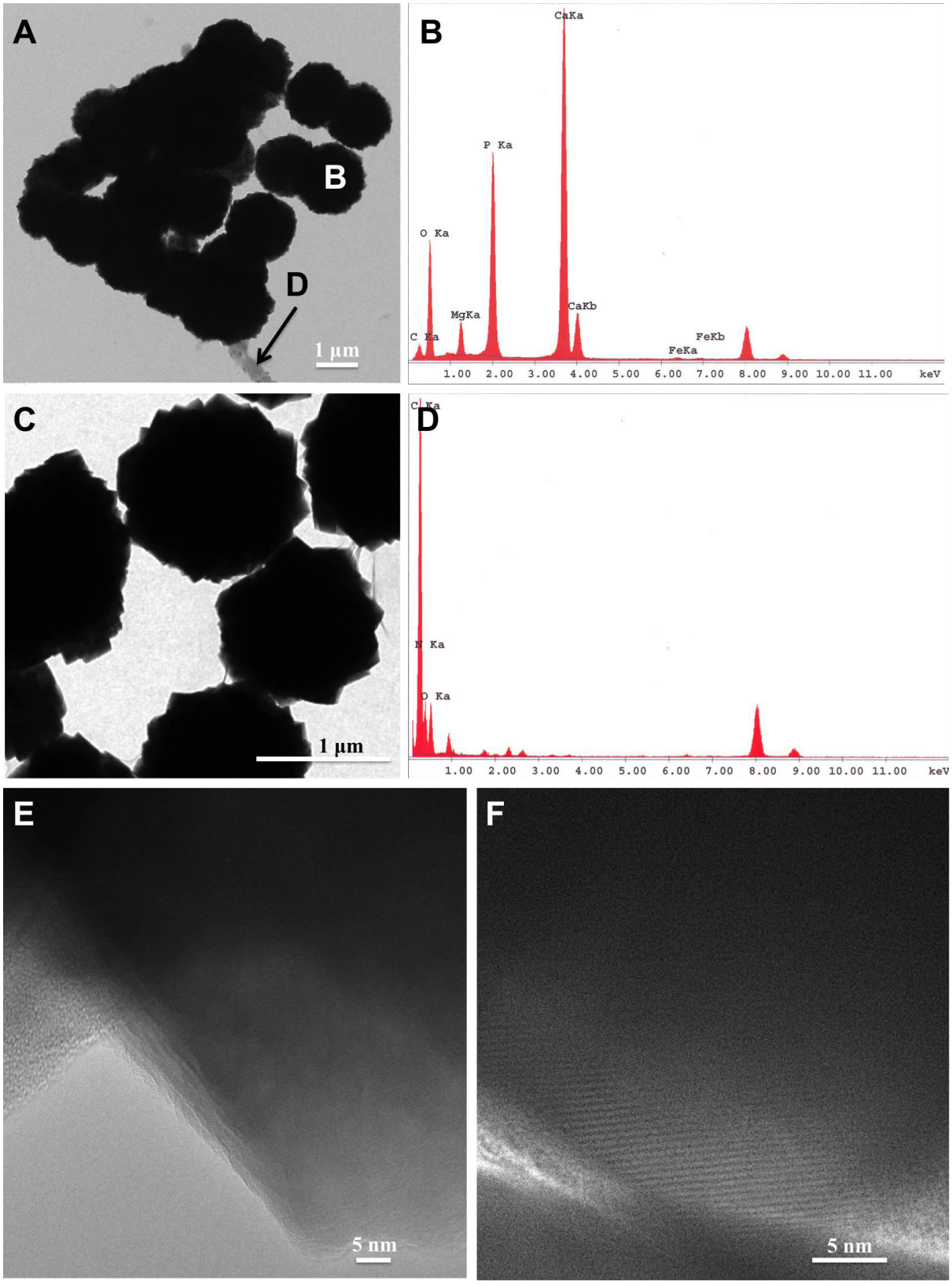
A
B
D
1 µm
B
CaKa
P Ka
O Ka
MgKa
CaKb
C Ka
FeKb
FeKa
1.00 2.00 3.00 4.00 5.00 6.00 7.00 8.00 9.00 10.00 11.00 keV
C
1 µm
D
C Ka
N Ka
O Ka
1.00 2.00 3.00 4.00 5.00 6.00 7.00 8.00 9.00 10.00 11.00 keV
E
5 nm
F
5 nm

Figure 8: Images (A, C) and corresponding TEM-EDS analysis (B, D) of two areas in a whole-mount sample recovered after 30 days from the inoculated DSMZ medium. (C) Magnification of the area in (A) showing biofilm covering and binding the granules, (B) Spectrum from the granule labelled B. (D) Spectrum from the organic material labelled D. (E, F) HR-TEM images of the granules' edges showing lattice fringes.

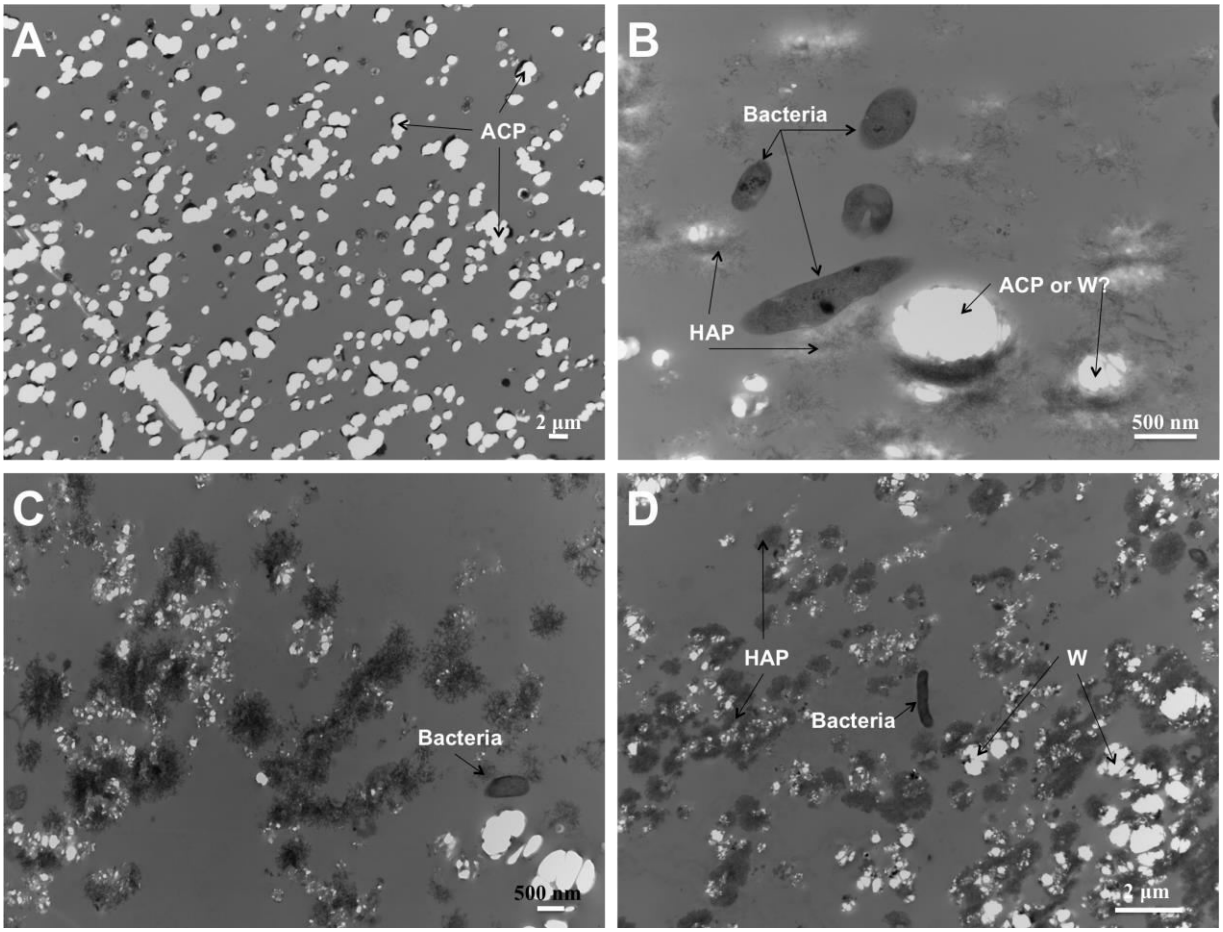

Figure 9: TEM imaging of solids identified in sterile and inoculated DSMZ media. (A) Sample recovered from the sterile DSMZ medium after 15 days of aging. ACP granules embedded in resin are visible. (B, C, D) Images from samples recovered after 3, 8 and 15 days respectively from a time course experiment in inoculated DSMZ medium. Three solid phases are distinct

and interpreted to be either amorphous CaP (ACP) or whitlockite (W) and nanocrystalline hydroxyl-apatite (HAP). Bacteria (B) are also visible.

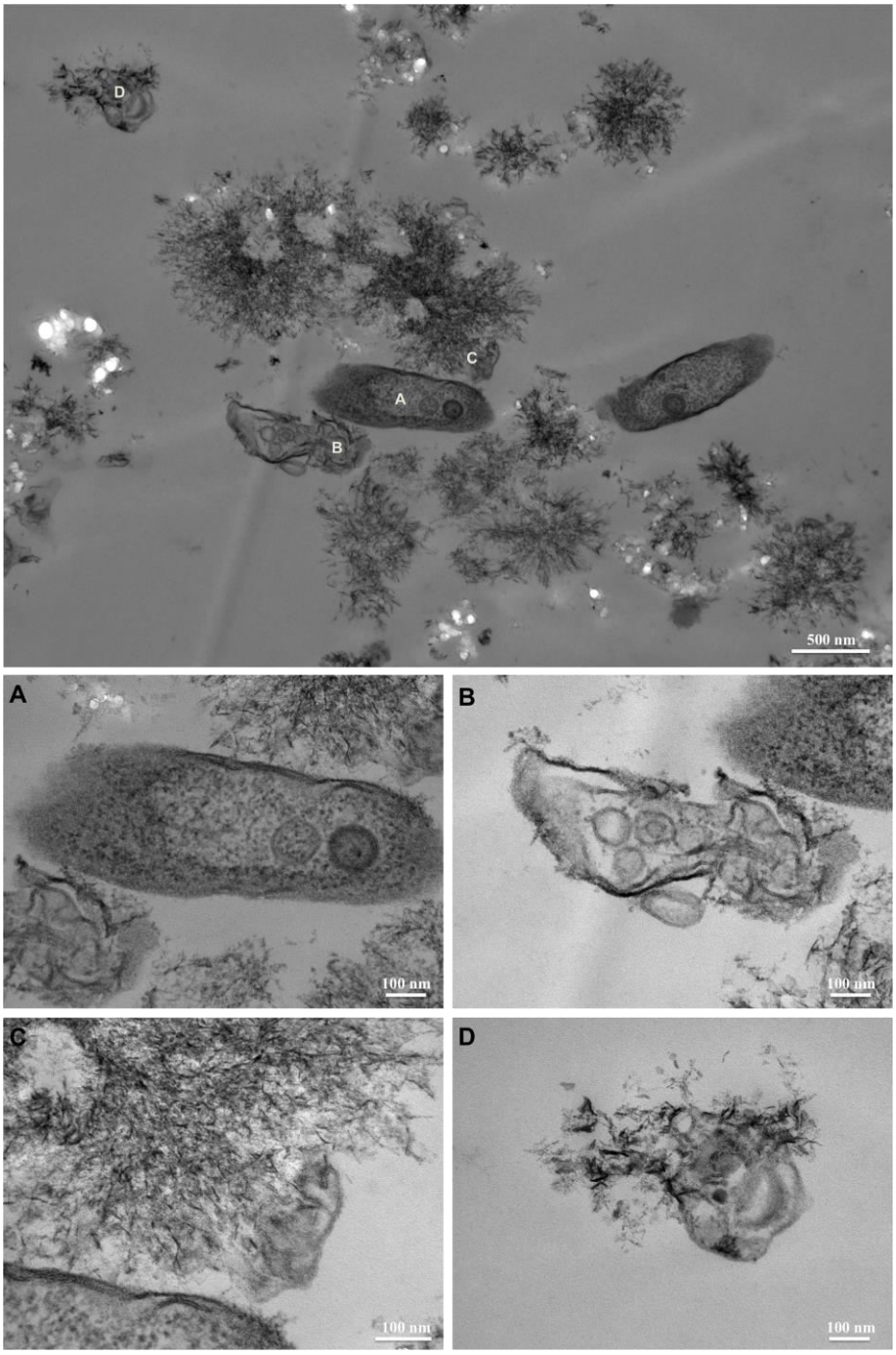

Figure 10: TEM imaging of the inoculated DSMZ medium sampled after 6 days of culture. A to D show magnification of cell lysis and spatial association of the lysed vesicle of C. hydrogenoformans and the interpreted HAP.

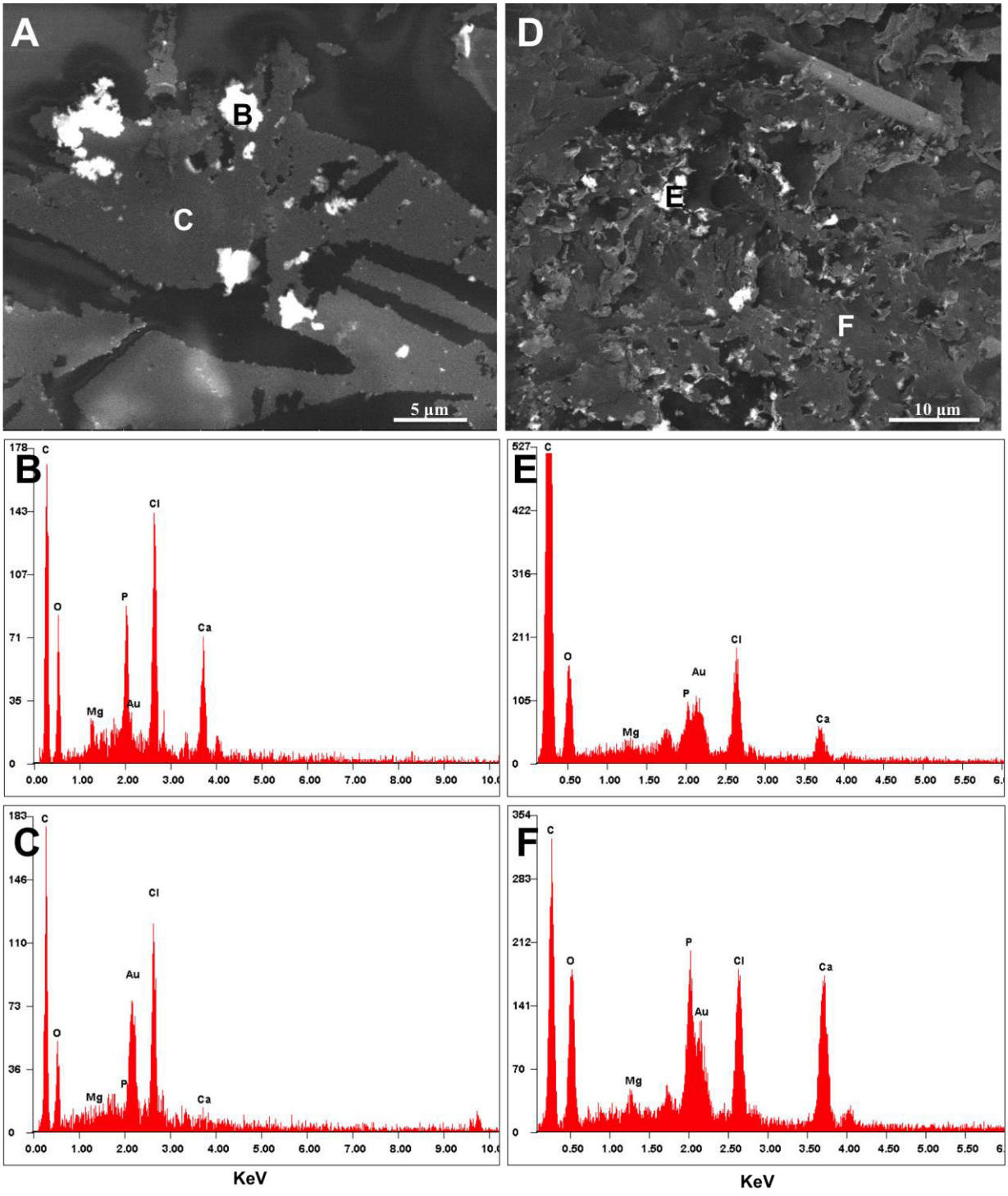
A
B
C
5 µm
D
E
F
10 µm
B
C
O
P
Cl
Ca
Mg
Au
E
C
O
Au
P
Cl
Ca
Mg
C
O
Au
Cl
P
Mg
Ca
F
C
O
P
Cl
Ca
Au
Mg
KeV
KeV

Figure 11: Backscatter electron image and EDS analysis by SEM of samples recovered after 15 days, also shown in Figure 9. (A) Sample recovered from sterile DSMZ medium, and (B) EDS analysis of its precipitate. (C) EDS analysis of the embedding epoxy matrix. (D) Sample recovered from the inoculated medium after 15 days of aging, and (E) EDS analysis of its solid precipitate, (F) EDS analysis of its embedding epoxy matrix showing that Ca and P are present.

Chapter 2: Calcium phosphate precipitation as a way to increase *Carboxydothermus hydrogenoformans* yield and CO solubility

Mathieu Haddad[a,b], Serge R. Guiot[a,b]

[a] Bioengineering Group, Energy, Mining and Environment, National Research Council Canada, 6100 Royalmount Avenue, Montreal, Canada H4P 2R2

[b] Department of Microbiology, Infectiology and Immunology, Université de Montréal, Montreal, Canada H3C 3J7

Keywords: *Carboxydothermus hydrogenoformans*, carbon monoxide; hydrogen; gas-liquid mass transfer; adsorption; CaP

Author contribution: MH designed the experiment, carried out the experimental work and interpreted the results; MH and SRG wrote the manuscript.

Article status: This article is in process of being submitted for publication to International Journal of Hydrogen Energy.

ABSTRACT

The objective of the present study was to investigate the impact of an endogenous calcium phosphate (CaP) precipitate on carbon monoxide (CO) mass transfer and hydrogen (H_2) production using *Carboxydothermus hydrogenoformans*. The endogenous precipitate formed in the DSMZ medium as formulated by the strain supplier (Deutsche Sammlung von Mikroorganismen und Zellkulturen GmbH) has been previously reported. H_2 production yield, CO specific uptake and CO mass transfer coefficient (K_La) were calculated in the DSMZ medium and in a modified growth medium deprived in calcium, phosphate and magnesium, in which no precipitation occurred. A physisorption analysis was then conducted to determine the adsorption capacity of CO on the CaP precipitate. In the DSMZ medium, the apparent K_La (0.22 ±0.005 min^{-1}) and H_2 production yield (89.11 ±6.69%) were higher than the ones obtained in the modified medium (0.19 ±0.015 min^{-1} and 82.60 ±3.62% respectively). The presence of the precipitate had no impact on *C. hydrogenoformans* CO uptake. Physisorption analysis resulted in a type III adsorption isotherm for CO with a maximal adsorption capacity of 12.6 $ml_{CO}/g_{precipitate}$. Overall, the CaP precipitate offers a novel strategy for gas-liquid mass transfer enhancement using CO hydrophobic properties.

INTRODUCTION

Today`s interest in a hydrogen (H_2) energy economy is based on many factors including reducing foreign oil imports, carbon dioxide (CO_2) emissions and global climate change, and the need to store renewable electricity supplies (Solomon & Banerjee 2006). About 50 million tons of hydrogen are generated worldwide and mainly used as a raw material in the organic chemical industry, especially for crude oil reforming and ammonia production (Roadmap 2002). 96% of the H_2 currently produced is obtained by thermocatalysis or gasification of fossil fuels (natural gas, oil and coal). Only 4% is generated from water using

electricity (B. Logan 2004). Steam reforming remains the main production process, accounting for 48% of the total hydrogen produced. It is a gasification step followed by a water gas shift reaction (WGS) (Padro & Putsche 1999) according to:

$$CH_4 + H_2O \rightarrow CO + 3H_2 \qquad (\Delta H = +206 \text{ kJ/mol})$$

$$CO + H_2O \rightarrow CO_2 + H_2 \qquad (\Delta H = -41 \text{ kJ/mol})$$

The water-gas shift reaction - widely utilized in the industry – is a process in which steam reacts with CO to produce carbon dioxide and hydrogen. Conventional processes include a 2-step transformation, in the presence of a nickel and metal catalyst, carried out at high (350-370°C) and subsequently low temperatures (200-220°C) respectively. The second step is mandatory in order to convert the CO remaining in the gaseous phase. The catalyst, used in this process, were shown to be highly intolerant to sulfur (Torres et al. 2007), especially copper-based catalysts being irreversibly poisoned by even small quantities of sulfur compounds (Newsome 1980).

A biological alternative that bypasses sulfur intolerance and is less energy intensive is possibly using thermophilic carboxydotrophic hydrogenogenic microorganisms (Henstra et al. 2007). *Carboxydothermus hydrogenoformans* is one of these microbial species that was isolated from a hot spring in Kunashir Island, Russia (Svetlichny et al. 1991). This extreme thermophilic bacillus uses CO as a sole source of carbon and energy and catalyses the WGS reaction thanks to its 5 carbon monoxide dehydrogenases (CODH) (Wu et al. 2005).

One major limitation for a biological WGS rate is the gas/liquid mass transfer, since CO is sparingly soluble in an aqueous medium (Klasson et al. 1992). *C. hydrogenoformans* being grown in the liquid phase, its WGS rate undergoes that constraint. Previous studies reported a high level of inorganic content in the original growth medium provided by the strain supplier (Henstra & Stams 2004). To prevent the clogging of membrane-based rectors, (Zhao et al. 2011) the medium was modified to inhibit the precipitation of inorganic calcium phosphate material, which resulted in lowering the cell mineral content to 13% dry weight and the calcium and phosphorus content at ca. 9% (as compared to ca. 94 and 56%, respectively, with the original medium).

In the present work, the impact of the endogenously and abiotically formed calcium phosphate precipitate on both the CO solubility and the biological WGS rates was investigated for planktonic-based systems using a pure culture C. *hydrogenoformans*.

MATERIALS AND METHODS

Culture medium for activity tests

C. hydrogenoformans (DSM 6008) was obtained from the German Collection of Microorganisms and Cell Cultures (DSMZ, Braunschweig, Germany). The strain was cultivated in shake-culture, at a 100 rpm, under strictly anaerobic conditions, at 70ºC, in a basal mineral medium, buffered with bicarbonate-phosphate. The medium contained (in g/L of demineralized water): KCl (0.33), $MgCl_2 \cdot 6H_2O$ (0.52), $CaCl_2 \cdot 2H_2O$ (0.29), NH_4Cl (0.33), KH_2PO_4 (0.33) and 10 mL of trace metals solution. The medium was boiled and then introduced anaerobically in sterilized serum bottles under N_2 air flush. After autoclaving, it was then complemented with (in $mL \cdot L^{-1}$ of medium): 5% NaHCO3 stock solution (20), 2.5% Na2S·9H2O stock solution (10), 0.5% yeast extract solution (10) and vitamin solution (1). The modified medium differed from the DSMZ one only in $MgCl_2 \cdot 6H_2O$, $CaCl_2 \cdot 2H_2O$, KH_2PO_4 and $NaHCO_3$ concentrations, which were (in $g \cdot L^{-1}$ of demineralized water): 0.102, 0.015, 0.136, 0.401, respectively (Zhao et al. 2011). The trace metals and vitamin stock solutions were prepared as described previously (Stams et al. 1993). All stock solutions were autoclaved, except the vitamin solution, which was sterilized by filtration through 0.22 µm filter membranes. The initial pH was adjusted between 6.8 and 7.0.

Activity tests

The impact of the endogenously formed abiotic precipitate on microbial activity was assessed. *C. hydrogenoformans* carboxydotrophic and hydrogenogenic activity obtained in

two different media (the DSMZ and the modified medium) were compared. Statistical analysis of the results was carried out using PRISM 4.0 (GraphPad Software, San Diego, CA). Activity assays were performed in 500-mL serum glass bottles using a final volume of 210 mL of culture media. Briefly, once inoculated with 2ml of an active culture, bottles were capped, sealed, and flushed with CO, as sole carbon source under 1 atm and placed in a rotary shaker (New Brunswick, Edison, NJ, USA), in a dark, thermostatically controlled environment (70 ±1°C) and gyrated at 150 rpm.

The biomass concentration was quantified using chemical oxygen demand (COD) measurements which were then converted to VSS using a factor of 1.37 $g_{COD}.g_{VSS}^{-1}$ based on the elemental formula of microbial biomass as $CH_{1.79}O_{0.5}N_{0.2}S_{0.005}$ (Roels 1983). The specific CO uptake or H_2 production rates, expressed as $mol_{CO}.g_{VSS}^{-1}.day^{-1}$ or $mol_{H2}.g_{VSS}^{-1}.day^{-1}$, respectively, were obtained by reporting the rate of CO consumed or H_2 produced (mole per day) to the VSS-based biomass as estimated in the bottle. The hydrogen yield (Y_{H2}) was expressed as a percentage of the H_2 gas produced per CO consumed (mole per mole).

CO volumetric gas-liquid mass transfer coefficient (K_La)

The CO volumetric gas-liquid mass transfer coefficient (K_La) was measured in batch tests and abiotic conditions for each medium. Tests were conducted in 500 mL serum bottles filled with 200 mL of complemented medium at 70°C and agitated at 150 rpm. The CO contained in the gas and liquid phases of each bottle was quantified immediately after flushing (CO_i) and at equilibrium (CO_f). The recovery percentage ($100*CO_f/CO_i$) was calculated for each condition. The dissolved CO concentration was calculated using Henry's law and the CO partial pressure in the headspace after equilibrium was reached at 70ºC as described elsewhere (Zhao et al. 2013).

Assuming that the dissolved CO concentration at the interface is at equilibrium with the CO concentration in the gaseous phase, the k_La was determined according to Munasinghe (Munasinghe & Khanal 2010). Briefly the slope of the following equation, which represents the k_La, was determined according to: $\ln((C_i-C_0)/(C_i-C)) = k_La*t$

Where C_0 is the initial CO concentration in the liquid phase ($mg.L^{-1}$), C is the CO concentration in the liquid phase ($mg.L^{-1}$) at any given time t (s) and C_i is the saturated CO concentration ($mg.L^{-1}$). The kLa values obtained with each medium were compared to evaluate the impact of the abiotic precipitate on CO mass transfer.

Analytical methods

The COD was determined according to Standard Methods using a DRB200 spectrophotometer (Hach Company, Loveland, CO) (Eaton et al. 2005).

The gas composition (H_2, CO, CO_2) was measured by injecting 300 µL of gas using a gas-tight syringe (model 1750, Hamilton, Reno, NV) taken from the bottle headspace after equilibrium at 70°C was reached. The gas was injected into an HP 6890 gas chromatograph (Hewlett Packard, Palo Alto, CA) equipped with a thermal conductivity detector (TCD) and a 11 m x 3.2 mm 60/80 mesh Chromosorb 102 packed column (Supelco, Bellafonte, PA). The column temperature was held at 60ºC for 7 min and increased to 225ºC at a rate of 60ºC per min. Argon was used as the carrier gas. The injector and detector were maintained at 125°C and 150°C respectively.

In order to test the endogenously produced precipitate for CO adsorption, physisorption analysis was conducted on a dried sample. Carbon monoxide adsorption–desorption isotherms were obtained at 77K using volumetric analysis Micromeritics Flowsorb ASAP 2020 (Micromeritics, Norcross, GA, USA), over the range 0 to 1 bar according to Singh (SING et al. 1985).

RESULTS

The CO apparent mass transfer coefficient (K_La) was measured in the DSMZ medium and compared to the one obtained with a modified medium, in which no precipitation occurs as formulated in the literature (Zhao et al. 2011). A T-test analysis of the obtained K_La in two

series of triplicates showed with a 95% confidence that this difference between the two media was significant (p = 0,025). When in presence of the precipitate, the apparent K_La reached 0.22 ±0.005 min^{-1} whereas in the modified medium it was of 0.19 ±0.015 min^{-1} (p = 0,025). This small difference was also supported by the fact that, at equilibrium, only 92,35 ±3,04% of the CO was recovered in the DSMZ medium. Full recovery of the CO injected was obtained in the modified medium (p = 0,023), leading to the possibility of an adsorption mechanism of CO on the precipitate.

Since no absorption or chemisorption phenomenon (covalent bonding) was possible between CO and the calcium phosphate precipitate, a physisorption analysis was conducted to confirm the adsorption hypothesis. Physisorption is an adsorption system in which the attractive forces between the adatoms and the surface are relatively non specific van der Waals or dispersion forces (Oura 2010). Results revealed that physisorption takes place as CO showed a type III adsorption isotherm and H3 hysteresis (desorption) in the presence of the amorphous precipitate (Figure 1). The maximal adsorption capacity was of 12.6 $ml_{CO}/g_{precipitate}$.

Carboxydotrophic and hydrogenogenic activities of *C. hydrogenoformans* were measured in both media. Results showed a statistically significant decrease in biological activity with biomass concentration (Figure 2, 3), confirming the finding of Zhao (Zhao et al. 2011) who concluded that consumption rates observed for biomass densities above 8 - 9 $mg_{VSS}.L^{-1}$ were limited by the volumetric gas–liquid mass transfer rate. Hence, comparison of biological activities in both media was carried on bottles with biomass concentration over 9 $mg_{VSS}.L^{-1}$. Results showed no significant impact ($p > 0.05$) of the medium on carboxydrotrophic activities, in agreement with the literature (Zhao et al. 2011).

Contrary to biological activity, hydrogen production yield was not impacted by biomass concentration regardless of the medium used ($p > 0.05$) (Figure 2, 3). A T-test analysis was conducted on the two media to establish whether or not there was a significant difference in the hydrogen production yields. Results showed that the two series of 12 independent bottles displayed, with a 95% confidence, a significant difference in yields (p =

0.006). Hydrogen production yield was lower in the modified medium (82.60 ±3.62%) compared to the one obtained in the DSMZ medium (89.11 ±6.69%).

DISCUSSION

The impact of the abiotic precipitate on CO mass transfer and *C. hydrogenoformans* carboxydotrophic activity and yield was assessed.

As described in the literature (Sing et al. 1985), a type III adsorption isotherm is characterized by weak adsorbate-adsorbent interactions. In these systems, gas adsorbs in thick layers prior to or without first forming a single monolayer. Type III isotherm arises from nonporous or macroporous surfaces (pore of internal width greater than 50 nm) (Kaneko 1994). Hysteresis describes desorption and is associated to specific pore structures. Isotherms with type H3 hysteresis are associated to non-rigid aggregates of plate-like particles or assemblages of slit-shaped pores (Thommes 2010). According to the results obtained, it appears that the presence of the precipitate offers an adsorption surface that circumvents the problem of CO low solubility (Ungerman & Heindel 2007). CO adsorption seems to enhance its apparent K_La as it allows more gas molecule in the liquid phase. Also, CO desorption showed similar profile and rate as the adsorption, thus demonstrating its potential availability for the microorganisms.

Even though CO adsorption on the calcium phosphate precipitate does not seem to increase *C. hydrogenoformans* activity as hypothesized, the DSMZ medium showed a significant effect on hydrogen production yield. Never the less, CO adsorption on the precipitate does not explain the difference in H_2 production yield between both media.

As reviewed by Norris (Norris et al. 1996), the calcium influx in bacteria is mainly based on passive transport mechanisms and comprises antiporters ($Ca^{2+}/2H^+$, $Ca^{2+}/2Na^+$). Calcium efflux is based on active transport (ATP-dependent) that conveys calcium against an electrochemical gradient at the expense of energy (ATP). Hence, a high concentration of extracellular calcium concentration creates a stressful environment for bacteria as passive

calcium influx will lead to intracellular calcium build-up and excessive proton expulsion. In order to restore suitable intracellular calcium concentration and compensate for proton loss, calcium ions will be actively exported at the expense of ATP (Hammes & Verstraete 2002). Accordingly, *C. hydrogenoformans* would need more energy when grown in the DSMZ medium, which comprises a high concentration of calcium ions, to regulate calcium flows.

A strategy would thus be to redirect its substrate (carbon monoxide) towards the production of ATP, needed for active calcium transportation instead of biomass growth. This could be done by overexpressing the CODH I, which drives the WGS reaction (Wu et al. 2005), or repressing the CODH III, which fixes CO using the acetyl-CoA pathway. This strategy would lead to a lower biomass production as less carbon is fixed while maximizing its energy yield, hence the higher hydrogen production yield observed with the DSMZ medium.

Techtmann (Techtmann et al. 2011) showed that CODH I and III are differentially regulated in response to CO availability in *C. hydrogenoformans*. When the intracellular concentration of CO > 6 μM, hydrogen production and acetyl CoA production are fully induced. Whereas under limiting CO conditions (CO < 2 μM), hydrogen production and energy conservation are limited in favour of acetyl CoA production and carbon fixation. We hereby emit the hypothesis that CODH enzymes might be also be regulated by the cell energy needs for calcium homeostasis.

CONCLUSION

The CO mass transfer limitation, due to the low gas solubility, is one of the major constrains for biological WGS reaction. The present work points to a new way, based on adsorption properties, to enhance CO solubility and availability for efficient utilization by bacteria.

Even though the DSMZ medium is not recommended for membrane-based rectors (Zhao et al. 2011), it can be suitable for any other type of reactor that would not be clogged by

the produced inorganic material. The obtained results demonstrate that the DSMZ medium displayed a positive impact on hydrogen production as its yield was enhanced by 12.40% compared to the one obtained in the modified medium.

An interesting finding resides in the fact that the present work offers a new strategy for gas-liquid mass transfer enhancement. Known techniques for increasing gas absorption in the liquid phase reside either in specific reactor design and configuration (Munasinghe & Khanal 2010 ; Merchuk & Gluz 2002a) or in headspace pressurization (Yang & Wang 1992). Here, we used the highly hydrophobic property of CO to trigger its adsorption on the calcium phosphate precipitate that is endogenously formed in the medium. Hence, this technique could be applied to any added material in the medium that would provide an adsorption surface for CO and enhance gas to liquid mass transfer.

ACKNOWLEDGEMENTS

The authors wish to thank Ruxandra Cimpoia and Punita Mehta for their assistance and discussions. One of the authors (M.H.) was supported by the Natural Sciences and Engineering Research Council of Canada (grant 185778-2009).

REFERENCES

Eaton, A., Clesceri, L., Rice, E., & Greenberg, A. (2005). *Standard methods for the examination of water and wastewater* (21st ed.). Washington, D.C.: American Public Health Association, American Water Works Association, Water Environment Federation.

Hammes, F., & Verstraete, W. (2002). Key roles of pH and calcium metabolism in microbial carbonate precipitation. *Reviews in Environmental Science and Biotechnology*, *1*(1), 3–7. doi:10.1023/A:1015135629155

Henstra, A. M., Sipma, J., Rinzema, A., & Stams, A. J. M. (2007). Microbiology of synthesis gas fermentation for biofuel production. *Current Opinion in Biotechnology*, *18*(3), 200–6. doi:10.1016/j.copbio.2007.03.008

Henstra, A. M., & Stams, A. J. M. (2004). Novel physiological features of *Carboxydothermus hydrogenoformans* and Thermoterrabacterium ferrireducens. *Applied and environmental microbiology*, *70*(12), 7236–40. doi:10.1128/AEM.70.12.7236-7240.2004

Kaneko, K. (1994). Determination of pore size and pore size distribution: 1. Adsorbents and catalysts. *Journal of Membrane Science*, *96*(1–2), 59–89. doi:10.1016/0376-7388(94)00126-X

Klasson, K. T., Ackerson, C. M. D., Clausen, E. C., & Gaddy, J. L. (1992). Biological conversion of synthesis gas into fuels. *International Journal of Hydrogen Energy*, *17*(4), 281–288.

Logan, B. (2004). Peer reviewed: extracting hydrogen and electricity from renewable resources. *Environmental Science & Technology*, *38*(9), 160A – 167A.

Merchuk, J. C., & Gluz, M. (2002). Bioreactors, Air-lift Reactors. In *Encyclopedia of Bioprocess Technology*. John Wiley & Sons, Inc. doi:10.1002/0471250589.ebt029

Munasinghe, P. C., & Khanal, S. K. (2010). Syngas fermentation to biofuel: evaluation of carbon monoxide mass transfer coefficient (kLa) in different reactor configurations. *Biotechnology progress*, *26*(6), 1616–21. doi:10.1002/btpr.473

Newsome, D. S. (1980). The Water-Gas Shift Reaction. *Catalysis Reviews*, *21*(2), 275–318. doi:10.1080/03602458008067535

Norris, V., Grant, S., Freestone, P., Canvin, J., Sheikh, F. N., Toth, I., … Norman, R. I. (1996). Calcium signalling in bacteria. *Journal of Bacteriology*, *178*(13), 3677–3682.

Oura, K. et al. (2010). *Surface Science: An Introduction* (p. 452). Springer.

Padro, C. E. G., & Putsche, V. (1999). Survey of the Economics of Hydrogen Technologies. *National Renewable Energy Laboratory*, (September).

Roadmap, E. (2002). National Hydrogen Energy Roadmap. *(US Department of Energy (DOE), 2002. National Hydrogen Energy Roadmap. Washington, DC.)*, (November).

Roels, J. A. (1983). *Energetics and kinetics in biotechnology*. Elsevier Biomedical Press.

Sing, K. S. W., Everett, D. H., Haul, R. A. W., Moscou, L., Pierotti, R. A., Rouquerol, J., & Siemieniewska, T. (1985). Reporting physisorption data for gas/solid systems, with special reference to the determination of surface area and porosity. *Pure and Applied Chemistry*, *57*(4), 603–619.

Solomon, B. D., & Banerjee, A. (2006). A global survey of hydrogen energy research, development and policy. *Energy Policy*, *34*(7), 781–792. doi:10.1016/j.enpol.2004.08.007

Stams, A. J., Van Dijk, J. B., Dijkema, C., & Plugge, C. M. (1993). Growth of syntrophic propionate-oxidizing bacteria with fumarate in the absence of methanogenic bacteria. *Applied and Environmental Microbiology*, *59*(4), 1114–1119.

Svetlichny, V. A., Sokolova, T. G., Gerhardt, M., Kostrikina, N. A., & Zavarzin, G. A. (1991). Anaerobic Extremely Thermophilic Carboxydotrophic Bacteria in Hydrotherms of Kuril Islands Light Microscopy, 1–10.

Techtmann, S., Colman, A., & Murphy, M. (2011). Regulation of multiple carbon monoxide consumption pathways in anaerobic bacteria. *Frontiers in Microbiology*, *2*(July), 12. doi:10.3389/fmicb.2011.00147

Thommes, M. (2010). Physical Adsorption Characterization of Nanoporous Materials. *Chemie Ingenieur Technik*, *82*(7), 1059–1073. doi:10.1002/cite.201000064

Torres, W., Pansare, S. S., & Goodwin, J. G. (2007). Hot Gas Removal of Tars, Ammonia, and Hydrogen Sulfide from Biomass Gasification Gas. *Catalysis Reviews*, *49*(4), 407–456. doi:10.1080/01614940701375134

Ungerman, A. J., & Heindel, T. J. (2007). Carbon Monoxide Mass Transfer for Syngas Fermentation in a Stirred Tank Reactor with Dual Impeller Configurations. *Biotechnology Progress*, *23*(3), 613–620. doi:10.1021/bp060311z

Wu, M., Ren, Q., Durkin, a S., Daugherty, S. C., Brinkac, L. M., Dodson, R. J., … Eisen, J. a. (2005). Life in hot carbon monoxide: the complete genome sequence of *Carboxydothermus hydrogenoformans* Z-2901. *PLoS Genetics*, *1*(5), e65. doi:10.1371/journal.pgen.0010065

Yang, J. D., & Wang, N. S. (1992). Oxygen mass transfer enhancement via fermentor headspace pressurization. *Biotechnology Progress*, *8*(3), 244–251. doi:10.1021/bp00015a010

Zhao, Y., Cimpoia, R., Liu, Z., & Guiot, S. (2011a). Kinetics of CO conversion into H_2 by *Carboxydothermus hydrogenoformans*. *Applied Microbiology and Biotechnology*, *91*(6), 1677–1684. doi:10.1007/s00253-011-3509-7

Zhao, Y., Cimpoia, R., Liu, Z., & Guiot, S. R. (2011b). Orthogonal optimization of *Carboxydothermus hydrogenoformans* culture medium for hydrogen production from carbon monoxide by biological water-gas shift reaction. *International Journal of Hydrogen Energy*, *36*(17), 10655–10665. doi:10.1016/j.ijhydene.2011.05.134

Zhao, Y., Haddad, M., Cimpoia, R., Liu, Z., & Guiot, S. R. (2013). Performance of a *Carboxydothermus hydrogenoformans*-immobilizing membrane reactor for syngas upgrading into hydrogen. *International Journal of Hydrogen Energy*, *38*(5), 2167 – 2175. doi:http://dx.doi.org/10.1016/j.ijhydene.2012.11.038

FIGURES

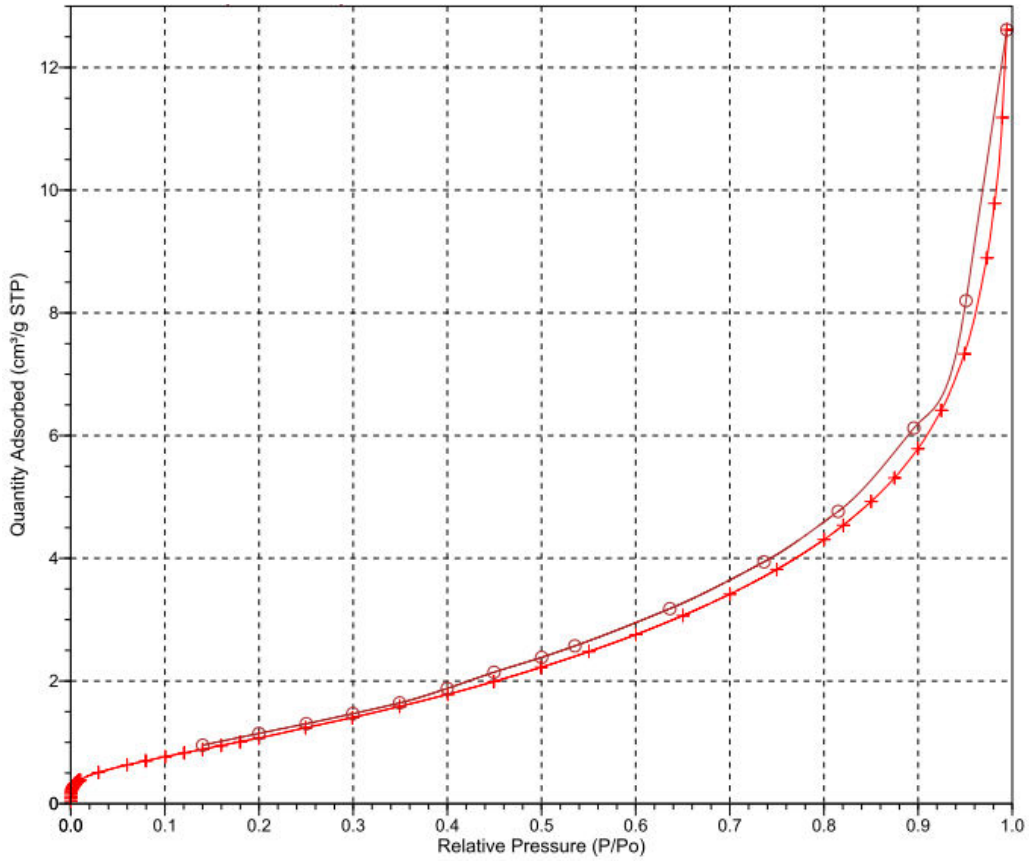

Figure 1: Adsorption of CO at 77K on the endogenously produced calcium phosphate in the DSMZ medium. (Cross) CO adsorption; (Circles) CO desorption.

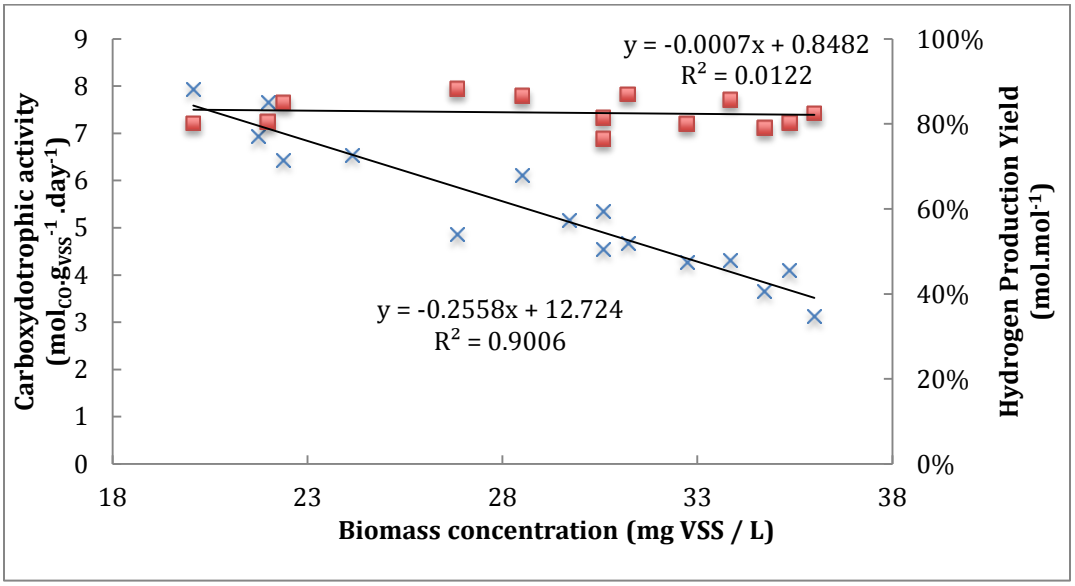

Figure 2: Carboxydrotrophic activity and hydrogen production yield obtained with different *C. hydrogenoformans* concentrations in the modified medium. (Cross) carboxydotrpohic activity; (Squares) Yield.

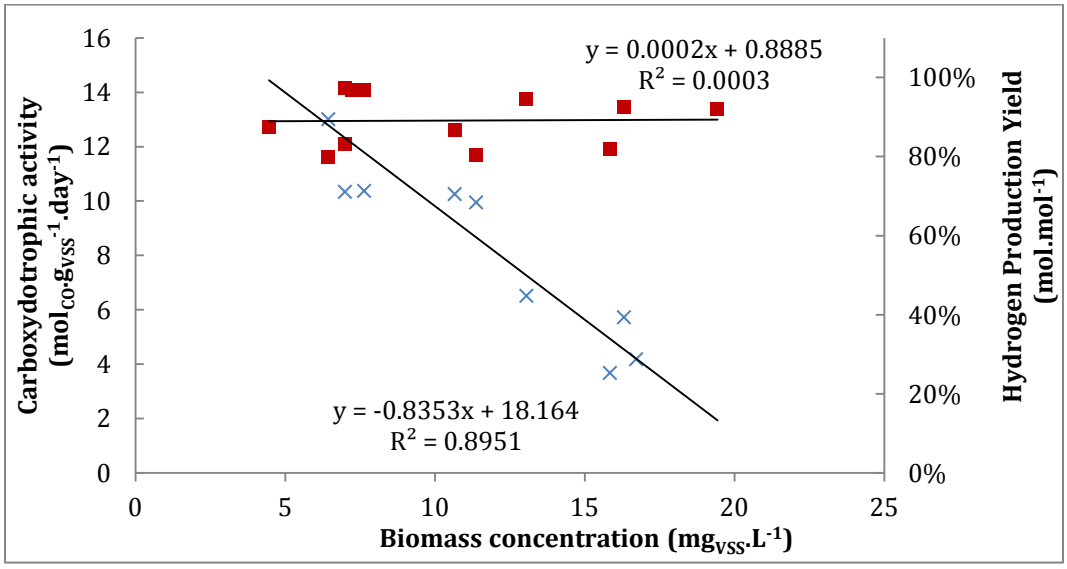

Figure 3: Carboxydrotrophic activity and hydrogen production yield obtained with different *C. hydrogenoformans* concentrations in the DSMZ medium. (Cross) carboxydotrpohic activity; (Squares) Yield.

Chapter 3: Performance of *Carboxydothermus hydrogenoformans* in a gas-lift reactor for syngas upgrading into hydrogen

Mathieu Haddad[a,b], Ruxandra Cimpoia[a], Serge R. Guiot[a,b]

[a] Bioengineering Group, Energy, Mining and Environment, National Research Council Canada, 6100 Royalmount Avenue, Montreal, Canada H4P 2R2

[b] Department of Microbiology, Infectiology and Immunology, Université de Montréal, Montreal, Canada H3C 3J7

Author contribution: MH designed the experiment, carried out the experimental work and interpreted the results; MH and RC interpreted the results; MH and SRG wrote the manuscript.

Article status: This article was submitted for publication to International Journal of Hydrogen Energy on 19 October 2013, accepted 2 December 2013 and published 14 February 2014.

Haddad, M., Cimpoia, R., & Guiot, S. R. (2014). Performance of *Carboxydothermus hydrogenoformans* in a gas-lift reactor for syngas upgrading into hydrogen. *International Journal of Hydrogen Energy*, *39*(6), 2543–2548. doi:10.1016/j.ijhydene.2013.12.022

Conference Presentation: This work was presented at two conferences: Bioenergy Australia 2013 conference (Hunter Valley, NSW, Australia), where it was awarded best poster presentation, and oral presentation at the Pacific Rim Summit on Industrial Biotechnology and Bioenergy 2013 (San Diego, CA, USA).

Keywords: *Carboxydothermus hydrogenoformans*, carbon monoxide; hydrogen; gas-lift reactor; continuous; gas-liquid mass transfer

ABSTRACT

The conversion of carbon monoxide (CO) into hydrogen (H_2) by a *Carboxydothermus hydrogenoformans* pure culture was investigated and optimized in a 35 L gas-lift reactor. The reactor was operated with a continuous supply of gas for 3 months. Reactor performance was evaluated under various operational conditions, such as gas recirculation rates (0.3 and 1.5 $L \cdot min^{-1}$), CO feeding rates (from 0.05 to 0.46 $mol \cdot L^{-1}_{reactor} \cdot day^{-1}$) and bacto-peptone addition to the medium. Overall, the H_2 yields were constant at 95±1% and 82±1% ($mol_{H2} \cdot mol^{-1}_{CO}$) with growth supported by peptone and unsupported respectively, regardless of the operational conditions tested. At the highest biomass density, a maximum CO conversion activity of 0.17 $mol_{CO} \cdot L^{-1}_{reactor} \cdot day^{-1}$ or 3.79 $L_{CO} \cdot L^{-1}_{reactor} \cdot day^{-1}$ was achieved. The ratio of gas recirculation over CO feed flow rates (Q_R:Q_{in}) was the major parameter that impacted both biological activity and volumetric gas-liquid mass transfer. The CO conversion performance of the gas lift reactor was kinetically limited over a Q_R:Q_{in} ratio of 40, and mass transfer limited below that ratio, resulting in a maximum conversion efficiency of 90.4±0.3% and a biological activity of 2.7±0.4 $mol_{CO} \cdot g^{-1}_{VSS} \cdot day^{-1}$. Overall, the CO conversion performance in the gas-lift reactor was limited by a low cell density, typical of *C. hydrogenoformans* planktonic growth. This limitation was found to be the most restrictive factor for higher CO loading rates.

INTRODUCTION

The water-gas shift (WGS) reaction, widely utilized in industry, is used to convert carbon monoxide (CO) to carbon dioxide (CO_2) and hydrogen (H_2) through a reaction with water (H_2O) according to: $CO + H_2O \rightarrow CO_2 + H_2$ (Newsome 1980). This process is achieved using a metallic catalyst in a heterogeneous gas-phase reaction with CO and steam. This reaction is the basis for most of the industrial H_2 produced in the world from methane (CH_4) in natural gas through steam-methane reforming (B. E. Logan 2004).

The WGS reaction has so far been reserved for large-scale gasification plants and requires high capital and operational expenditures. Hence, smaller scale plants that process low-grade materials, would not have access to such technology. The only possible outcome with the synthesis gas (syngas) produced and which generally has a poor calorific value, is to generate heat or at best, electricity. In order to offer small plants access to the WGS reaction and to a higher range of products from their syngas, an alternative to the expensive and energy-intensive established catalyst-based WGS is here considered, such as extreme-thermophilic microbial processes carried out by hydrogenogens (Henstra et al. 2007). Indeed, despite its deleterious effects on many species, CO is the basis for many food chains, especially in hydrothermal environments such as the deep sea, hot springs, and volcanoes (Bonch-Osmolovskaya et al. 1999). Among these microorganisms, is the obligate anaerobic *Carboxydothermus hydrogenoformans*. This extreme thermophilic bacillus was first isolated from a hot spring in Kunashir Island, Russia (Svetlichny et al. 1991). Due to its five CO dehydrogenases (CODH) and its autotrophy, *C. hydrogenoformans* can survive efficiently on CO as its sole carbon and energy source by catalyzing the WGS reaction (Wu et al. 2005). Hence, this makes it an excellent candidate for possible industrial biological WGS reactions.

Previous use of *C. hydrogenoformans* in a Hollow Fiber Membrane Reactor (HFMBR) for syngas upgrading in hydrogen showed that despite the steady performances and a bioactivity potential of 5 $mol_{CO} \cdot L_{reactor(rxr)}^{-1} \cdot day^{-1}$, membrane fouling and aging affected the membrane permeability as well as CO transfer making this kind of reactor of limiting interest for long run use and higher CO feeding rates (Zhao et al. 2013).

The gas-lift bioreactor represents an alternative solution to the HFMBR. In a gas-lift reactor, the medium is pneumatically agitated by a stream of gas that is fed at the bottom of the reactor through a sparkler. The liquid is conveyed in an internal tube, which creates circulation channels. This allows a constant agitation without the need of moving parts, hence easy maintenance as well as mass transfer enhancement between the gas and the liquid phase (Merchuk & Gluz 2002b). Also, when studying different reactor configurations, Munasinghe

and Khanal (Munasinghe & Khanal 2010) showed that the highest mass transfer coefficient (k_La) for CO was obtained in a air-lift reactor combined with a 20 µm bubble diffuser.

The objectives of this study were to evaluate at bench scale the efficiency and technology-based limitations of a gas-lift reactor inoculated with a pure strain of *C. hydrogenoformans* for continuous conversion of carbon monoxide into hydrogen gas.

MATERIALS AND METHODS

Bacterial strain and growth conditions

Carboxydothermus hydrogenoformans (DSM 6008) was obtained from the German Collection of Microorganisms and Cell Cultures (DSMZ, Braunschweig, Germany). The strain was cultivated in shake-culture at 100 rpm under strictly anaerobic conditions at 70ºC in a basal mineral medium buffered with a bicarbonate-phosphate buffer. The medium as formulated by Zhao et al (Zhao et al. 2011) contained (in $mg \cdot L^{-1}$ of demineralized water): KCl (330), $MgCl_2 \cdot 6H_2O$ (102), $CaCl_2 \cdot 2H_2O$ (15), NH_4Cl (330), KH_2PO_4 (136), $NaHCO_3$ (420), yeast extract (50). The medium was supplemented with 10 $ml \cdot L^{-1}$ trace metals solution and 10 $mL \cdot L^{-1}$ of vitamins solution prepared as described previously (Stams et al. 1993). All stock solutions were autoclaved, except for the vitamin solution, which was sterilized by filtration through 0.22 µm filter membranes. The initial pH was adjusted between 6.8 and 7.0. During phase I (unsupported growth), *C. hydrogenoformans* was grown on CO only whereas in phase II (supported growth), Bacto-peptone (Becton Dickinson, MD) was injected in the growth medium at a concentration of 1.0 $g \cdot L^{-1}$.

Reactor set-up and operation

The closed-loop gas lift reactor (internal diameter 0.2 m; height 1.13 m; working liquid volume 30 L; headspace 5 L) used in this study enclosed an internal draft-tube of 0.6 m height and 0.1 m diameter (Fig. 1). The reactor temperature was controlled by two probes (DP-41,

Omega Engineering Inc, Stamford, CT) placed in the upper and lower levels and maintained at 70ºC using an electric heating jacket covering the reactor and linked by a custom made controller to the temperature probes. The pH was measured (electrode 405-DPAS-SC-K8S, Mettler Toledo GmbH, Urdorf, CH), read on a pH controller (PHP-194, Omega Engineering Inc, Stamford, CT) and controlled manually between 6.8 and 7.2 using 1M NaOH or 1M HCl.

The CO content of the feeding gas was composed of 100% CO (Praxair Canada Inc, Mississauga, ON, CA). The gas was bubbled at the center of the reactor bottom. The gas flow rates were measured and controlled by thermal mass flow meters (M100B, M10MB, 247D, MKS, Wilmington, MA). The gas exited the reactor through a pressure valve (TM Swagelok, Solon, OH) to maintain the reactor headspace at 1.5 atm (manometer 0-20PSI, US Gauge, Ira Township, MI). The gas phase was recycled with a gas pump (model UN726.1.2 FTP, KNF Neuberger Inc., Trenton, NJ) at 0.3 and 1.5 $L \cdot min^{-1}$. In the gas recycle line, a 0.5 m^2 condenser (Chemap, Volketswil, Switzerland) was placed before the exit valve and was kept at 0°C using a 50/50 (volume) water and propylene glycol mix that was cooled using a thermostated bath (RM6; MGW Lauda, Konigshofen, Germany). Prior to inoculation, the growth medium was bubbled with N_2 gas to establish anaerobic conditions. A hundred milliliters of liquid were sampled daily from the center of the reactor and analyzed for its dissolved CO, chemical oxygen demand (COD), volatile fatty acid (VFA) and alcohol content using the method presented below. A hundred milliliters of fresh sterile medium was injected back in the reactor.

Analytical methods

To quantify the biomass concentration, two 35 mL aliquots of liquid suspension were sampled from the reactor and centrifuged at 10000 rpm for 10 min at 4°C. The pellets were resuspended in 2 mL of distilled water and the solid concentration was quantified using chemical oxygen demand (COD) measurements determined according to Standard Methods (Eaton et al. 2005). The COD values were then converted to VSS using a factor of 1.37

$g_{COD} \cdot g_{VSS}^{-1}$ based on the elemental formula of anaerobic bacteria as $CH_{1.79}O_{0.5}N_{0.2}S_{0.005}$ (Roels 1983).

Measurements of H_2, N_2, O_2, CO, CH_4 and CO_2 were made on an Agilent 7820 gas chromatograph (Wilmington, DE) coupled to a thermal conductivity detector (TCD). Three hundred µL of headspace gas was sampled and injected on a 2 m x 2 mm I.D. ShinCarbon ST packed column from RESTEK. The column was heated at 40°C for 5 minutes then raised to 200°C at a rate of 20°C·min^{-1} maintained for 2 minutes. Argon was used as carrier gas at a flow rate of 10 mL·min^{-1}. The injector and detector were maintained at 125°C and 250°C respectively.

VFAs (i.e. acetic, propionic and butyric acids) were measured on an Agilent 6890 gas chromatograph (Wilmington, DE) equipped with a flame ionization detector (FID) on 0.2 µL samples diluted 1:1 (vol./vol.) with an internal standard of iso-butyric acid in 6% formic acid, directly injected on a glass column of 1 m x 2 mm Carbopack C (60-80 mesh) coated with 0.3 % Carbowax 20M and 0.1% H_3PO_4. The column was held at 130 °C for 4 min. Helium was the carrier gas fed at a rate of 20 mL·min^{-1}. The injector and the detector were both maintained at 200°C.

To measure the solvents produced (methanol, ethanol, acetone, 2-propanol, tert-butanol, n-propanol, sec-butanol, n-butanol) 100 µL of liquid was transferred into a vial that had 20 mL of headspace and was closed with a crimped Teflon-coated septum. The vial was heated at 80ºC for 2 min, then 1000 µL of headspace gas were injected on a DB-ACL2 capillary column of 30 m x 530 m x 2 µm using a Combipal autosampler (CTC Analytics AG, Zwingen, Swizerland). The column was held at 40ºC for 10 min. Helium was the carrier gas at a head pressure of 5 psi. The injector and the detector were maintained at 200ºC and 250ºC, respectively.

Dissolved carbon monoxide analysis in culture medium

An approximate 8 mL volume of liquid culture medium to be tested was transferred with a gas-tight syringe into a 20 mL gas-tight glass vial, which was pre-tared, both empty and

fully filled with water, including stopper and cap and flushed with N_2. Once the sample transferred, the vial was weighted. The difference between this weight, empty tare and filled tare determined accurately the liquid sample volume and the headspace volume, respectively. The vials were then placed in a 100°C thermostatic water bath during 30 min so that all dissolved CO (dCO) was released in the headspace. Afterwards the CO content in the headspace was determined by GC, allowing for the calculation of the dCO concentration (Zhao et al. 2013).

Gas-liquid mass transfer rate of the abiotic gas-lift reactor

The volumetric gas-liquid mass transfer coefficient (k_La) of the gas-lift reactor was determined by dynamic method at 70° C under abiotic conditions, as described elsewhere (Zhao et al. 2013). The reactor was fed with CO at a flow rate (Q_{in}) ranging from 24 to 110 $mL \cdot min^{-1}$. The headspace was recirculated at flow rates (Q_R) of 300 and 1500 $mL \cdot min^{-1}$. Assuming that the dCO concentration at the interface is in equilibrium with the CO concentration in the gaseous phase, k_La in the previously described conditions was determined according to Munasinghe and Khanal (Munasinghe & Khanal 2010). The k_La values obtained with each medium were compared to evaluate the impact of the abiotic precipitate on the CO mass transfer.

RESULTS

CO removal performance of the gas-lift reactor

Once inoculated with a pure culture of *C. hydrogenoformans*, the gas lift reactor was operated under anaerobic conditions with a continuous supply of CO and a constant gas recirculation flow rate (2160 $L \cdot day^{-1}$). During the unsupported growth phase (Table 1), the CO feeding rate (Q_{CO}) was increased from 0.05 to 0.13 $mol.L_{rxr}^{-1} \cdot day^{-1}$. The average H_2 production yield (Y_{H2}) for this phase was around 80 ± 4 % whereas a maximum of 79 ± 0.5% efficiency

of CO conversion (E_{CO}) was obtained at Q_{CO} of 0.05 $mol \cdot L_{rxr}^{-1} \cdot day^{-1}$. This value also corresponded to the maximal specific activity reached during this phase (2.30 ± 0.4 $mol_{CO} \cdot g_{VSS}^{-1} \cdot d^{-1}$). Augmenting the Q_{CO} to 0.13 $mol \cdot L_{rxr}^{-1} \cdot day^{-1}$ resulted in a sharp decrease in the volumetric activity and ultimately in a general failure, with the dCO concentration reaching 0.74 $mmol \cdot L^{-1}$. Here the E_{CO} was clearly biologically limited since the *C. hydrogenoformans* concentration was not sufficient to handle such a substrate load.

In the next phase (supported growth), a solution of peptone was injected into the reactor to reach a final concentration of 1.0 $g \cdot L^{-1}$. The CO feeding conditions were reset to the same rate as in phase I: Q_{CO} of 0.05 $mol.L_{rxr}^{-1}.day^{-1}$. This resulted in volumetric rates of CO removal of 90.4 ± 0.3 % and 82.8 ± 1.2 % for Q_{CO} of 0.05 and 0.08 $mol \cdot L_{rxr}^{-1}.day^{-1}$ respectively. The obtained E_{CO} values were significantly higher than the ones obtained during unsupported growth whereas the specific activity values for CO consumption remained similar for Q_{CO} below 0.10 $mol_{CO} \cdot g_{VSS}^{-1} \cdot d^{-1}$. Also, the CO feeding rates were increased up to 0.30 $mol \cdot L_{rxr}^{-1} \cdot day^{-1}$ without leading to a sharp decrease of biological activity. The CO overload occurred at a Q_{CO} of 0.46 $mol \cdot L_{rxr}^{-1} \cdot day^{-1}$ leading to a dCO of 0.49 $mol \cdot L^{-1}$ and a failure of the biological reaction. The average Y_{H2} for phase II remained relatively constant through all runs at 95.6 ± 1.3 %.

When plotting the *C. hydrogenoformans* specific CO uptake and E_{CO} against the gas recirculation to feed volumetric flow rates ratio (Q_R:Q_{in} ratio), the results showed a logarithmic correlation for both parameters (Fig. 2). This presumably indicates that a Q_R:Q_{in} ratio of 40 is the boundary domain between mass transfer (below this point) and biokinetic (over this point) limitations. Indeed, over a Q_R:Q_{in} ratio of 40, both specific CO consumption and E_{CO} reach a plateau regardless of the Q_R:Q_{in} ratio increase; whereas under that Q_R:Q_{in} ratio of 40, a sharp decrease can be noticed for both parameters, clearly indicating a gas-liquid mass transfer limitation of the CO. Another indication of limitation by mass transfer was the dCO concentrations which were decreasing under a Q_R:Q_{in} ratio of 20 and equal to zero.

Amongst the liquid metabolites, acetate was the most significant with 30 $mg \cdot L^{-1}$. Only traces of ethanol and methanol were detected: maximum 4 and 8 $mg \cdot L^{-1}$ respectively. Other potential metabolites (butyric acid, propanol, butanol and acetone) were not detected.

C. hydrogenoformans development and growth

The observed specific growth rate can be expressed as a function of the cellular density as follows (Herbert et al. 1956):

$$X_t = X_o \cdot e^{\mu_o \cdot (t - t_o)}$$

where X_t is the microbial density at a given time t ($mg_{VSS} \cdot L^{-1}$) and μ_o, the actual (observed) specific growth rate (d^{-1}).

The obtained growth curve showed that the *C. hydrogenoformans* duplication rate depended on the biomass content in the gas-lift reactor (Fig. 3). Under 20 $mg_{VSS} \cdot L^{-1}$, observed growth rates were of 0.10 ± 0.01 h^{-1} whereas above this concentration, rates were of 0.01 ± 0.003 h^{-1}. This therefore translates to a duplication time of 6.80 hours under nominal conditions. Prior to peptone addition, the population density reached a plateau of around 23 ± 4 $mg_{VSS} \cdot L^{-1}$. After medium complementation with peptone, this threshold was exceeded and the population density reached 106 $mg_{VSS} \cdot L^{-1}$. The growth curves obtained after peptone addition showed the characteristic S shape of bacterial culture growth, at each CO feeding rate increase with an exponential phase, plateau and decay.

Two decay rates were obtained in the gas-lift reactor (Fig. 3). The first one was noticeable after medium complementation with peptone. Once population density reached a plateau following an increase of CO feeding, *C. hydrogenoformans* displayed a constant decay rate of 0.01 ± 0.003 h^{-1}. The second decay rate of 0.04 ± 0.01 h^{-1} occurred following an overload of gaseous substrate or under substrate limiting condition.

CO gas-liquid mass transfer: the impact of gas recirculation

The k_La values obtained varied linearly regardless of the recirculation volumetric flow rates with Q_{CO} from 24 to 110 $mL \cdot min^{-1}$ (Fig. 4). The increase of both gas recirculation and CO feed flow rates had a positive impact on the k_La value. Nevertheless, the increase of the gas recirculation flow rate had a higher impact on the k_La than the Q_{CO}, probably because of a better solubilisation of the gas phase. The k_La values were significantly smaller than those obtained with a similar experimental set-up (Munasinghe & Khanal 2010). This is likely the result of the elevated temperature used in this work, since other work has reported k_La values for tap water at 25°C.

DISCUSSION

In regards to the CO conversion, the addition of bacto-peptone resulted in a remarkable increase of growth, yield and conversion rates, in accordance with the literature (Gerhardt et al. 1991). The optimal conditions for maximizing the gas-lift performance were found to be controlled by both the gas recirculation to feed volumetric flow rates ratio (Q_R:Q_{in} ratio) and biomass concentration. Overall, the CO conversion performance of the gas lift reactor is kinetically limited over a Q_R:Q_{in} ratio of 40 and gas-liquid mass transfer limited below that ratio. With a fixed recirculation flow rate 2160 $L \cdot day^{-1}$, Run 3 conditions with Q_{CO} of 0.05 $mol \cdot L_{rxr}^{-1} \cdot d^{-1}$ seemed to be optimal for maximizing the gas-lift reactor performance with an E_{CO} of 90.4 ± 0.3 % and a bacterial activity of 2.7 ± 0.8 $mol_{CO} \cdot g_{VSS}^{-1} \cdot day^{-1}$. A higher Q_{CO} resulted in lowering the conversion efficiency and the strain activity. This activity was found to be very close to the maximal activity rate usually reported in the literature, at an optimal substrate concentration i.e. ca. 3 $mol_{CO} \cdot g^{-1}_{VSS} \cdot day^{-1}$ (Zhao et al. 2011). This confirms the previous observation according to which the gas-liquid mass transfer limitation did not occur under these conditions.

During growth of *C. hydrogenoformans* on CO, the unsupported medium did not allow a cell density higher than 23 ± 4 $mg_{VSS} \cdot L^{-1}$ and a rise in CO feeding would result in population

decay (Fig. 3). Once complementing the medium with 1.0 $g \cdot L^{-1}$ of bacto-peptone, each reasonable increase of Q_{CO} led to a continuous augmentation in bacterial concentration. The observed growth rates were inversely related to cell density, since the highest rate (0.10 ± 0.01 h^{-1}) was observed at a low bacterial density. The corresponding doubling time (6.8 h) was significantly higher than the doubling time observed in previous studies: 2 h (Gerhardt et al. 1991), 3.75 h (Henstra & Stams 2004) and 5.5 h (Svetlichny et al. 1991). This might be related to some deficiency in essential minerals of the medium used in this study as compared to previous studies: calcium, magnesium and phosphorus contents were 19.3, 2.4 and 5.1 times lower compared to the medium used previously (Gerhardt et al. 1991). The nominal decay rate was found to be in accordance with the literature (Zhao et al. 2013). Interestingly, the decay rate reaches 0.04 h^{-1} under starvation or under an overload of dCO concentration in the medium. Despite the fact that medium complementation with bacto-peptone led to a 4.6-fold increase in *C. hydrogenoformans* population, the final concentration remained low (0.1 $g_{VSS} \cdot L_{rxr}^{-1}$ after 68 days of growth) compared to a sessile growth system (6.1 $g_{VSS} \cdot L_{rxr}^{-1}$ after 126 days of growth), confirming previous observations according to which *C. hydrogenoformans* prefers sessile growth (Zhao et al. 2013).

CONCLUSION

To conclude, considering that the highest cell concentration in the reactor was of 0.106 $g_{VSS} \cdot L_{rxr}^{-1}$, with a potential bioactivity rate of 2.7 $mol_{CO} \cdot g_{VSS}^{-1} \cdot day^{-1}$, it may be deduced from this work that the volumetric CO conversion performance of such a gas lift reactor would be at the most in the range of 0.28 $mol_{CO} \cdot L_{rxr}^{-1} \cdot day^{-1}$, i.e. ~ 8 $m^3_{CO} \cdot m^3_{rxr} \cdot day^{-1}$ (70ºC). Despite the very good performances (H_2 yield, bioactivity potential and removal efficiency), the low cell density affected the volumetric activity as it was found to be 18 times lower than that of a biofilm based system (Zhao et al. 2013), making the process limiting for higher syngas feeding rates.

Overall this experimental study demonstrated the importance of bacto-peptone in triggering cell growth and enhancing the H_2 production yield as well as the feasibility of CO fermentation in a gas-lift reactor. Should a process scale up be considered, an ideal model should combine the gas-lift technology, which enhances gas-liquid mass transfer while lowering maintenance costs and energy consumption, with a biofilm-based technology, such as a fixed bed, which will allow for a higher cell density and retention thus higher volumetric activity.

ACKNOWLEDGEMENTS

The authors wish to thank R. Cimpoia, J. Breton, L. Fisher, P. Mehta, A. Corriveau and S. Deschamps for their assistance and discussions. One of the authors (M.H.) was supported by the Natural Sciences and Engineering Research Council of Canada (grant 185778-2009). NRCC paper No. NRC-EME-5563.

REFERENCES

Bonch-Osmolovskaya, E. et al., 1999. Biodiversity of anaerobic lithotrophic prokaryotes in terrestrial hot springs of Kamchatka. *Microbiology*, 68, pp.343–351.

Eaton, A. et al., 2005. *Standard methods for the examination of water and wastewater* 21st ed., Washington, D.C.: American Public Health Association, American Water Works Association, Water Environment Federation.

Gerhardt, M. et al., 1991. Bacterial CO utilization with H_2 production by the strictly anaerobic lithoautotrophic thermophilic bacterium *Carboxydothermus hydrogenus* DSM 6008 isolated from a hot swamp. *FEMS Microbiology Letters*, 83(3), pp.267–271.

Henstra, A.M. et al., 2007. Microbiology of synthesis gas fermentation for biofuel production. *Current Opinion in Biotechnology*, 18(3), pp.200–6.

Henstra, A.M. & Stams, A.J.M., 2004. Novel physiological features of *Carboxydothermus hydrogenoformans* and Thermoterrabacterium ferrireducens. *Applied and Environmental Microbiology*, 70(12), pp.7236–40.

Herbert, D., Elsworth, R. & Telling, R.C., 1956. The Continuous Culture of Bacteria; a Theoretical and Experimental Study. *Journal of General Microbiology* , 14 (3), pp.601–622.

Logan, B.E., 2004. Extracting hydrogen and electricity from renewable resources. *Environmental Science Technology*, 38(9), p.160A–167A.

Merchuk, J.C. & Gluz, M., 2002. Bioreactors, Air-lift Reactors. In *Encyclopedia of Bioprocess Technology*. John Wiley & Sons, Inc.

Munasinghe, P.C. & Khanal, S.K., 2010. Syngas fermentation to biofuel: evaluation of carbon monoxide mass transfer coefficient (kLa) in different reactor configurations. *Biotechnology Progress*, 26(6), pp.1616–21.

Newsome, D.S., 1980. The Water-Gas Shift Reaction. *Catalysis Reviews*, 21(2), pp.275–318.

Roels, J.A., 1983. *Energetics and kinetics in biotechnology*, Elsevier Biomedical Press.

Stams, A.J. et al., 1993. Growth of syntrophic propionate-oxidizing bacteria with fumarate in the absence of methanogenic bacteria. *Applied and Environmental Microbiology*, 59(4), pp.1114–1119.

Svetlichny, V.A. et al., 1991. Anaerobic Extremely Thermophilic Carboxydotrophic Bacteria in Hydrotherms of Kuril Islands Light Microscopy. , pp.1–10.

Wu, M. et al., 2005. Life in hot carbon monoxide: the complete genome sequence of *Carboxydothermus hydrogenoformans* Z-2901. *PLoS Genetics*, 1(5), p.e65.

Zhao, Y., Cimpoia, R., Liu, Z. & Guiot, S., 2011. Kinetics of CO conversion into H_2 by *Carboxydothermus hydrogenoformans*. *Applied Microbiology and Biotechnology*, 91(6), pp.1677–1684.

Zhao, Y., Cimpoia, R., Liu, Z. & Guiot, S.R., 2011. Orthogonal optimization of *Carboxydothermus hydrogenoformans* culture medium for hydrogen production from carbon monoxide by biological water-gas shift reaction. *International Journal of Hydrogen Energy*, 36(17), pp.10655–10665.

Zhao, Y. et al., 2013. Performance of a *Carboxydothermus hydrogenoformans*-immobilizing membrane reactor for syngas upgrading into hydrogen. *International Journal of Hydrogen Energy*, 38(5), pp.2167 – 2175.

FIGURES

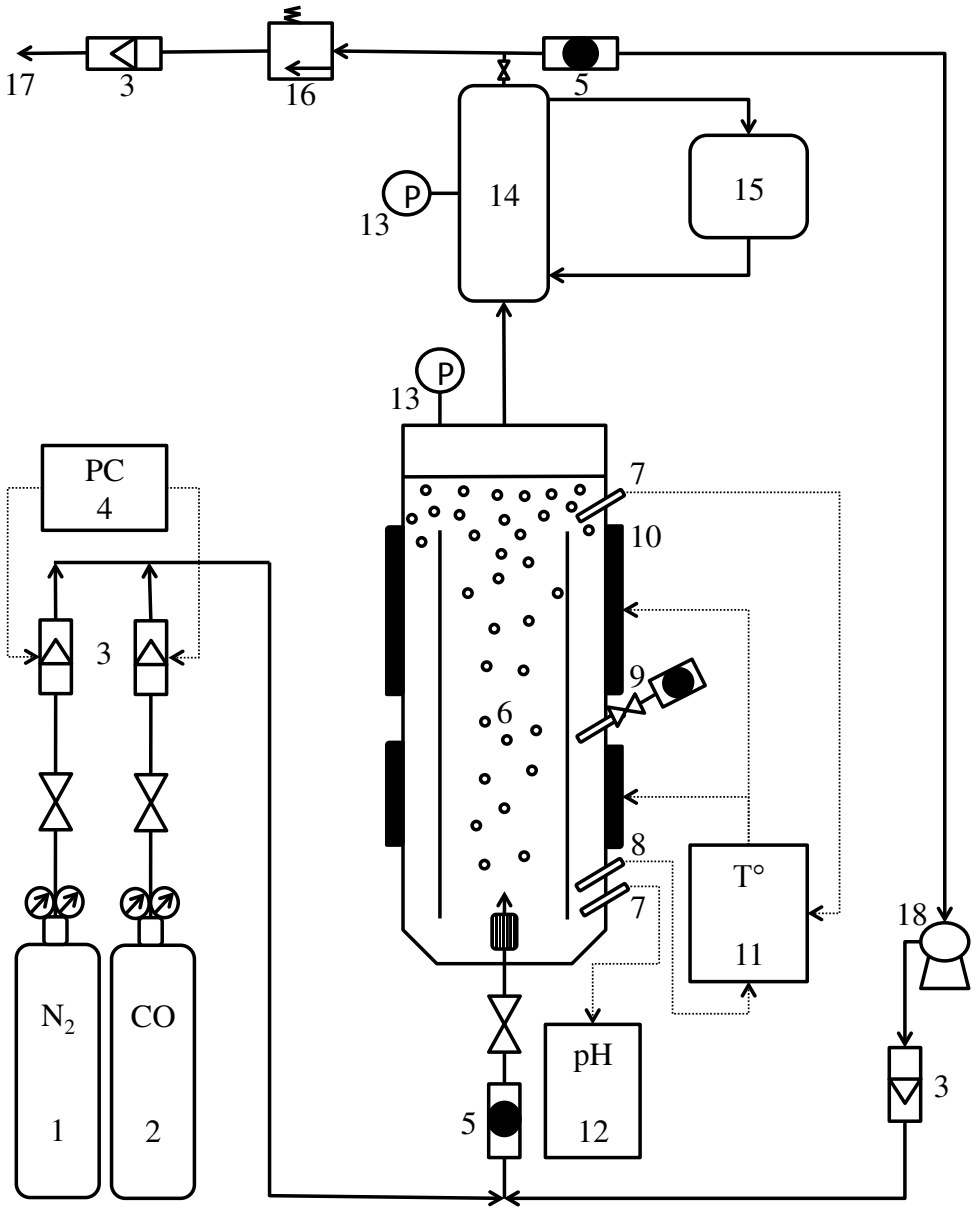

Figure 1: Schematic representation of the gas-lift reactor set-up used for hydrogen production from carbon monoxide. 1) N_2 gas cylinder; 2) CO gas cylinder; 3) gas flow meter; 4) flow controller; 5) gas sampling port; 6) gas lift reactor; 7) temperature sensor; 8) pH probe; 9) liquid sampling port; 10) electrical heating jacket; 11) temperature controller; 12) pH meter and controller; 13) pressure gauge; 14) heat exchanger; 15) water bath; 16) pressure release valve; 17) venting; 18) gas recirculation pump.

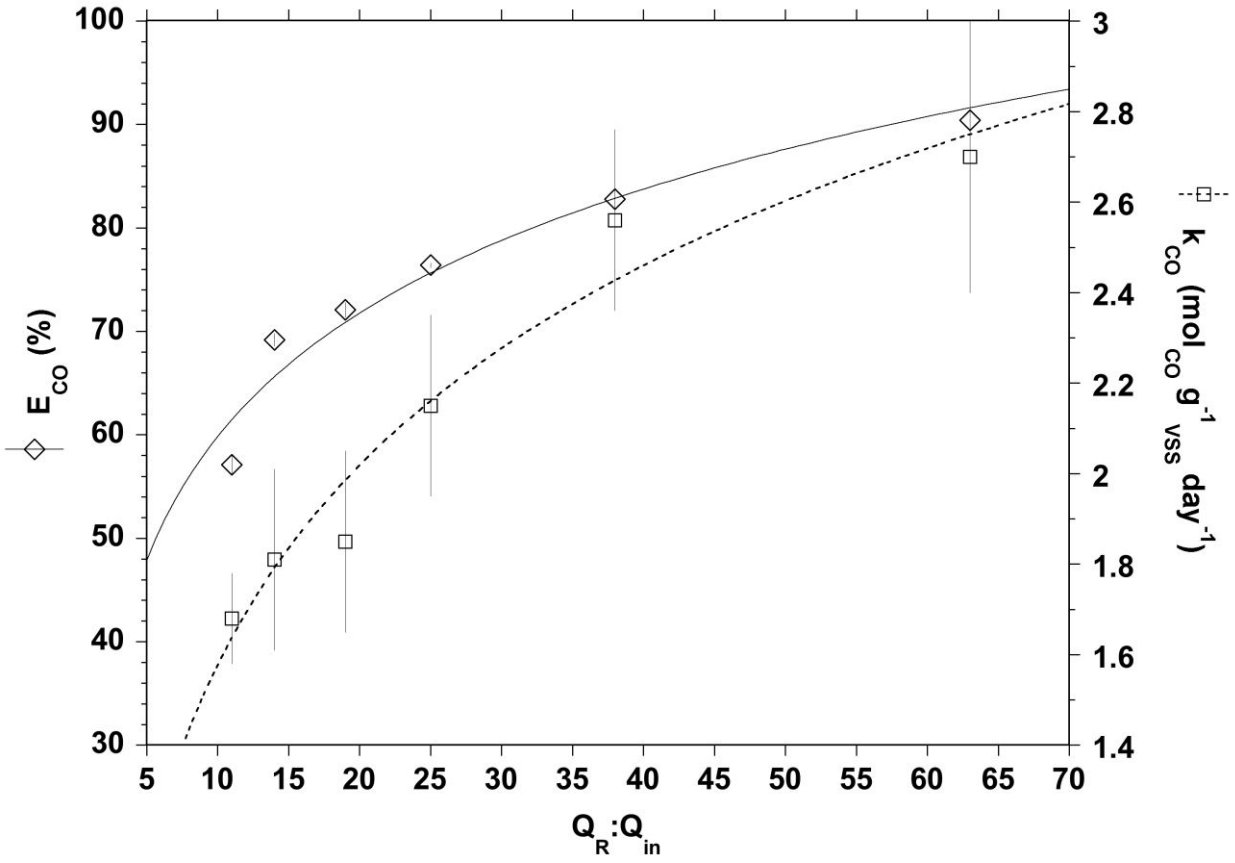

Figure 2: Performance of the gas-lift reactor under supported growth of *C. hydrogenoformans*: E_{CO}, carbon monoxide conversion efficiency (diamonds) and k_{CO}, CO specific conversion rate (squares) as a function of the ratio of gas recirculation over CO feed flow rates (Q_R:Q_{in}).

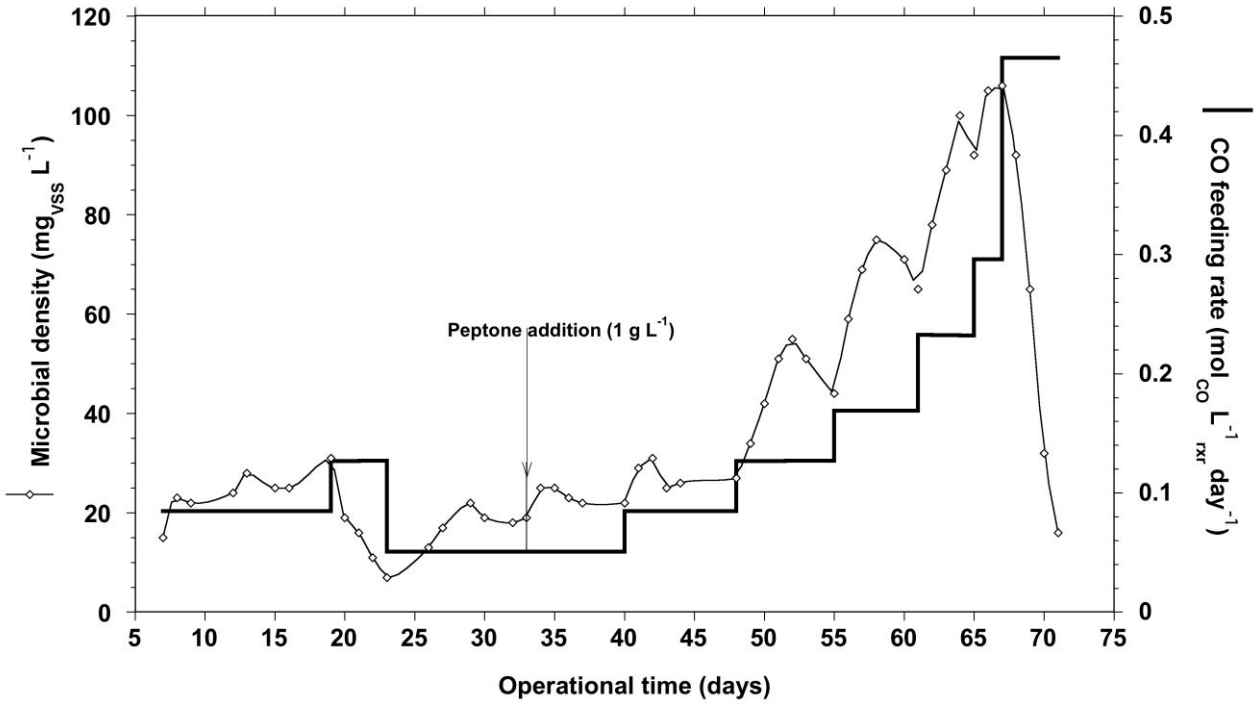

Figure 3: *C. hydrogenoformans* concentration (diamonds) in the gas-lift bioreactor as a function of time and CO feeding rate (bold line) modification prior to and after the medium complementation with peptone at 1.0 $g \cdot L^{-1}$ (vertical arrow).

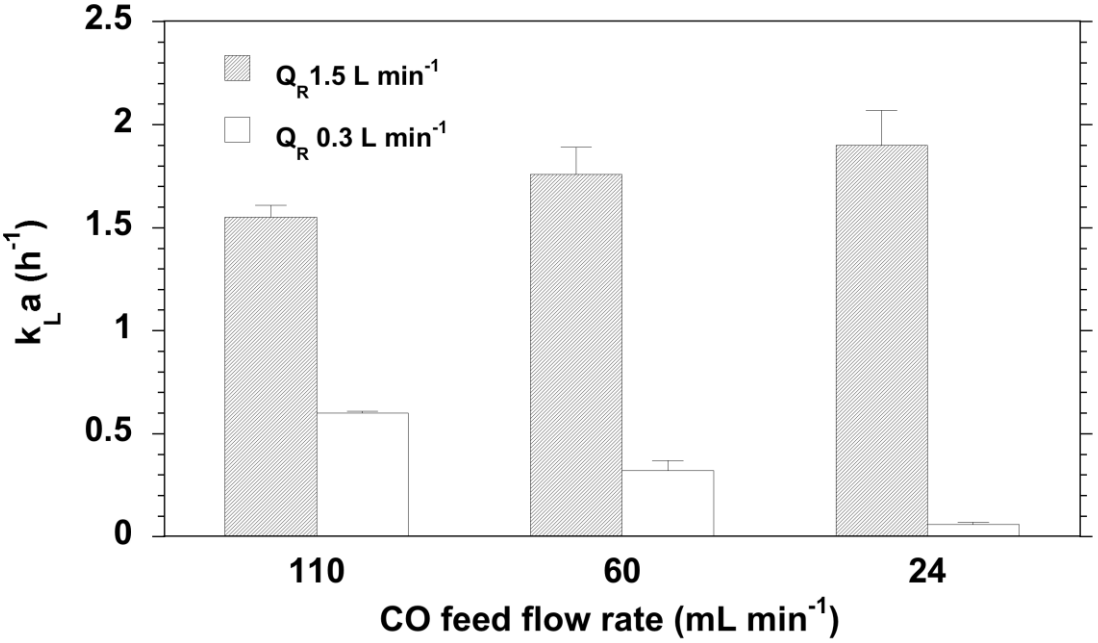

Figure 4: Effect of the gas recirculation and CO feed flow rates on the volumetric gas-liquid mass transfer coefficient (k_La) in the abiotic gas-lift reactor. Hatched columns represent the k_La obtained with a gas recirculation flow rate (Q_R) of 1.5 L·min^{-1}. Plain columns represent the k_La obtained with a Q_R of 0.3 L·min^{-1}.

Phase	Run		Q_{CO}[a]	R_{CO}[a]	E_{CO}[a]	Y_{H2}[a]	Q_R/Q_{in}	dCO[a]	k_{CO}[a]
	#	days	$mol \cdot L_{rxr}^{-1} \cdot day^{-1}$	$mol \cdot L_{rxr}^{-1} \cdot day^{-1}$	%	% $mol \cdot mol^{-1}$ CO	dl	$mmol \cdot L^{-1}$	$mol_{CO} \cdot g_{VSS}^{-1} \cdot d^{-1}$
Unsupported growth	1	6 – 19	0.08	0.05 ± 0.001	64.0 ± 0.6	74.6 ± 1.8	38	0.11 ± 0.03	2.16 ± 0.2
	2	22 – 32	0.05	0.04 ± 0.0002	78.9 ± 0.5	83.3 ± 1.6	63	0.08 ± 0.02	2.30 ± 0.4
Supported Growth	3	33 – 40	0.05	0.05 ± 0.0001	90.4 ± 0.3	96.7 ± 2.2	63	0.05 ± 0.05	2.7 ± 0.8
	4	40 – 48	0.08	0.07 ± 0.001	82.8 ± 1.2	95.1 ± 0.9	38	0.05 ± 0.04	2.56 ± 0.2
	5	48 – 55	0.13	0.10 ± 0.0003	76.4 ± 0.2	96.3 ± 0.8	25	0.07 ± 0.01	2.15 ± 0.2
	6	55 – 61	0.17	0.12 ± 0.001	72.1 ± 0.7	96.6 ± 0.7	19	0.04 ± 0.04	1.85 ± 0.2
	7	61 – 65	0.23	0.16 ± 0.001	69.2 ± 0.6	94.2 ± 0.9	14	0.00 ± 0.00	1.81 ± 0.2
	8	65 – 68	0.30	0.17 ± 0.003	57.1 ± 0.9	94.7 ± 0.7	11	0.00 ± 0.00	1.68 ± 0.1

Table 1: Performance of the gas lift reactor as a function of operational time and conditions. Phase I, unsupported growth (100% CO); Phase II, supported growth (100% CO, 1.0 $g \cdot L^{-1}$ peptone). Q_{CO}, CO feed molar flow rate; E_{CO}, CO conversion efficiency; Q_R, gas recirculation volumetric flow rate; Q_{in}, gas feed volumetric flow rates; R_{CO}, volumetric CO removal rate; Y_{H2}, hydrogen yield from CO; dCO, dissolved CO concentration; k_{CO}, specific rate of CO consumption; dl, dimensionless; [a] averages ± standard deviation.

Chapter 4: Growth profile of *Carboxydothermus hydrogenoformans* on Pyruvate

Mathieu Haddad[a,b], Ruxandra Cimpoia[b], Ya Zhao[b,c], Serge R. Guiot[a,b]

[a] Department of Microbiology and Immunology, Université de Montréal, Montreal, Canada H3C 3J7

[b] Bioengineering Group, Energy, Mining and Environment, National Research Council Canada, 6100 Royalmount Avenue, Montreal, Canada H4P 2R2

[c] Institute of Biophysics, Chinese Academy of Sciences, Chaoyang District, Beijing 100101, P.R. China

Author contribution: RC and YZ designed the experiment; YZ and MH carried out the experimental work; RC, MH and SRG interpreted the results; MH and SRG wrote the manuscript..

Article status: This article was submitted for publication to AMB express on 11 June 2013, accepted 27 September 2013 and published online 7 October 2013.

Haddad, M., Cimpoia, R., Zhao, Y., & Guiot, S. R. (2013). Growth profile of *Carboxydothermus hydrogenoformans* on pyruvate. *AMB Express*, *3*(1), 60. doi:10.1186/2191-0855-3-60

Keywords: Carbon monoxide; Water-gas shift reaction; *C. hydrogenoformans*; Pyruvate

ABSTRACT

Carboxydothermus hydrogenoformans is a thermophilic anaerobic strain most widely known for its ability to produce hydrogen (H_2) when grown on carbon monoxide (CO). Although relatively well studied, growth characterization on pyruvate has never been assessed. The present work fully characterizes growth of the bacterium on pyruvate as a sole carbon source. *C. hydrogenoformans* demonstrated a growth rate of 0.03 h^{-1}, with pyruvate consumption ranging between 0.21 and 0.48 $mol \cdot g^{-1}$ volatile suspended $solid \cdot d^{-1}$. A lag phase was also observed when switching from pyruvate to CO. When grown simultaneously on pyruvate and CO, pyruvate consumption was initiated upon CO depletion. This was attributed to pyruvate oxidation inhibition by CO, and not to a diauxic phenomenom. The strain also showed homoacetogenic activity.

INTRODUCTION

Gasification of biomass and waste is a way to produce non-fossil hydrogen and involves a high temperature (750–1500°C) conversion of any carbonaceous material into a synthesis gas (syngas) mainly composed of carbon monoxide (CO), carbon dioxide (CO_2) and hydrogen (H_2) (Rezaiyan & Cheremisinoff 2005; Song 2009). The water-gas shift (WGS) reaction widely utilized in industry can be used to augment the H_2 content of syngas. In this process, steam reacts with CO to produce carbon dioxide and hydrogen ($CO + H_2O \rightarrow CO_2 + H_2$).

Despite its deleterious effects on many living species, carbon monoxide is also the starting point for many food chains, especially in hydrothermal environments such as the deep sea, hot springs, and volcanoes. *Carboxydothermus hydrogenoformans* is one such organism that was isolated from a hot spring on Kunashir Island, Russia (Svetlichny et al. 1991). This

extreme thermophilic bacillus uses CO as sole source of carbon and energy while catalyzing the WGS reaction.

Gasifiers, as all industrial machinery, may need to be stopped for maintenance or for emergency intervention. Considering the high decay rate of *C. hydrogenoformans* (Zhao et al. 2013), it is mandatory to have a secondary carbon and energy source that would act as a back-up system in case CO fails to be delivered over an extended period of time to the biomass. That way, biomass concentration can be maintained, allowing a smooth restart of the WGS reaction with no lag time or the need to rebuild the bacterial population. In this regard, pyruvate could prove to be an interesting substitution substrate since *C. hydrogenoformans* was reported to be able to grow on it as an alternative carbon and electron source to carbon monoxide (Svetlichny et al. 1994). Pyruvate fermentation in anaerobic fermentative organisms leads to the production of acetyl-CoA and hydrogen (Hallenbeck & Benemann 2002). This reaction is catalyzed by two enzymes (Thauer et al. 1972; Carere et al. 2008): the pyruvate:ferredoxin oxidoreductase (POR), which catalyzes: $\text{pyruvate} + \text{CoA} + 2\ \text{Fd}_{ox} \rightarrow \text{acetyl-CoA} + \text{CO}_2 + \text{Fd}_{red} + 2\text{H}^+$; and the pyruvate: formate lyase (PFL), which catalyzes: $\text{pyruvate} + \text{CoA} \rightarrow \text{acetyl-CoA} + \text{formate}$.

As the reported growth information of *C. hydrogenoformans* on pyruvate was only qualitative, the objective of this study was to quantitatively assess its growth and activity kinetics on pyruvate and elucidate a potential impact of substrate alternation on both activities and products formation.

MATERIALS AND METHODS

Culture medium

C. hydrogenoformans (DSM 6008) was obtained from the German Collection of Microorganisms and Cell Cultures (DSMZ, Braunschweig, Germany). The strain was cultivated in shake-culture at 100 rpm under strictly anaerobic conditions at 70°C in a basal

mineral medium buffered with a bicarbonate-phosphate buffer. The medium as formulated by Zhao et al. (Zhao et al. 2011) contained (in $g \cdot L^{-1}$ of demineralized water): KCl 0.33, $MgCl_2 \cdot 6H_2O$ 0.102, $CaCl_2 \cdot 2H_2O$ 0.015, NH_4Cl 0.33, KH_2PO_4 0.136, $NaHCO_3$ 0.42, yeast extract 0.05, $Na_2S \cdot 9H_2O$ 0.7. The medium was supplemented with 10 $mL \cdot L^{-1}$ trace metals solution and 10 $ml \cdot L^{-1}$ of vitamins solution prepared as described previously (Stams et al. 1993). All stock solutions were autoclaved, except for the vitamin solution, which was sterilized by filtration through 0.22 μm filter membranes. The initial pH was adjusted between 6.8 and 7.0.

Growth quantification

The pyruvate activity tests were conducted in 120 mL serum bottles in quintuplicate. Bottles were filled with 30 mL of the growth medium, inoculated with 2 mL of C. hydrogenoformans at an initial concentration of 6.65 mg volatile suspended solid (VSS) $\cdot L^{-1}$, capped, and flushed with a gas mixture of N_2/CO_2 to establish anaerobic conditions. Starter cultures were active *C. hydrogenoformans* cultures that were cultivated on CO as sole source of carbon and energy. Headspace monitoring of these cultures was done prior to inoculation to ensure that they were not in latency phase. Bottles were then flushed with a high purity CO gas (100%) and set to atmospheric pressure or spiked with a pyruvate solution to an initial concentration of 3.0 ± 0.1 $g \cdot L^{-1}$, and incubated in the absence of light at 70°C and 100 rpm in a rotary shaker (New Brunswick, Edison, NJ).

Microbial quantification in the bottles was performed immediately after substrate feeding (time 0), then intermittently until the end of experiment. Biomass quantification was achieved using chemical oxygen demand (COD) measurements which were then converted to VSS using a factor of 1.37 g COD $\cdot g^{-1}$ VSS based on the elemental formula of microbial biomass as $CH_{1.79}O_{0.5}N_{0.2}S_{0.005}$ (Roels 1983).

Both substrate (CO, pyruvate) depletion and catabolite (H_2, CO_2, volatile fatty acids (VFA) and alcohols) production were monitored. The specific substrate uptake or product

formation rates, expressed as $mol \cdot g^{-1}$ $VSS \cdot d^{-1}$, were obtained by the rate of depletion or accumulation ($mol \cdot d^{-1}$) per bottle divided by the number of grams of biomass-VSS as estimated in the bottle. The hydrogen yield (Y_{H2}) was expressed as a percentage of the H_2 gas produced per CO consumed (mol/mol).

Analytical methods

The COD was determined according to Standard Methods (Eaton et al. 2005), using a spectrophotometer DRB 200 (Hach Company, Loveland, CO).

Gas samples were obtained by withdrawing 300 μL of gas from the bottle headspace using a gas-tight syringe (model 1750 Hamilton, Reno, NV). Gas composition (H_2, CO, CO_2) was measured by injecting this gas into a HP 6890 gas chromatograph (Hewlett Packard, Palo Alto, CA) equipped with a thermal conductivity detector (TCD) and a 11 $m \times 3.2$ mm 60/80 mesh Chromosorb 102 packed column (Supelco, Bellafonte, PA). The column temperature was held at 60°C for 7 min and increased to 225°C at a rate of 60°C per min. Argon was used as the carrier gas. The injector and detector were maintained at 125°C and 150°C respectively. VFAs (i.e. acetic, propionic and butyric acids) were measured on an Agilent 6890 (Wilmington, DE) gas chromatograph (GC) equipped with a flame ionization detector (FID). 0.2 μL samples were diluted 1:1 (vol./vol.) with an internal standard of iso-butyric acid in 6% formic acid, directly injected on a glass column of 1 $m \times 2$ mm Carbopack C (60–80 mesh) coated with 0.3% Carbowax 20M and 0.1% H_3PO_4. The column was held at 130°C for 4 min. Helium was the carrier gas, fed at a rate of 20 $mL \cdot min–1$. Both injector and detector were maintained at 200°C.

For measurement of solvents (methanol, ethanol, acetone, 2-propanol, tert-butanol, n-propanol, sec-butanol, n-butanol) 100 μL of liquid was transferred into a vial that had 20 mL of headspace and was crimp sealed with a Teflon-coated septum. The vial was heated at 80°C for 2 min, then 1000 μL of headspace gas was injected onto a DB-ACL2 capillary column of 30 $m \times 530$ $mm \times 2$ μm using a Combipal autosampler (CTC Analytics AG, Zwingen, Switzerland). The column was held at 40°C for 10 min. Helium was the carrier gas at a head

pressure of 5 psi. The injector and the detector were maintained at 200°C and 250°C, respectively.

Pyruvate was monitored using a high performance liquid chromatograph (HPLC) (Waters, Milford, MA) equipped with a model 600 pump, a model 717 Plus autosampler and a refractive index detector (model 2414) linked to a photodiode array (PDA) detector (model 2996). The separation was made on a 300 $mm \times 7.8$ mm ICSep IC ION-300 column (Transgenomic, Omaha, NE). The mobile phase was 0.01 N H_2SO_4 at 0.4 $mL \cdot min^{-1}$. Analyses were carried out at 35°C.

RESULTS

C. hydrogenoformans was reported to grow on pyruvate as an alternative carbon and electron source to carbon monoxide (Svetlichny et al. 1994). *C. hydrogenoformans* activity and formed products were first quantified on pyruvate (3.0 ± 0.1 $g \cdot L^{-1}$) with an initial microbial concentration of 6.65 mg $VSS \cdot L^{-1}$ for a feed-to-microorganisms ratio (F/M) of 515. (Figure 1, Phase I). Over phase I, the highest pyruvate consumption activity (initial rate reported on initial biomass concentration) and the lowest activity (final rate reported on final biomass concentration) were 0.48 ± 0.27 and 0.21 ± 0.03 $mol \cdot g\ VSS^{-1}.d^{-1}$, respectively. The corresponding product yields were 77, 7, 13 and 75% (mol/mol pyruvate) for acetate, ethanol, hydrogen and CO_2, respectively. The formation of trace methanol and 2-propanol were also observed. Once pyruvate was depleted, the cultures were flushed with CO (90 mL headspace filled with 100% CO, 1 bar) only (phase II, Figure 1), then with CO and pyruvate simultaneously (phase III, Figure 1), at the same concentrations used in phases I and II. Substrate consumption (CO and pyruvate) and products formation (H_2, CO_2, acetate, ethanol) were continuously monitored. The results showed that substrate alternation had neither an impact over products yield nor on CO or pyruvate consumption rates. The 17 hours lag time in pyruvate consumption at the beginning of phase III was expected due to the simultaneous

addition of CO and pyruvate at the end of phase II. Pyruvate consumption did not begin before 90% of the CO was consumed, indicating clear sequential substrate consumption. A significant discrepancy of 0.72 mmol between CO_2 and H_2 content occurred when *C. hydrogenoformans* was grown on pyruvate in both phases I and III, clearly indicating that part of the H_2 produced was also consumed. This difference could not be explained by the production of ethanol alone (0.16 mmol). Interestingly, hydrogen consumption stopped once ethanol concentration in the medium reached 5.33 $mmol \cdot L^{-1}$ (phase III).

Concurrently, an independent fresh growth experimental set was conducted on pyruvate alone to accurately assess the *C. hydrogenoformans* growth rate and yield on pyruvate, verify the reproducibility of the above results (Figure 2) and confirm the absence of lag time for growth and substrate consumption when CO is not present. The initial pyruvate concentration was 3.0 ± 0.1 $g \cdot L^{-1}$, with an initial microbial concentration of 71.9 mg $VSS \cdot L^{-1}$ for F/M of 43. Pyruvate consumption started within the first 4 hours compared to over 22 hours when in simultaneous presence of CO and pyruvate (Figure 1, Phase III). The observed growth rate was 0.03 ± 0.005 h^{-1}. Pyruvate consumption activity was stable throughout the experiment with the highest and lowest activity of 0.24 and 0.21 $mol \cdot g\ VSS^{-1}.d^{-1}$, respectively. This corresponded to apparent growth yields of 3.51 ± 0.69 $g\ VSS \cdot mol^{-1}$ pyruvate (i.e. 4.28 ± 0.54% by weight), respectively. The product yields were 72, 24 and 3% (mol/mol pyruvate) for acetate, hydrogen and ethanol, respectively.

DISCUSSION

Since pyruvate consumption by *C. hydrogenoformans* has not been thoroughly described in literature (Svetlichny et al. 1994), the present work allows a better understanding of this metabolism. When switching from CO to pyruvate, little lag time was observed versus the 17h lag observed for the inverse (pyruvate to CO). This could be explained by the number of steps involved in pyruvate degradation (Knappe & Sawers 1990; Bock & Schönheit 1995)

as compared to CO. Indeed, *C. hydrogenoformans* is able to convert pyruvate to acetyl-CoA in a single step, using its pyruvate-ferredoxin oxidoreductase (POR) (Perumal et al. 2012). On the other hand, CO transformation to acetyl-coA requires 4 steps and three enzymes (Lu et al. 1990): the bifunctional CODH/ACS complex, the monofunctional CODH, and a methylated corrinoid iron–sulfur protein (Ragsdale 2008). Also, the CO-related genes (coo operon) were found to be induced upon CO binding on the sensor and the transcriptional regulatory CooA protein (He et al. 1996; Aono et al. 2000; Wu et al. 2005). When assessing the activity profiles of the enzymes involved in pyruvate catabolism in *Clostridium thermocellum* (Rydzak et al. 2009), it was found that the expression level of the POR enzyme remained constant as growth progressed from early exponential to stationary phase. Hence, it was concluded that the changes of enzyme expression involved in pyruvate catabolism were negligible in response to growth (Rydzak et al. 2009). Assuming that the expression pattern of the POR superfamily is similar across *Clostridia*, these findings suggest that the POR enzyme is constantly expressed under anaerobic conditions as opposed to the CO-induced CODH (Sawers & Böck 1989; Knappe & Sawers 1990).

When *C. hydrogenoformans* was simultaneously fed with pyruvate and CO, the substrates were sequentially consumed, the pyruvate being consumed only when CO is depleted. This has the appearance of a diauxie phenomenon, also named carbon catabolite repression (CCR) (Görke & Stülke 2008), and defined as a regulatory phenomenon during which, in the presence of two carbon sources, gene expression and protein activity of the secondary carbon source are reduced. However in this case, the thermodynamics suggested that pyruvate should have been consumed before CO. The Gibbs free energy changes at 70°C and neutral pH were as follows: $\Delta G' = -45$ kJ/mol for the the reaction $CO + H_2O \rightarrow CO_2 + H_2$, with p_{CO} at 1.1 atm, p_{CO2} at 0.06 atm and p_{H2} at 0.01 atm; $\Delta G' = -81$ kJ/mol, for the reaction $CH_3COCOO^- + 2\ H_2O \rightarrow CH_3COO^- + HCO_3^- + H^+ + H_2$, with p_{H2} 0.01 atm, $[CH_3COCOO^-]$ 0.04 M, $[CH_3COO^-]$ 0.03 M, $[HCO_3^-]$ 0.005 M. This thermodynamic prediction is consistent with the observed growth kinetics, with a faster rate for pyruvate (μ 0.03 h^{-1}) than on CO (μ

0.01 h^{-1}) (Zhao et al. 2013). Thus diauxie, *sensu stricto*, cannot be retained as an explanation. The substrate consumption sequence as observed, is probably due to CO toxicity to the pyruvate pathway present in *C. hydrogenoformans* (Uniprot accession numbers: Q3ADQ7; Q3AFU1; Q3AFU0; Q3ACZ5). CO has proven to be a potent inhibitor to pyruvate oxidation in another strictly anaerobic hyperthermophile, *Pyrococcus furiosus* (Blamey & Adams 1993) and inhibited the hydrogenase activity of the POR in *Clostridium thermoaceticum* (Menon & Ragsdale 1996).

The observed discrepancy between H_2 and CO_2 content during pyruvate fermentation (Figure 1) with no subsequent by-product formation besides acetate strongly suggests a homoacetogenic activity of the bacterial strain. All the genes in the acetyl-CoA pathway have been identified in the *C. hydrogenoformans* genome (Wu et al. 2005) making CO_2 reduction to acetate possible ($2\ CO_2 + 4\ H_2 \rightarrow CH_3COO^- + H^+ + 2\ H_2O$). The stoichiometry-based combination of this homoacetogenic reaction with the pyruvate-to-acetate and pyruvate-to-ethanol reactions predicts a CO_2 net production which is nearly 4 times higher than that of hydrogen, when the yields observed for acetate, ethanol and hydrogen are used as actual stoichiometric coefficients of the balanced chemical equation: this is quite in line with the phase I observations. Adding to this, acetogenic shift of *C. hydrogenoformans* from CO was showed in final stages of incubation(Henstra & Stams 2011). Hence, homoacetogenesis would explain the linear increase in acetate in phase III (Figure 1) prior to pyruvate consumption.

In phase III (Figure 1), although hydrogen (issued from the WGS reaction) and pyruvate were present in large amounts, and that ethanol production from pyruvate and hydrogen ($\Delta G^{\circ\prime} = -57$ kJ/reaction) is more thermodynamically favourable than acetate production from pyruvate ($\Delta G^{\circ\prime} = -47$ kJ/reaction), hydrogen was not significantly consumed while ethanol did not reach a concentration higher than 5.3 mM. This could be explained by the fact that the alcohol dehydrogenase present in *C. hydrogenoformans* (NCBI Accession AF244667) is inhibited by ethanol as it was demonstrated in another thermophilic clostridium, *C. thermocellum*, at an even lower ethanol concentration (0.14 mM) (Lamed & Zeikus 1980; Lovitt et al. 1988).

To conclude, the present work revealed new growth-related features of *C. hydrogenoformans.* Growth of the bacterium on pyruvate as sole C source was fully characterized. When grown simultaneously on pyruvate and CO, pyruvate consumption was initiated upon CO depletion. This was attributed to inhibition of pyruvate oxidation by CO. While the bulk of acetate derived from pyruvate, it is likely that there was also some homoacetogenic activity, thus contributing to the formation of acetate from H_2 and CO_2, which had never previously been shown with *C. hydrogenoformans*.

REFERENCES

Aono, S., Honma, Y., Ohkubo, K., Tawara, T., Kamiya, T., & Nakajima, H. (2000). CO sensing and regulation of gene expression by the transcriptional activator CooA. *Journal of Inorganic Biochemistry*, *82*(1–4), 51–56. doi:http://dx.doi.org/10.1016/S0162-0134(00)00139-2

Blamey, J. M., & Adams, M. W. (1993). Purification and characterization of pyruvate ferredoxin oxidoreductase from the hyperthermophilic archaeon Pyrococcus furiosus. *Biochimica et Biophysica Acta*, *1161*(1), 19–27.

Bock, a K., & Schönheit, P. (1995). Growth of Methanosarcina barkeri (Fusaro) under nonmethanogenic conditions by the fermentation of pyruvate to acetate: ATP synthesis via the mechanism of substrate level phosphorylation. *Journal of Bacteriology*, *177*(8), 2002–7.

Carere, C., Kalia, V., Sparling, R., Cicek, N., & Levin, D. (2008). Pyruvate catabolism and hydrogen synthesis pathway genes of Clostridium thermocellum ATCC 27405. *Indian Journal of Microbiology*, *48*(2), 252–266 LA – English. doi:10.1007/s12088-008-0036-z

Eaton, A., Clesceri, L., Rice, E., & Greenberg, A. (2005). *Standard methods for the examination of water and wastewater* (21st ed.). Washington, D.C.: American Public Health Association, American Water Works Association, Water Environment Federation.

Görke, B., & Stülke, J. (2008). Carbon catabolite repression in bacteria: many ways to make the most out of nutrients. *Nature reviews. Microbiology*, *6*(8), 613–24. doi:10.1038/nrmicro1932

Hallenbeck, P. C., & Benemann, J. R. (2002). Biological hydrogen production ; fundamentals and limiting processes, *27*, 1185–1193.

He, Y., Shelver, D., Kerby, R. L., & Roberts, G. P. (1996). Characterization of a CO-responsive Transcriptional Activator from *Rhodospirillum rubrum*. *Journal of Biological Chemistry* , *271* (1), 120–123. doi:10.1074/jbc.271.1.120

Henstra, A. M., & Stams, A. J. M. (2011). Deep Conversion of Carbon Monoxide to Hydrogen and Formation of Acetate by the Anaerobic Thermophile *Carboxydothermus hydrogenoformans*. *International Journal of Microbiology*, *2011*, 641582. doi:10.1155/2011/641582

Knappe, J., & Sawers, G. (1990). A radical-chemical route to acetyl-CoA: the anaerobically induced pyruvate formate-lyase system of *Escherichia coli*. *FEMS microbiology reviews*, *6*(4), 383–98.

Lamed, R., & Zeikus, J. G. (1980). Ethanol Production by Thermophilic Bacteria: Relationship Between Fermentation Product Yields of and Catabolic Enzyme Activities in *Clostridium thermocellum* and *Thermoanaerobium brockii*. *Journal of Bacteriology* , *144* (2), 569–578.

Lovitt, R. W., Shen, G. J., & Zeikus, J. G. (1988). Ethanol production by thermophilic bacteria: biochemical basis for ethanol and hydrogen tolerance in *Clostridium thermohydrosulfuricum*. *Journal of Bacteriology* , *170* (6), 2809–2815.

Lu, W. P., Harder, S. R., & Ragsdale, S. W. (1990). Controlled potential enzymology of methyl transfer reactions involved in acetyl-CoA synthesis by CO dehydrogenase and the corrinoid/iron-sulfur protein from *Clostridium thermoaceticum*. *The Journal of Biological Chemistry*, *265*(6), 3124–33.

Menon, S., & Ragsdale, S. W. (1996). Unleashing Hydrogenase Activity in Carbon Monoxide Dehydrogenase/Acetyl-CoA Synthase and Pyruvate:Ferredoxin Oxidoreductase†. *Biochemistry*, *35*(49), 15814–15821. doi:10.1021/bi9615598

Perumal, R., Selvaraj, A., Ravichandran, S., & Kumar, G. (2012). Computational kinetic studies of pyruvate metabolism in *Carboxydothermus hydrogenoformans* Z-2901 for improved hydrogen production. *Biotechnology and Bioprocess Engineering*, *17*(3), 565–575. doi:10.1007/s12257-011-0396-9

Ragsdale, S. W. (2008). Enzymology of the Wood–Ljungdahl Pathway of Acetogenesis. *Annals of the New York Academy of Sciences*, *1125*(1), 129–136. doi:10.1196/annals.1419.015

Rezaiyan, J., & Cheremisinoff, N. P. (2005). *Gasification technologies: a primer for engineers and scientists*. Portland, OR: Boca Raton: Taylor & Francis.

Roels, J. A. (1983). *Energetics and kinetics in biotechnology*. Elsevier Biomedical Press.

Rydzak, T., Levin, D. B., Cicek, N., & Sparling, R. (2009). Growth phase-dependant enzyme profile of pyruvate catabolism and end-product formation in Clostridium thermocellum ATCC 27405. *Journal of Biotechnology*, *140*(3–4), 169–175. doi:http://dx.doi.org/10.1016/j.jbiotec.2009.01.022

Sawers, G., & Böck, a. (1989). Novel transcriptional control of the pyruvate formate-lyase gene: upstream regulatory sequences and multiple promoters regulate anaerobic expression. *Journal of Bacteriology*, *171*(5), 2485–98.

Song, C. (2009). Introduction to Hydrogen and Syngas Production and Purification Technologies. In *Hydrogen and Syngas Production and Purification Technologies* (pp. 1–13). John Wiley & Sons, Inc. doi:10.1002/9780470561256.ch1

Stams, A. J., Van Dijk, J. B., Dijkema, C., & Plugge, C. M. (1993). Growth of syntrophic propionate-oxidizing bacteria with fumarate in the absence of methanogenic bacteria. *Applied and Environmental Microbiology*, *59*(4), 1114–1119.

Svetlichny, V. A., Sokolova, T. G., Gerhardt, M., Kostrikina, N. A., & Zavarzin, G. A. (1991). Anaerobic Extremely Thermophilic Carboxydotrophic Bacteria in Hydrotherms of Kuril Islands Light Microscopy, 1–10.

Svetlichny, V., Sokolova, T., Kostrikina, N., & Lysenko, A. (1994). A new thermophilic anaerobic carboxydotrophic bacterium *Carboxydothermus restrictus* sp. nov. *Mikrobiologiya*, *63*, 294–297.

Thauer, R. K., Kirchniawy, F. H., & Jungermann, K. A. (1972). Properties and function of the pyruvate-formate-lyase reaction in clostridiae. *European Journal of Biochemistry / FEBS*, *27*(2), 282–90.

Wu, M., Ren, Q., Durkin, a S., Daugherty, S. C., Brinkac, L. M., Dodson, R. J., Eisen, J. A. (2005). Life in hot carbon monoxide: the complete genome sequence of *Carboxydothermus hydrogenoformans* Z-2901. *PLoS Genetics*, *1*(5), e65. doi:10.1371/journal.pgen.0010065

Zhao, Y., Cimpoia, R., Liu, Z., & Guiot, S. R. (2011). Orthogonal optimization of *Carboxydothermus hydrogenoformans* culture medium for hydrogen production from

carbon monoxide by biological water-gas shift reaction. *International Journal of Hydrogen Energy*, *36*(17), 10655–10665. doi:10.1016/j.ijhydene.2011.05.134

Zhao, Y., Haddad, M., Cimpoia, R., Liu, Z., & Guiot, S. R. (2013). Performance of a *Carboxydothermus hydrogenoformans*-immobilizing membrane reactor for syngas upgrading into hydrogen. *International Journal of Hydrogen Energy*, *38*(5), 2167 – 2175. doi:http://dx.doi.org/10.1016/j.ijhydene.2012.11.038

FIGURES

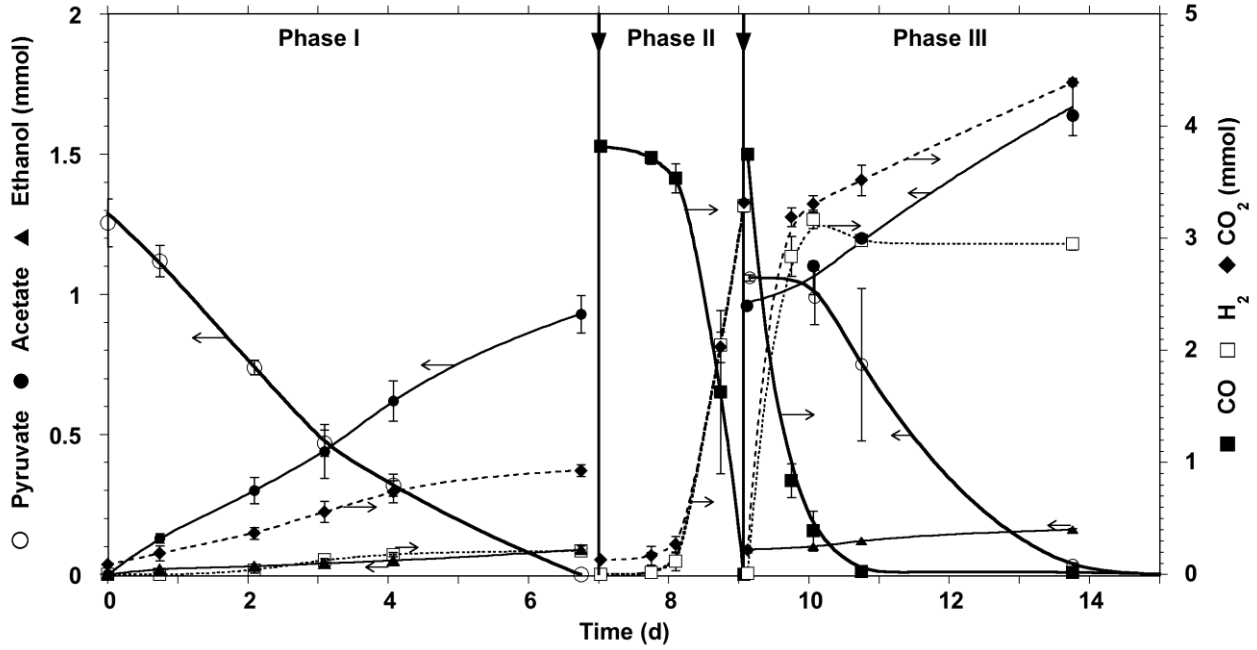

Figure 1: Time-course of CO and pyruvate consumption and hydrogen CO_2, acetate and ethanol production, by the *C. hydrogenoformans* culture when alternating substrate. Phase I, Pyruvate only; Phase II, CO only; Phase III: CO and pyruvate; the vertical arrows indicate the change of substrate; horizontal arrows indicate the axis which the data refer to.

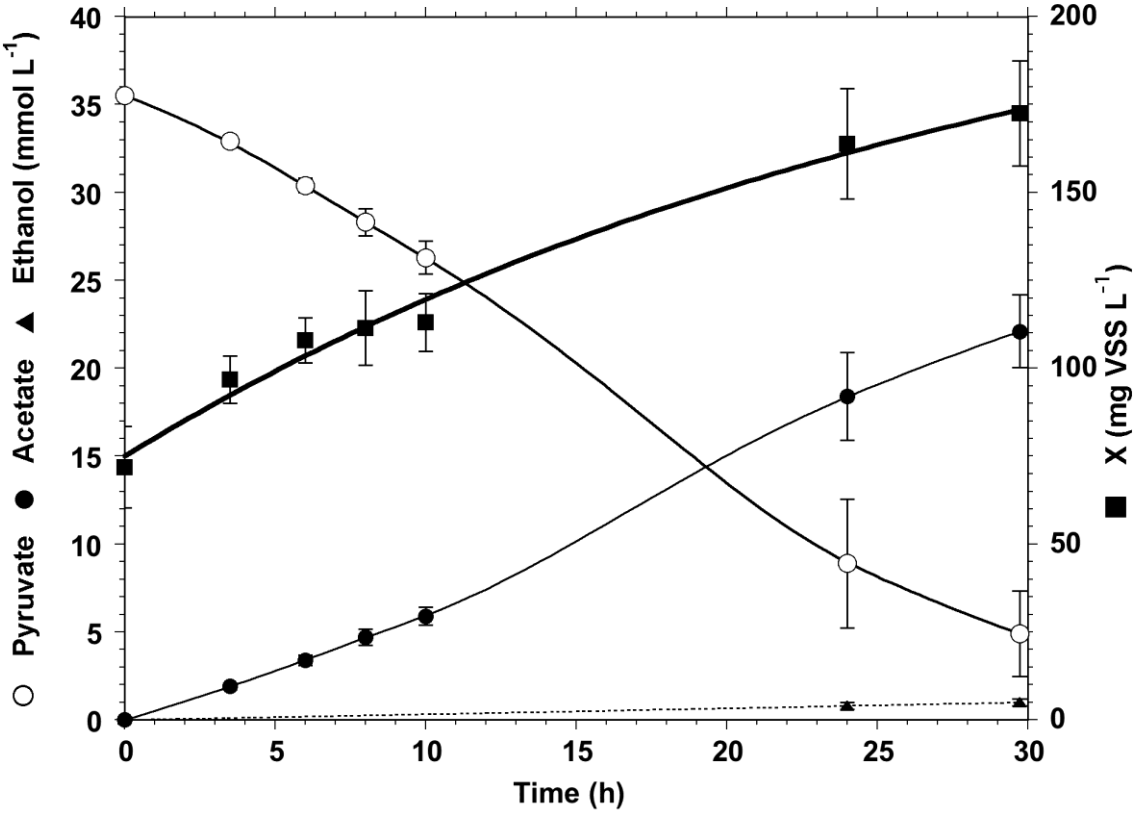

Figure 2: Time courses of *C. hydrogenoformans* growth (X), pyruvate consumption, and acetate and ethanol production.

Conclusion et perspectives

Cette thèse se divise en deux volets de recherche. La première consiste à caractériser un phénomène de biominéralisation de deux phases de phosphate de calcium (CaP) ainsi que l'impact de ce matériau sur la production d'hydrogène (H_2) et le transfert de masse du monoxyde de carbone (CO) des phases gazeuse à liquide. La seconde se concentre sur la mise à l'échelle de la production d'H_2 à partir de CO par *C. hydrogenoformans* dans un procédé en continu ainsi que la caractérisation de la consommation d'une source de carbone alternative : le pyruvate.

1. Biomineralization de whitlockite et nano-hydroxyapatite par *C. hydrogenoformans* et impact sur la production d'hydrogène

1.1. Conclusion

Lors de la croissance de *C. hydrogenoformans* dans le milieu de culture DSMZ formulé par le fournisseur de la souche (Deutsche Sammlung von Mikroorganismen und Zellkulturen GmbH), deux modes de biominéralisation ont été observés, menant à la formation de deux solides cristallins: des cristaux micrométriques de whitlockite associés à un biofilm bactérien ainsi que des cristaux nanométriques qui semblent être une hydroxyapatite nanocristalline, dispersés parmi les produits organiques de lyse bactérienne. Ce mélange biphasique est nettement dominé par la première phase.

Le premier mode de minéralisation implique la conversion d'un CaP amorphe, issu d'une précipitation abiotique suite à l'ajout du tampon $NaHCO_3$, en granules polycristallins de whitlockite. Le recouvrement de ces granules par le biofilm microbien suggère que ce dernier

crée des conditions favorables à un mécanisme de dissolution - reprécipitation. Cela est appuyé par les analyses de phosphate total qui montrent une redissolution du phosphate observée au cours des 25 premières heures après inoculation du milieu avec *C. hydrogenoformans*. Ce phénomène de transformation d'un CaP amorphe en whitlockite cristalline a été décrit par Lagier et Baud (Lagier & Baud 2003). Selon les auteurs, les phospholipides seraient responsables de l'initiation de la nucléation du cristal. Cette nucléation serait au profit de la whitlockite en raison de la teneur en magnésium (Mg) dans le précurseur amorphe qui inhiberait la nucléation d'une phase apatite (Blumenthal 1989; Boskey & Posner 1974). Au vu de la teneur en Mg dans le CaP et le milieu, les résultats obtenus semblent montrer que le biofilm bactérien a joué non seulement un rôle de support de la nucléation mais aussi comme potentiel chélateur de Mg, limitant ainsi l'inhibition de la dissolution du CaP amorphe ou favorisant la nucléation des phases cristallines.

Le second mode de minéralisation implique la formation de nanotiges cristallines s'apparentant à de l'hydroxyapatite (HA) obtenue dans d'autres cas de biominéralisation décrite chez *Serratia*, où la présence d'une concentration élevée de calcium et de phosphate dans le milieu de croissance couplée à la présence d'une matrice organique, avait engendré la nucléation d'HA (Medina Ledo et al. 2008). Les vésicules issues de la lyse des cellules bactériennes semblent jouer ici le rôle de la matrice organique initiant la nucléation de nano-HA. En effet, un lien direct entre les nanotiges de HA et ces vésicules a été observé. Cela est en accord avec les travaux de Mann (Mann 1993) qui démontre qu'une membrane cellulaire peut servir de plate-forme pour la nucléation de l'HA.

Dans les deux cas, le mode de biominéralisation s'apparente fortement à un cas de biominéralisation induite (Frankel & Bazylinski 2003) plutôt qu'à celui d'une biominéralisation contrôlée (Bazylinski 2003). En effet, les analyses des sous-produits métaboliques (mono ou disaccharides, acides gras volatiles, alcools) et protéiques n'ont révélé la présence d'aucune biomolécule incluse ou fortement adsorbée à la surface du biomatériau.

L'utilisation première de *C. hydrogenoformans* étant la production d'H_2, l'impact du précipité amorphe abiotique sur le transfert de masse du CO et le rendement en H_2 a donc été évalué en comparant les résultats obtenus dans les milieux de croissance DSMZ et modifié où aucune précipitation abiotique n'a lieu (Zhao et al. 2011). Les résultats obtenus montrent une augmentation du coefficient de transfert de masse apparent (K_La) de 0.19 ± 0.015 min^{-1} à 0.22 ± 0.005 min^{-1} dans le milieu DSMZ comparé au milieu modifié. Cela serait dû à un phénomène de physisorption au cours duquel le CO dissous s'adsorbe sur la phase solide, augmentant ainsi le transfert entre les phases gazeuse et liquide. L'analyse de physisorption du CO sur le précipité abiotique vient consolider ces résultats en démontrant l'existence d'un isotherme d'adsorption de type III caractérisé par de faibles interactions adsorbat - adsorbant (Sing et al. 1985). Ainsi, ce précipité offrirait non seulement une surface d'adsorption, palliant la faible solubilité du CO (Ungerman & Heindel 2007) mais aussi l'augmentation de la biodisponibilité du CO dans le milieu de culture. Cela s'inscrirait donc comme une nouvelle stratégie pour l'amélioration du transfert de masse gaz-liquide, basée sur les propriétés hydrophobes du CO.

Même si l'adsorption du CO sur le précipité abiotique n'a pas eu d'impact sur l'activité microbienne, *C. hydrogenoformans* a démontré un meilleur rendement en H_2 lorsqu'incubé dans le milieu de croissance DSMZ (89.11 ±6.69%) comparativement au milieu modifié (82.60 ±3.62%).

1.2. Perspectives

Les phosphates de calcium sont connus pour leur biocompatibilité et biodégradabilité en raison de leur similitude chimique avec les tissus calcifiés (Dorozhkin & Epple 2002; Chevalier & Gremillard 2009; Yuan et al. 1998). Leur utilisation en médecine pour la régénération de ces tissus est largement répandue aujourd'hui (LeGeros 2002). Malgré le fait

que la biocompatibilité de la whitlockite avec les tissus osseux humain ne soit pas documentée, des études antérieures (Ramselaar et al. 1991; Sader et al. 2009) ont conclu que ce matériau pourrait avoir une gamme intéressante d'applications dans l'ingénierie osseuse puisqu'en terme de résorbabilité, il se situe entre l'hydroxyapatite et le β-phosphate de tricalcium (β-TCP). Aussi, la présence de magnésium dans le matériau est connu pour stimuler la prolifération des ostéoblastes humains (Sader et al. 2009), faisant donc de la whitlockite un matériau moins rapidement résorbable que le β-TCP, mais plus osteoinductif. Ainsi, la biominéralisation de ce précipité biphasique à dominante whitlockite par *C. hydrogenoformans* offre une possibilité de production d'un sous-produit biologique à haute valeur ajoutée et cela avec un effet positif sur le rendement en H_2 sans pour autant affecter l'activité microbienne.

Les résultats présentés montrent que la cristallisation du précipité abiotique qui apparaît dans le milieu de culture DSMZ, se déroule entre 10 et 30 jours en présence d'une culture active de *C. hydrogenoformans*. La caractérisation cinétique de ce phénomène de biominéralisation devient alors un facteur déterminant pour l'optimisation du temps de rétention du milieu dans un système en continu. En effet, le milieu de culture doit être renouvelé afin d'éviter l'accumulation de déchets cellulaire potentiellement inhibiteurs de l'activité biologique. L'obtention du taux de cristallinité, tel que décrit dans le chapitre 1, sur du précipité échantillonné quotidiennement, permet de déterminer la cinétique de transformation de l'état amorphe à cristallin (Liou & Chen 2002) et ainsi de calculer la vitesse de cristallisation. En rapportant ce taux à la concentration de biomasse, on peut déterminer le temps de rétention optimal du milieu. De plus, les valeurs de cristallinité peuvent être transformées en utilisant l'équation Avrami (Hulbert 1969). La représentation graphique de cette transformation permet de déterminer la pente m et l'ordonnée ln k:

$$\ln\left\{\ln\left(\frac{1}{1-X}\right)\right\} = \ln k + m \ln t$$

où X (%) est le taux de cristallinité de la whitlockite formée à l'instant t (s), k (s^{-1}), la constante de vitesse de cristallisation, et m le nombre d'Avrami. La valeur de m est spécifique du mécanisme de réaction de nucléation. Cette valeur permettrait donc une meilleure compréhension de la transformation de la phase CaP amorphe en whitlockite cristalline à une température donnée. En obtenant la valeur de k pour au moins 3 températures différentes auxquelles *C. hydrogenoformans* peut subsister (60°, 65° et 70°C) et selon l'équation d'Arrhénius (Sarkar et al. 2003), il est alors possible de déterminer l'énergie d'activation de la réaction en traçant la droite ayant pour abscisse l'inverse de la température (1/T) (K) et en ordonnées, la constante de vitesse de cristallisation (k) obtenue précédemment selon l'équation suivante:

$$\ln k = \ln A - \frac{E\mathrm{a}}{RT}$$

où Ea ($J.mol^{-1}$) est l'énergie d'activation de la réaction de biominéralisation, R ($J.K^{-1}.mol^{-1}$), la constante des gaz parfait et A (s^{-1}), la constante pré-exponentielle obtenue par l'intersection de la droite avec l'axe des ordonnées. La valeur Ea de la minéralisation pourra ensuite être comparée à celle du procédé chimique de 308 $kJ.mol^{-1}$ (Unyi et al. 2000). Ea permettra aussi une compréhension thermodynamique du procédé microbien et son rôle dans la production des sous produits cristallins.

2. Mise en place d'un procédé continu pour la production d'hydrogène à partir de monoxyde de carbone par *C. hydrogenoformans* et caractérisation de l'utilisation d'une source alternative de carbone et d'énergie

2.1. Conclusion

La deuxième partie de ce travail consiste à la mise en place et l'optimisation d'un procédé de conversion en continu de CO en H_2 par *C. hydrogenoformans* se basant sur la

technologie d'un bioréacteur gazosiphone de 35L. Une précédente étude utilisant la technologie d'un bioréacteur à fibre creuse avait dévoilé de nombreuses limitations techniques (Zhao et al. 2013). Ces limitations consistaient en un vieillissement prématuré de la membrane à cause de la croissance en condition hyperthermophile ainsi que l'obstruction des pores par le biofilm, résultant en une limitation et du transfert de masse du CO, et de l'activité bactérienne. Ces deux effets cumulés entrainent donc des coûts de maintenance et de capital trop élevés pour avoir un procédé économiquement viable.

Dans un premier temps, les paramètres de croissance de *C. hydrogenoformans* et les performances du bioréacteur gazosiphon ont été étudiés en fonction de l'addition au milieu de culture, de 1.0 $g.L^{-1}$ de bacto-peptone, préalablement utilisé pour palier la faible concentration bactérienne dans des cultures planctoniques (Gerhardt et al. 1991). Les résultats montrent que l'ajout de bacto-peptone a entrainé une augmentation de la croissance cellulaire d'environ 20 $mg_{VSS}.L_{rxr}^{-1}$ à 106 $mg_{VSS}.L_{rxr}^{-1}$ au plateau et une amélioration du rendement en H_2 de 82 ± 1% à 95 ± 1%.

Ensuite, l'alimentation du bioréacteur en CO a été augmentée afin de tester les performances de la réaction biologique de conversion du CO en hydrogène et déterminer les limites cinétiques et de transfert de masse du procédé. Les résultats montrent que les performances sont contrôlées par le ratio du débit de recirculation sur celui de l'alimentation en CO ($Q_r : Q_{CO}$). Au delà d'un ratio de 40, la conversion catalytique à la vapeur d'eau est limité cinétiquement ; l'activité maximal de la souche étant atteinte tel que décrite dans la littérature (Zhao et al. 2011). En deçà d'un ratio de 40, la réaction est limitée par le transfert de masse. Dans ces conditions, les performances maximales ont été atteintes avec un taux de recirculation de la phase gazeuse de 71 $L.L_{rxr}^{-1}.d^{-1}$ et un Q_{CO} de 0.05 $mol.L_{rxr}^{-1}.d^{-1}$ conduisant à une efficacité de conversion de 90.4 ± 0.3% et une activité bactérienne de 2.7 ± 0.8 $mol_{CO}.g_{VSS}^{-1}.d^{-1}$.

Somme toute, la limitation majeure réside dans la faible densité cellulaire, typique de *C. hydrogenoformans* en croissance planctonique (Gerhardt et al. 1991), qui empêche une activité volumique plus élevée et donc une charge plus élevée en CO. Compte tenu d'une activité biologique de 2.7 $mol_{CO}.g_{VSS}^{-1}.d^{-1}$ et de la concentration cellulaire maximale obtenue, les performances volumique du bioréacteur seraient tout au plus de l'ordre de 0.28 $mol_{CO}.L_{rxr}^{-1}.d^{-1}$ (≈8 m^3_{CO} m^3_{rxr} d^{-1} à 70°C).

Afin de proposer une source de carbone auxiliaire dans un système continu de bioaugmentation d'H_2 dans le gaz de synthèse, la caractérisation de croissance de *C. hydrogenoformans* sur le pyruvate a été caractérisée. La capacité de croissance sur pyruvate comme seule source de carbone et d'énergie a déjà été démontrée mais jamais quantifiée (Gerhardt et al. 1991). Les résultats montrent une activité bactérienne entre 0.24 and 0.21 $mol_{pyruvate}.g_{VSS}^{-1}.d^{-1}$ qui ne débute que lorsque les ressources en CO sont épuisées. Ce phénomène a été attribué à l'inhibition de la voie enzymatique de dégradation du pyruvate par le CO et non à un phénomène de diauxie. Cette consommation séquentielle offre ainsi une excellente solution de substitution dans un procédé industrielle, permettant l'arrêt de l'alimentation en CO sans pour autant engendrer un déclin de la biomasse. La croissance sur pyruvate a également démontré que la bactérie était capable d'activité homoacétogène et de générer de l'acétate à partir de l'H_2 et du CO_2, ce qui n'avait jamais été relaté auparavant.

2.2. Perspectives

La présente étude démontre que la conversion du monoxyde de carbone en hydrogène est faisable par voie biologique, et qu'ainsi la biovalorisation du gaz de synthèse en hydrogène pourrait être opérée en continu dans un bioréacteur gazosiphon. Malgré des résultats prometteurs en terme d'efficacité de conversion du CO, d'activité carboxydotrophique, de transfert de masse et de rendement en H_2, la limitation majeure reste la faible densité cellulaire de *C. hydrogenoformans* qui affecte l'activité volumique du bioréacteur. Afin de palier à cette

restriction et dans l'optique d'une mise à l'échelle du procédé, le couplage de la technologie de bioréacteur gazosiphone avec une croissance sessile semble être la meilleure approche. En effet, la technologie du bioréacteur gazosiphon offre une base idéale permettant la maximisation simultanée du transfert de masse de CO et de l'activité carboxydotrophique tout en minimisant les coûts de maintenance et d'opération (Merchuk & Gluz 2002b). D'autre part, on a observé une préférence naturelle de la souche à croître en biofilm et obtenu une concentration cellulaire, lors d'une croissance en biofilm, 18 fois supérieur au maximum obtenu dans le présent travail (Zhao et al. 2013). Ainsi, un support physique sous forme de billes, tel que décrit dans la littérature (Nicolella et al. 2000), pourrait décupler la densité cellulaire et donc l'activité volumique. Cela permettrait également la rétention de la biomasse dans le réacteur et ainsi le renouvellement de la phase liquide en continu.

Bibliographie

Anon, 2009. HarvestGas process. Available at: http://www.syngest.com/technology.html [Accessed November 19, 2013].

Aono, S. et al., 2000. CO sensing and regulation of gene expression by the transcriptional activator CooA. *Journal of Inorganic Biochemistry*, 82(1–4), pp.51–56.

ASTM Standard D5291, 2010. *Instrumental determination of carbon, hydrogen, and nitrogen in petroleum products and lubricants.*, West Conshohocken, PA.

ASTM Standard D5373, 2008. *Instrumental Determination of Carbon, Hydrogen, and Nitrogen in Laboratory Samples of Coal.*, West Conshohocken, PA.

Azari, F. et al., 2008. Intracellular precipitation of hydroxyapatite mineral and implications for pathologic calcification. *Journal of Structural Biology*, 162(3), pp.468–479.

Balat, H. & Kırtay, E., 2010. Hydrogen from biomass – Present scenario and future prospects. *International Journal of Hydrogen Energy*, 35(14), pp.7416–7426.

Barker, D.J. & Stuckey, D.C., 1999. A review of soluble microbial products (SMP) in wastewater treatment systems. *Water Research*, 33(14), pp.3063–3082.

Basile, A. et al., 1996. Membrane reactor for water gas shift reaction. *Gas Separation & Purification*, 10(4), pp.243–254.

Bäuerlein, E., 2007. Growth and Form: What is the Aim of Biomineralization? In E. Buerlein, ed. *Handbook of Biomineralization*. Weinheim, Germany: Wiley-VCH Verlag GmbH, pp. 1–20.

Bazylinski, D. a., Frankel, R.B. & Konhauser, K.O., 2007. Modes of Biomineralization of Magnetite by Microbes. *Geomicrobiology Journal*, 24(6), pp.465–475.

Bazylinski, D.A. & Richard, F.B., 2003. Biologically Controlled Mineralization in Prokaryotes. *Reviews in Mineralogy and Geochemistry*, 54(1), pp.217–247.

Belgiorno, V. et al., 2003. Energy from gasification of solid wastes. *Waste management (New York, N.Y.)*, 23(1), pp.1–15.

Berman, A. et al., 1993. Biological control of crystal texture: a widespread strategy for adapting crystal properties to function. *Science (New York, N.Y.)*, 259(5096), pp.776–9.

Bičáková, O. & Straka, P., 2012. Production of hydrogen from renewable resources and its effectiveness. *International Journal of Hydrogen Energy*, 37(16), pp.11563–11578.

Blamey, J.M. & Adams, M.W., 1993. Purification and characterization of pyruvate ferredoxin oxidoreductase from the hyperthermophilic archaeon *Pyrococcus furiosus*. *Biochimica et Biophysica Acta*, 1161(1), pp.19–27.

Blokhuis, T.J. et al., 2000. Properties of Calcium Phosphate Ceramics in Relation to Their In Vivo Behavior. *The Journal of Trauma: Injury, Infection, and Critical Care*, 48(1), p.179.

Blumenthal, N.C., 1989. Mechanisms of inhibition of calcification. *Clinical orthopaedics and Related Research*, 247, pp.279–89.

Bock, a K. & Schönheit, P., 1995. Growth of Methanosarcina barkeri (Fusaro) under nonmethanogenic conditions by the fermentation of pyruvate to acetate: ATP synthesis via the mechanism of substrate level phosphorylation. *Journal of Bacteriology*, 177(8), pp.2002–7.

Bonam, D., Murrell, S.A. & Ludden, P.W., 1984. Carbon monoxide dehydrogenase from *Rhodospirillum rubrum*. *J. Bacteriol.*, 159(2), pp.693–699.

Bonch-Osmolovskaya, E. et al., 1999. Biodiversity of anaerobic lithotrophic prokaryotes in terrestrial hot springs of Kamchatka. *Microbiology*, 68, pp.343–351.

Boskey, A.L. & Posner, A.S., 1974. Magnesium stabilization of amorphous calcium phosphate: A kinetic study. *Materials Research Bulletin*, 9(7), pp.907–916.

Bouhabila, E., 2001. Fouling characterisation in membrane bioreactors. *Separation and Purification Technology*, 22-23(1-2), pp.123–132.

Carere, C. et al., 2008. Pyruvate catabolism and hydrogen synthesis pathway genes of *Clostridium thermocellum* ATCC 27405. *Indian Journal of Microbiology*, 48(2), pp.252–266 LA – English.

CEAEQ, 2004. *Détermination de la spéciation de l'arsenic: méthode par chromatographie à haute pression couplé à un spectromètre de masse à source ionisante au plasma d'argon. MA.200-As 1.1*, Québec, QC, Canada.

Chang, I.-S. et al., 2002. Membrane Fouling in Membrane Bioreactors for Wastewater Treatment. *Journal of Environmental Engineering*, 128(11), pp.1018–1029.

Chevalier, J. & Gremillard, L., 2009. Ceramics for medical applications: A picture for the next 20 years. *Journal of the European Ceramic Society*, 29(7), pp.1245–1255.

Cölfen, H. & Qi, L., 2001. A Systematic Examination of the Morphogenesis of Calcium Carbonate in the Presence of a Double-Hydrophilic Block Copolymer. *Chemistry – A European Journal*, 7(1), pp.106–116.

Coward, H.F. & Georgeson, E.H.M., 1937. 226. The diffusion coefficient of methane and air. *Journal of the Chemical Society (Resumed)*, p.1085.

Das, D. & Veziroglu, T.N., 2001. Hydrogen production by biological processes: a survey of literature. *International Journal of Hydrogen Energy*, 26(1), pp.13–28.

DoE-NETL, 2010. *Gasification 2010 Worldwide Database*,

Dorozhkin, S. V & Epple, M., 2002. Biological and medical significance of calcium phosphates. *Angewandte Chemie (International ed. in English)*, 41(17), pp.3130–46.

Eaton, A. et al., 2005. *Standard methods for the examination of water and wastewater* 21st ed., Washington, D.C.: American Public Health Association, American Water Works Association, Water Environment Federation.

Emsley, J., 1991. *The elements* 2d ed., Oxford, UK.: Clarendon Press.

Epple, M. & Kovtun, A., 2010. Functionalized Calcium Phosphate Nanoparticles for Biomedical Application. *Key Engineering Materials*, 441, pp.299–305.

De Filippis, P. et al., 2004. Prediction of syngas quality for two-stage gasification of selected waste feedstocks. *Waste Management (New York, N.Y.)*, 24(6), pp.633–9.

Flickinger, M. & Drew, S., 2002. Fermentation, Biocatalysis and Bioseparation. In M. C. Flickinger & S. W. Drew, eds. *Encyclopedia of Bioprocess Technology, 1st ed.* Hoboken, NJ, USA: John Wiley & Sons, Inc., pp. 267 – 291.

Frankel, R.B. & Bazylinski, D.A., 2003. Biologically Induced Mineralization by Bacteria. *Reviews in Mineralogy and Geochemistry* , 54 (1), pp.95–114.

Frondel, C., 1943. Mineralogy of the calcium phosphates in insular phosphate rock. *American Mineralogist*, 28, pp.215–232.

Gabelman, A. & Hwang, S.-T., 1999. Hollow fiber membrane contactors. *Journal of Membrane Science*, 159(1-2), pp.61–106.

Gerhardt, M., Svetlichny, V., Sokolova, T.G., et al., 1991. Bacterial CO utilization with H_2 production by the strictly anaerobic lithoautotrophic thermophilic bacterium *Carboxydothermus hydrogenus* DSM 6008 isolated from a hot swamp. *FEMS Microbiology Letters*, 83(3), pp.267–271.

Gilliland, E.R. et al., 1974. Diffusion on Surfaces. I. Effect of Concentration on the Diffusivity of Physically Adsorbed Gases. *Industrial & Engineering Chemistry Fundamentals*, 13(2), pp.95–100.

Gopal, R. et al., 1974. Crystal Structure of Synthetic Mg-Whitlockite, $Ca_{18}Mg_2H_2(PO_4)_{14}$. *Canadian Journal of Chemistry*, 52(7), pp.1155–1164.

Gopal, R. & Calvo, C., 1972. Structural Relationship of Whitlockite and βCa3(PO4)2. *Nature Physical Science*, 237, pp.30–32.

Görke, B. & Stülke, J., 2008. Carbon catabolite repression in bacteria: many ways to make the most out of nutrients. *Nature Reviews. Microbiology*, 6(8), pp.613–24.

Guillory, J.K., 2010. Book Review of CRC Handbook of Chemistry and Physics. 91st Edition CRC Handbook of Chemistry and Physics. 91st Edition . Edited by W. M. Haynes CRC

Press (Taylor and Francis Group) , Boca Raton, FL . 2010 . xi +2610 pp. 22 × 29 cm. ISBN 978-1-4398-2077-3. *Journal of Medicinal Chemistry*, 53(24), pp.8780–8780.

Hallenbeck, P.C. & Benemann, J.R., 2002. Biological hydrogen production ; fundamentals and limiting processes. , 27, pp.1185–1193.

Hammes, F. & Verstraete, W., 2002. Key roles of pH and calcium metabolism in microbial carbonate precipitation. *Reviews in Environmental Science and Biotechnology*, 1(1), pp.3–7.

He, Y. et al., 1996. Characterization of a CO-responsive Transcriptional Activator from *Rhodospirillum rubrum*. *Journal of Biological Chemistry* , 271 (1), pp.120–123.

Hench, L.L., 1991. Bioceramics: From Concept to Clinic. *Journal of the American Ceramic Society*, 74(7), pp.1487–1510.

Henstra, A.M. et al., 2007. Microbiology of synthesis gas fermentation for biofuel production. *Current Opinion in Biotechnology*, 18(3), pp.200–6.

Henstra, A.M. & Stams, A.J.M., 2011. Deep Conversion of Carbon Monoxide to Hydrogen and Formation of Acetate by the Anaerobic Thermophile *Carboxydothermus hydrogenoformans*. *International Journal of Microbiology*, 2011(Article ID 641582), p.4 pages.

Henstra, A.M. & Stams, A.J.M., 2004. Novel physiological features of *Carboxydothermus hydrogenoformans* and *Thermoterrabacterium ferrireducens*. *Applied and Environmental Microbiology*, 70(12), pp.7236–40.

Herbert, D., Elsworth, R. & Telling, R.C., 1956. The Continuous Culture of Bacteria; a Theoretical and Experimental Study. *Journal of General Microbiology* , 14 (3), pp.601–622.

Higman, C., 2013. Gasification Technologies Conference. In *State of the Gasification Industry – the Updated Worldwide Gasification Database*. Colorado Springs (CO).

Higman, C. & Van der Burgt, M., 2008. *Gasification*, Gulf Professional Publishing.

Hoornweg, D. & Bhada-Tata, P., 2012. *What a Waste: A Global Review of Solid Waste Management*,

Hoornweg, D., Bhada-Tata, P. & Kennedy, C., 2013. Environment: Waste production must peak this century. *Nature*, 502(7473), pp.615–617.

Huang, L.-N., De Wever, H. & Diels, L., 2008. Diverse and Distinct Bacterial Communities Induced Biofilm Fouling in Membrane Bioreactors Operated under Different Conditions. *Environmental Science & Technology*, 42(22), pp.8360–8366.

Huber, R., Huber, H. & Stetter, K.O., 2000. Towards the ecology of hyperthermophiles: biotopes, new isolation strategies and novel metabolic properties. *FEMS Microbiology Reviews*, 24(5), pp.615–623.

Hulbert, S.F., 1969. Models of solid-state reactions in powder compacts: A review. *Journal of the British Ceramics Society*, 6, pp.11–20.

ISO, 2007. *ISO. Rigid cellular plastics — Determination of water vapour transmission properties*,

Joannis, C., Delia, M.L. & Riba, J.P., 1998. Comparison of four methods for quantification of biofilms in biphasic cultures. *Biotechnology Techniques*, 12(10), pp.777–782.

Jones, S.T., 2007. *Gas liquid mass transfer in an external airlift loop reactor for syngas fermentation*. Iowa State, Ames, IOWA.

Kaneko, K., 1994. Determination of pore size and pore size distribution: 1. Adsorbents and catalysts. *Journal of Membrane Science*, 96(1–2), pp.59–89.

Kapic, A., 2005. *Mass Transfer Measurements for Syngas Fermentation*. Iowa State University, Ames, IA.

Kapic, A., Jones, S.T. & Heindel, T.J., 2006. Carbon Monoxide Mass Transfer in a Syngas Mixture. *Industrial & Engineering Chemistry Research*, 45(26), pp.9150–9155.

Karatan, E. & Watnick, P., 2009. Signals, regulatory networks, and materials that build and break bacterial biofilms. *Microbiology and Molecular Biology Reviews : MMBR*, 73(2), pp.310–47.

Karoor, S. & Sirkar, K.K., 1993. Gas absorption studies in microporous hollow fiber membrane modules. *Industrial & Engineering Chemistry Research*, 32(4), pp.674–684.

Kashefi, K. & Lovley, D.R., 2000. Reduction of Fe(III), Mn(IV), and Toxic Metals at 100 C by Pyrobaculum islandicum. *Applied and Environmental Microbiology*, 66(3), pp.1050–1056.

Kirkels, A.F. & Verbong, G.P.J., 2011. Biomass gasification: Still promising? A 30-year global overview. *Renewable and Sustainable Energy Reviews*, 15(1), pp.471–481.

Klasson, K.T. et al., 1992. Biological conversion of synthesis gas into fuels. *International Journal of Hydrogen Energy*, 17(4), pp.281–288.

Knappe, J. & Sawers, G., 1990. A radical-chemical route to acetyl-CoA: the anaerobically induced pyruvate formate-lyase system of *Escherichia coli*. *FEMS Microbiology Reviews*, 6(4), pp.383–98.

Kweh, S.W., Khor, K.. & Cheang, P., 2000. Plasma-sprayed hydroxyapatite (HA) coatings with flame-spheroidized feedstock: microstructure and mechanical properties. *Biomaterials*, 21(12), pp.1223–1234.

Lagier, R. & Baud, C.-A., 2003. Magnesium Whitlockite, a Calcium Phosphate Crystal of Special Interest in Pathology. *Pathology - Research and Practice*, 199(5), pp.329–335.

Lamed, R. & Zeikus, J.G., 1980. Ethanol Production by Thermophilic Bacteria: Relationship Between Fermentation Product Yields of and Catabolic Enzyme Activities in *Clostridium thermocellum* and *Thermoanaerobium brockii*. *Journal of Bacteriology* , 144 (2), pp.569–578.

Lan, R., Irvine, J.T.S. & Tao, S., 2012. Ammonia and related chemicals as potential indirect hydrogen storage materials. *International Journal of Hydrogen Energy*, 37(2), pp.1482–1494.

Layrolle, P., Ito, A. & Tateishi, T., 1998. Sol-Gel Synthesis of Amorphous Calcium Phosphate and Sintering into Microporous Hydroxyapatite Bioceramics. *Journal of the American Ceramic Society*, 81(6), pp.1421–1428.

LeGeros, R.Z., 2002. Properties of Osteoconductive Biomaterials: Calcium Phosphates. *Clinical Orthopaedics and Related Research*, 395(395), pp.81–98.

Lide Frederikse, H.P.R.,, D.R., 1995. *CRC handbook of chemistry and physics, 1995-1996 : a ready-reference book of chemical and physical data*, Boca Raton (Florida): CRC Press.

Lindahl, P.A., 2002. Current Topics The Ni-Containing Carbon Monoxide Dehydrogenase Family : Light at the End of the Tunnel ? †. , 41(7).

Liou, S.-C. & Chen, S.-Y., 2002. Transformation mechanism of different chemically precipitated apatitic precursors into beta-tricalcium phosphate upon calcination. *Biomaterials*, 23(23), pp.4541–7.

Littlewood, K., 1977. Gasification: Theory and application. *Progress in Energy and Combustion Science*, 3(1), pp.35–71.

Liu, H. et al., 2007. Carbon membrane-aerated biofilm reactor for synthetic wastewater treatment. *Bioprocess and Biosystems Engineering*, 30(4), pp.217–24.

Logan, B., 2004. Peer reviewed: extracting hydrogen and electricity from renewable resources. *Environmental science & Technology*, 38(9), p.160A – 167A.

Logan, B.E., 2004. Extracting hydrogen and electricity from renewable resources. *Environmental Science & Technology*, 38(9), p.160A–167A.

Lovitt, R.W., Shen, G.J. & Zeikus, J.G., 1988. Ethanol production by thermophilic bacteria: biochemical basis for ethanol and hydrogen tolerance in *Clostridium thermohydrosulfuricum*. *Journal of Bacteriology* , 170 (6), pp.2809–2815.

Lowenstam, H., 1981. Minerals formed by organisms. *Science*, 211(4487), pp.1126–1131.

Lu, W.P., Harder, S.R. & Ragsdale, S.W., 1990. Controlled potential enzymology of methyl transfer reactions involved in acetyl-CoA synthesis by CO dehydrogenase and the corrinoid/iron-sulfur protein from *Clostridium thermoaceticum*. *The Journal of Biological Chemistry*, 265(6), pp.3124–33.

Mandel, S. & Tas, a. C., 2010. Brushite ($CaHPO_4 \cdot 2H_2O$) to octacalcium phosphate ($Ca_8(HPO_4)_2(PO_4)_4 \cdot 5H_2O$) transformation in DMEM solutions at 36.5°C. *Materials Science and Engineering: C*, 30(2), pp.245–254.

Mann, S., 1993. Molecular tectonics in biomineralization and biomimetic materials chemistry. *Nature*, 365(6446), pp.499–505.

Medina Ledo, H. et al., 2008. Microstructure and composition of biosynthetically synthesised hydroxyapatite. *Journal of Materials Science. Materials in medicine*, 19(11), pp.3419–27.

Menon, S. & Ragsdale, S.W., 1996. Unleashing Hydrogenase Activity in Carbon Monoxide Dehydrogenase/Acetyl-CoA Synthase and Pyruvate:Ferredoxin Oxidoreductase. *Biochemistry*, 35(49), pp.15814–15821.

Merchuk, J.C. & Gluz, M., 2002a. Bioreactors, Air-lift Reactors. In *Encyclopedia of Bioprocess Technology*. John Wiley & Sons, Inc.

Merchuk, J.C. & Gluz, M., 2002b. Bioreactors, Air-lift Reactors. In *Encyclopedia of Bioprocess Technology*. John Wiley & Sons, Inc.

Milliken, J., 2001. Alternative catalysts offer high activity , low cost Contacts. , (April).

Miura, Y., Watanabe, Y. & Okabe, S., 2007. Membrane Biofouling in Pilot-Scale Membrane Bioreactors (MBRs) Treating Municipal Wastewater: Impact of Biofilm Formation. *Environmental Science & Technology*, 41(2), pp.632–638.

Mohammadi, M. et al., 2011. Bioconversion of synthesis gas to second generation biofuels: A review. *Renewable and Sustainable Energy Reviews*, 15(9), pp.4255–4273.

Montoya, J.P., 2010. Membrane gas exchange: Using hollow fiber membranes to separate gases from liquid and gaseous streams. *Ann Arbor; MI: MedArray; Inc.* Available at: http://www.permselect.com/files/Using_Membranes_for_Gas_Exchange.pdf [Accessed July 18, 2010].

Munasinghe, P.C. & Khanal, S.K., 2010. Syngas fermentation to biofuel: evaluation of carbon monoxide mass transfer coefficient (kLa) in different reactor configurations. *Biotechnology progress*, 26(6), pp.1616–21.

Newsome, D.S., 1980. The Water-Gas Shift Reaction. *Catalysis Reviews*, 21(2), pp.275–318.

Nicolella, C., van Loosdrecht, M.C.M. & Heijnen, S.J., 2000. Particle-based biofilm reactor technology. *Trends in Biotechnology*, 18(7), pp.312–320.

Norris, V. et al., 1996. Calcium signalling in bacteria. *Journal of Bacteriology*, 178(13), pp.3677–3682.

Oelgeschläger, E. & Rother, M., 2008. Carbon monoxide-dependent energy metabolism in anaerobic bacteria and archaea. *Archives of Microbiology*, 190(3), pp.257–69.

Okubo, T. et al., 1991. Equilibrium shift of dehydrogenation at short space-time with hollow fiber ceramic membrane. *Industrial & Engineering Chemistry Research*, 30(4), pp.614–616.

Oura, K. et al., 2010. *Surface Science: An Introduction*, Springer.

Padro, C.E.G. & Putsche, V., 1999. Survey of the Economics of Hydrogen Technologies. *National Renewable Energy Laboratory*, (September).

Perry , Green, Don W., Maloney, James O.,, R.H., 1984. *Perry's Chemical engineers' handbook.*, New York: McGraw-Hill.

Perumal, R. et al., 2012. Computational kinetic studies of pyruvate metabolism in *Carboxydothermus hydrogenoformans* Z-2901 for improved hydrogen production. *Biotechnology and Bioprocess Engineering*, 17(3), pp.565–575.

Pfaff, J.D., 1993. *US EPA Method 300.0, Methods for the determination of inorganic substances in environmental samples. EPA-600/R-93-100, NTIS PB94-121811.*, Cincinnati, OH, USA.

Ragsdale, S.W., 2008. Enzymology of the Wood–Ljungdahl Pathway of Acetogenesis. *Annals of the New York Academy of Sciences*, 1125(1), pp.129–136.

Ragsdale, S.W., 2004. Life with carbon monoxide. *Critical reviews in biochemistry and molecular biology*, 39(3), pp.165–95.

Ramselaar, M.M.A. et al., 1991. Biodegradation of four calcium phosphate ceramics;in vivo rates and tissue interactions. *Journal of Materials Science: Materials in Medicine*, 2(2), pp.63–70.

Rey, C. et al., 1991. Resolution-enhanced fourier transform infrared spectroscopy study of the environment of phosphate ion in the early deposits of a solid phase of calcium phosphate in bone and enamel and their evolution with age: 2. Investigations in thev 3 PO4 domain. *Calcified Tissue International*, 49(6), pp.383–388.

Rey, C. et al., 1990. Resolution-enhanced fourier transform infrared spectroscopy study of the environment of phosphate ions in the early deposits of a solid phase of calcium-phosphate in bone and enamel, and their evolution with age. I: Investigations in thev 4 PO4 domain. *Calcified Tissue International*, 46(6), pp.384–394.

Rezaiyan, J. & Cheremisinoff, N.P., 2005. *Gasification technologies: a primer for engineers and scientists*, Portland, OR: Boca Raton: Taylor & Francis.

Riggs, S.S., 2004. *Carbon Monoxide and Hydrogen Mass Transfer in a Stirred Tank Reactor*. Iowa State University, Ames, IA.

Riggs, S.S. & Heindel, T.J., 2006. Measuring carbon monoxide gas-liquid mass transfer in a stirred tank reactor for syngas fermentation. *Biotechnology progress*, 22(3), pp.903–6.

Roadmap, E., 2002. National Hydrogen Energy Roadmap. *(US Department of Energy (DOE), 2002. National Hydrogen Energy Roadmap. Washington, DC.)*, (November).

Roels, J.A., 1983. *Energetics and Kinetics in Biotechnology*, Elsevier Biomedical Press.

Rouf, M. a, 1964. Spectrochemical Analysis of Inorganic Elements in Bacteria. *Journal of Bacteriology*, 88, pp.1545–9.

Ruiz Careri, M.N., 2005. *Advantages and disadvantages of microporous membranes in a hollow fiber bioreactor for space applications*. Texas Tech University.

Rydzak, T. et al., 2009. Growth phase-dependant enzyme profile of pyruvate catabolism and end-product formation in *Clostridium thermocellum* ATCC 27405. *Journal of Biotechnology*, 140(3–4), pp.169–175.

Sader, M.S., Legeros, R.Z. & Soares, G. a, 2009. Human osteoblasts adhesion and proliferation on magnesium-substituted tricalcium phosphate dense tablets. *Journal of Materials Science. Materials in Medicine*, 20(2), pp.521–7.

Sapra, R., Bagramyan, K. & Adams, M.W.W., 2003. A simple energy-conserving system: proton reduction coupled to proton translocation. *Proceedings of the National Academy of Sciences of the United States of America*, 100(13), pp.7545–50.

Sarkar, M., Acharya, P.K. & Bhattacharya, B., 2003. Modeling the adsorption kinetics of some priority organic pollutants in water from diffusion and activation energy parameters. *Journal of Colloid and Interface Science*, 266(1), pp.28–32.

Sauer, K., 2003. The genomics and proteomics of biofilm formation. *Genome biology*, 4(6), p.219.

Sawers, G. & Böck, a, 1989. Novel transcriptional control of the pyruvate formate-lyase gene: upstream regulatory sequences and multiple promoters regulate anaerobic expression. *Journal of Bacteriology*, 171(5), pp.2485–98.

Sidaway, D.A., 1978. A microbiological study of dental calculus. *Journal of Periodontal Research*, 13(4), pp.349–359.

Sing, K. S. W., Everett, D. H., Haul, R. A. W., Moscou, L., Pierotti, R. A., Rouquerol, J., & Siemieniewska, T. (1985). Reporting physisorption data for gas/solid systems, with special reference to the determination of surface area and porosity. Pure and applied chemistry (Vol. 57, pp. 603–619). *Pure and Applied Chemistry*. doi:10.1002/9783527610044

Sipma, J., 2006. *Microbial hydrogenogenic CO conversions: applications in synthesis gas purification and biodesulfurization*. Wageningen University, Wageningen, the Netherlands.

Smith R J, B., Loganathan, M. & Shantha, M.S., 2010. A Review of the Water Gas Shift Reaction Kinetics. *International Journal of Chemical Reactor Engineering*, 8(1).

Sokolova, T.G. et al., 2009. Diversity and ecophysiological features of thermophilic carboxydotrophic anaerobes. *FEMS Microbiology Ecology*, 68(2), pp.131–41.

Solomon, B.D. & Banerjee, A., 2006. A global survey of hydrogen energy research, development and policy. *Energy Policy*, 34(7), pp.781–792.

Sombatsompop, K., Visvanathan, C. & Ben Aim, R., 2006. Evaluation of biofouling phenomenon in suspended and attached growth membrane bioreactor systems. *Desalination*, 201(1-3), pp.138–149.

Song, C., 2009. Introduction to Hydrogen and Syngas Production and Purification Technologies. In *Hydrogen and Syngas Production and Purification Technologies*. John Wiley & Sons, Inc., pp. 1–13.

Stams, A.J. et al., 1993. Growth of syntrophic propionate-oxidizing bacteria with fumarate in the absence of methanogenic bacteria. *Applied and Environmental Microbiology*, 59(4), pp.1114–9.

Stoodley, P. et al., 2002. Biofilms as complex differentiated communities. *Annual Review of Microbiology*, 56, pp.187–209.

Stoodley, P. et al., 1999. Structural deformation of bacterial biofilms caused by short-term fluctuations in fluid shear: an in situ investigation of biofilm rheology. *Biotechnology and Bioengineering*, 65(1), pp.83–92.

Sun, X., Meng, F. & Yang, F., 2008. Application of seawater to enhance SO2 removal from simulated flue gas through hollow fiber membrane contactor. *Journal of Membrane Science*, 312(1-2), pp.6–14.

Svetlichny, V. et al., 1994. A new thermophilic anaerobic carboxydotrophic bacterium *Carboxydothermus restrictus* sp. nov. *Mikrobiologiya*, 63, pp.294–297.

Svetlitchnyi, V. et al., 2001. Two Membrane-Associated NiFeS-Carbon Monoxide Dehydrogenases from the Anaerobic Carbon-Monoxide-Utilizing Eubacterium *Carboxydothermus hydrogenoformans*. *Journal of Bacteriology*, 183(17), pp.5134–5144.

SynGest Inc. (2009). HarvestGas process. Retrieved November 19, 2013, from http://www.syngest.com/technology.html

Techtmann, S., Colman, A. & Murphy, M., 2011. Regulation of multiple carbon monoxide consumption pathways in anaerobic bacteria. *Frontiers in Microbiology*, 2(July), p.12.

Thauer, R.K., Kirchniawy, F.H. & Jungermann, K. a, 1972. Properties and function of the pyruvate-formate-lyase reaction in clostridiae. *European Journal of Biochemistry / FEBS*, 27(2), pp.282–90.

Thommes, M., 2010. Physical Adsorption Characterization of Nanoporous Materials. *Chemie Ingenieur Technik*, 82(7), pp.1059–1073.

Torres, W., Pansare, S.S. & Goodwin, J.G., 2007. Hot Gas Removal of Tars, Ammonia, and Hydrogen Sulfide from Biomass Gasification Gas. *Catalysis Reviews*, 49(4), pp.407–456.

Tung, M.S., 1998. Calcium Phosphates in Biological and Industrial Systems. In Z. Amjad, ed. *Biological and Industrial Systems*. Boston, MA: Springer US, pp. 1–19.

Ungerman, A.J. & Heindel, T.J., 2007. Carbon Monoxide Mass Transfer for Syngas Fermentation in a Stirred Tank Reactor with Dual Impeller Configurations. *Biotechnology Progress*, 23(3), pp.613–620.

Unyi, T. et al., 2000. Changes of the mechanical properties during the crystallization of bio-active glass-ceramics. *Journal of Materials Science*, 35(12), pp.3059–3068.

Wang, J. & Wan, W., 2009. Factors influencing fermentative hydrogen production: A review. *International Journal of Hydrogen Energy*, 34(2), pp.799–811.

Weiner, S., 2003. An Overview of Biomineralization Processes and the Problem of the Vital Effect. *Reviews in Mineralogy and Geochemistry*, 54(1), pp.1–29.

Wise, D.L. & Houghton, G., 1968. Diffusion coefficients of neon, krypton, xenon, carbon monoxide and nitric oxide in water at 10–60°C. *Chemical Engineering Science*, 23(10), pp.1211–1216.

Wu, M. et al., 2005. Life in hot carbon monoxide: the complete genome sequence of *Carboxydothermus hydrogenoformans* Z-2901. *PLoS Genetics*, 1(5), p.e65.

Xie, H. et al., 2002. Validated methods for sampling and headspace analysis of carbon monoxide in seawater. *Marine Chemistry*, 77(2-3), pp.93–108.

Yang, J.D. & Wang, N.S., 1992. Oxygen mass transfer enhancement via fermentor headspace pressurization. *Biotechnology Progress*, 8(3), pp.244–251.

Yuan, H. et al., 1998. Osteoinduction by calcium phosphate biomaterials. *Journal of Materials Science: Materials in Medicine*, 9(12), pp.723–726.

Zakkour, P. & Cook, G., 2010. *CCS Roadmap for Industry: High-purity CO_2 sources*,

Zhang, J. et al., 2006. Factors affecting the membrane performance in submerged membrane bioreactors. *Journal of Membrane Science*, 284(1-2), pp.54–66.

Zhao, Y., Cimpoia, R., Liu, Z. & Guiot, S., 2011. Kinetics of CO conversion into H_2 by *Carboxydothermus hydrogenoformans*. *Applied Microbiology and Biotechnology*, 91(6), pp.1677–1684.

Zhao, Y., Cimpoia, R., Liu, Z. & Guiot, S.R., 2011. Orthogonal optimization of *Carboxydothermus hydrogenoformans* culture medium for hydrogen production from carbon monoxide by biological water-gas shift reaction. *International Journal of Hydrogen Energy*, 36(17), pp.10655–10665.

Zhao, Y., Haddad, M., Cimpoia, R., Liu, Z. & Guiot, S.R., 2013. Performance of a *Carboxydothermus hydrogenoformans*-immobilizing membrane reactor for syngas upgrading into hydrogen. *International Journal of Hydrogen Energy*, 38(5), pp.2167–2175.

Zhao, Y., Haddad, M., Cimpoia, R., Liu, Z. & Guiot, S.R., 2013. Performance of a *Carboxydothermus hydrogenoformans*-immobilizing membrane reactor for syngas upgrading into hydrogen. *International Journal of Hydrogen Energy*, 38(5), pp.2167 – 2175.

Annexe 1: Performance of a *Carboxydothermus hydrogenoformans*-immobilizing membrane reactor for syngas upgrading into hydrogen

Ya Zhao[a,b], Mathieu Haddad[b,c], Ruxandra Cimpoia[b], Zhijun Liu[a], Serge R. Guiot[b,c]

[a] Faculty of Chemical, Environmental and Biological Engineering, Dalian University of Technology, Dalian 116012, P.R. China

[b] Bioengineering Group, Energy, Mining and Environment, National Research Council of Canada, 6100 Royalmount Avenue, Montreal, Quebec, Canada H4P 2R2

[c] Department of Microbiology, Infectiology and Immunology, Université de Montréal, Montreal, Canada H3C 3J7

Author contribution: RC and YZ designed the experiment; YZ and MH carried out the experimental work; RC, MH and SRG interpreted the results; MH and SRG wrote the manuscript.

Article status: This article was submitted for publication to International Journal of Hydrogen Energy on 13 June 2012, accepted on 6 November 2012 and published online 24 December 2012.

Zhao, Y., Haddad, M., Cimpoia, R., Liu, Z., & Guiot, S. R. (2013). Performance of a *Carboxydothermus hydrogenoformans*-immobilizing membrane reactor for syngas upgrading into hydrogen. *International Journal of Hydrogen Energy*, *38*(5), 2167 – 2175. doi:http://dx.doi.org/10.1016/j.ijhydene.2012.11.038

Keywords: *Carboxydothermus hydrogenoformans*, carbon monoxide; hydrogen; hollow fiber membrane; bioreactor; continuous; gas-liquid mass transfer; biofilm; fouling

ABSTRACT

Hydrogen conversion of CO by a pure culture of *Carboxydothermus hydrogenoformans* was investigated and optimized in a lab-scale hollow fiber membrane bioreactor (HFMBR). The reactor was operated under strict anaerobic, extremely thermophilic (70 °C) conditions with a continuous supply of gas, for four months. Reactor performance was evaluated under various operational conditions, such as liquid velocity (v_{liq}) (13, 65 and 130 m h^{-1}), temperature (70, 65, and 60 °C), CO pressure (from 1 to 2.5 atm) and CO loading rate (from 1.3 to 16.5 mol.L_{rxr}^{-1}.d^{-1}). Overall, results indicated a relatively constant H_2 yield of 92 ± 4% (mol mol^{-1}) regardless of the operational condition tested. Permeation across the colonized membrane was improved by three orders of magnitude as compared to the abiotic membrane, because of dissolved CO concentration was constantly maintained low in the liquid on the shell side of the membrane as continually depleted by the microorganisms. Once the biofilm was sufficiently developed, a maximum CO conversion activity of 0.44 $mol_{CO}.g^{-1}_{volatile\ suspended\ solid\ (VSS)}.d^{-1}$ was achieved at a p_{CO} of 2 atm or above and a v_{liq} of 65 m h^{-1}. However, this highest activity represented only 15% of the maximal activity potential of the strain under non-limiting conditions, attributed to the low concentration of dissolved CO (0.01–0.07 mM) present in the HFMBR liquid. Higher v_{liq} (130 m h^{-1}) produced shearing stress, which detached a significant portion of the biofilm from the membrane, and/or prevented less sessile growth (57% total biomass as biofilm, as opposed to 84–86% at lower v_{liq}). One may deduce from this work that the volumetric CO conversion performance of such a membrane bioreactor would be at the most in the range of 5 $mol_{CO}.L_{rxr}^{-1}.d^{-1}$. Overall, the CO conversion performance in the HFMBR was biokinetically limited, when not limited by gas–liquid mass transfer. Additionally, over time, membrane fouling and aging decreased membrane permeability such that the CO transfer rate would be the most limiting factor in the long run.

INTRODUCTION

Hydrogen, to be sustainable, has to be produced from renewable electricity (solar, wind, hydropower), or from biomass sources (Das & Veziroglu 2001; Balat & Kırtay 2010). Gasification of biomass and waste is a way to produce non-fossil hydrogen through high temperature (750–1500 °C) conversion of carbonaceous material into a synthesis gas (syngas) mainly composed of carbon monoxide (CO), carbon dioxide (CO_2) and hydrogen (H_2). The final calorific value of syngas, that is its H_2 to CO ratio, varies depending on the feedstock type used and gasification conditions (Song 2009; Rezaiyan & Cheremisinoff 2005). One typical way of achieving augmentation of the H_2 content of syngas in industry is through the use of the water–gas shift (WGS) reaction. In this process, steam reacts with carbon monoxide to produce carbon dioxide and hydrogen ($CO + H_2O \rightarrow CO_2 + H_2$). The WGS is catalyzed at either high temperatures (350–450 °C) using iron-based shift catalysts or at lower temperatures (160–250 °C) using copper-based shift catalysts. However these catalysts are highly intolerant to sulfur (Torres et al. 2007), especially copper-based catalysts being irreversibly poisoned by even small quantities of sulfur compounds (Newsome 1980). The sulfur content of syngas depends on the gasified material used. For instance, syngas derived from municipal solid waste (MSW) and sludge (Torres et al. 2007) can generate sulfur compounds in amounts which may inhibit the WGS reaction. Moreover, *in situ* pre-reduction steps for catalyst regeneration should also be considered (Milliken 2001). Finally, the process is energy-intensive, namely for steam generation.

Alternatively, biologically-mediated WGS reactions possess several advantages over conventional chemically mediated WGS mechanisms; such as enzyme specificity, improved yields, overall cost efficiency and environmental attractiveness (Mohammadi et al. 2011). Of interest to this study is the obligate anaerobic *Carboxydothermus hydrogenoformans* which was first isolated from a hot spring in Kunashir Island, Russia (Svetlichny et al. 1991). This extreme thermophilic bacillus uses CO as sole source of carbon and energy and catalyses the

WGS reaction. Interest in this organism in its ability to produce H_2 from CO has possible application in downstream syngas processes where elevated temperatures are probable.

The bioreactor technology selected must be able to process the syngas into a hydrogen-rich biogas at a continuous volumetric rate, in an efficient and cost-effective manner. In principle the higher the reactor cell density, the greater the volumetric bioconversion rate. However, since the main components of syngas are sparingly soluble, from a certain level of cell density, the gas-to-liquid mass transfer may become rate limiting. Most studies on fermentative hydrogen production conducted in continuous stirred tank reactor (CSTR) – due to its simple operation – have demonstrated performance limitations due to low biomass concentration and biomass wash out at short hydraulic retention times (HRT) (Wang & Wan 2009). Hence, using *C. hydrogenoformans* in a CSTR could be problematic, since growth is poor and would result in low concentrations of cell mass (Gerhardt et al. 1991). The culture however would not be prone to washout since the HRT could be kept high as feeding is gaseous. However gaseous feeding in a CSTR would require elevated pressure and stirring so that gas–liquid mass transfer is not limited; as such, a higher power consumption is envisioned with this process (Henstra et al. 2007).

The hollow fiber membrane bioreactor (HFMBR) represents an alternative solution to conventional fermentation reactors. In the HFMBR, gas fed at an elevated pressure at one end of the cartridge, is conveyed along the inside of the fibers, then diffuses laterally out through the fiber membrane then through the attached biofilm outside the fiber. Therefore in addition to providing a physical support for microbial immobilization, the microporous membranes in an HFMBR achieve gas–liquid contact through the fibers and offer a large gas–liquid interface area that may enhance gas–liquid mass transfer (Karoor & Sirkar 1993; Sun et al. 2008). On the other hand the use of a pure culture at high temperature and strictly anaerobic conditions are also significant challenges to the use of an HFMBR. Hence the objectives of the study are to analyze the advantages and disadvantages of using an HFMBR inoculated with *C. hydrogenoformans* for continuous conversion of carbon monoxide into hydrogen gas, by evaluating (a) the CO conversion efficiency, the H_2 yield and the gas–liquid mass transfer

efficacy of the HFMBR under various operational conditions, (b) the amount and distribution of biofilm growth within the reactor, and (c) the consequence of membrane aging and fouling.

MATERIALS AND METHODS

Bacterial strain and growth conditions

C. hydrogenoformans DSM6008 was obtained from the German Collection of Microorganisms and Cell Cultures, DSMZ (Deutsche Sammlung von Mikroorganismen und Zellkulturen GmbH, Braunschweig, Germany). The strain was cultivated in shake-culture at 100 rpm under strictly anaerobic conditions at 70 °C under 100% CO in a basal mineral medium buffered with bicarbonate-phosphate. The medium contained (in mg L^{-1} demineralized water): NH_4Cl (1000), $MgCl_2 \cdot 6H_2O$ (102), $CaCl_2 \cdot 2H_2O$ (15), $KH_2PO_4 \cdot H_2O$ (78), Na_2HPO_4 (74), $NaHCO_3$ (360), yeast extract (50), $Na_2S \cdot 9H_2O$ (700), $NiCl_2 \cdot 6H_2O$ (1), resazurin (0.05). The medium was then completed with 10 mL L^{-1} trace metals solution and 10 mL L^{-1} of vitamins solution as described by Stams (Stams et al. 1993). All solutions were autoclaved, except the calcium and magnesium stock solutions and vitamins solution, which were sterilized by filtration through 0.22 μm filter membranes. The initial pH was adjusted between 6.8 and 7.0.

Reactor set-up and operation

The reactor set-up included a hollow fiber membrane bioreactor (HFMBR) and devices for gas and nutrients supply and online monitoring (Figure 1). The HFMBR consisted of a cartridge including 100 hollow fibers (210 mm length, outer surface area of 9 cm^2) in polyvinyldenedifluoride (PVDF) (UMP-1047R, Pall, Ann Arbor, MI), as shown in Figure S1 (Supplementary content). The HFMBR had a working volume of 160 mL. The HFMBR cartridge was immersed in a custom-made temperature-controlled water bath (DP-41, Omega Engineering Inc, Stamford, CT USA). The feeding gas was supplied at elevated pressure at

one end of the cartridge and conveyed inside the fibers to diffuse through the fiber membrane, without gas recirculation. The gas loading and pressure was controlled by thermal mass flow meters (M100B, M10MB, 247D, MKS, Wilmington, MA, USA) linked to a computer, and two pressure gauges (Glass100, Dixon Valve & Coupling, Chestertown, MD). Possible oxygen contamination was eliminated by an oxygen trap (4003-Large oxy-trap column, Alltech Associates Inc, Deerfield, IL). The shell side of the HFMBR was fed (77300-50 Masterflex Pump, Cole-Parmer, Vernon Hills, IL, USA) through two lateral ports with a defined media solution for an average hydraulic retention time (HRT) of 16 days. Liquid was recirculated (77300-50 Masterflex Pump, Cole-Parmer, Vernon Hills, IL, USA) through the HFMBR in the opposite direction to the gas injection. The recirculation flow was controlled at given levels (77300-80 Masterflex Controller, Cole-Parmer, Vernon Hills, IL, USA). The recirculation loop traversed a custom-made glass–Teflon vessel, where pH of liquid was monitored and where the surplus gas was captured. The gas was released to the exhaust through a gasmeter (model L1, Wohlgroth SA, Schwerzenbach, CH). The liquid pressure in the HFMBR was monitored with a manometer (0-60PSI, US Gauge, Ira Township, MI, USA). The pH was controlled (PHP-194, Omega Engineering Inc, Stamford, CT; electrode 405-DPAS-SC-K8S, Mettler Toledo GmbH, Urdorf, CH) between 6.9 and 7.8 using either 0.1 M NaOH or 0.1 M HCl. The fiber membrane served as a support for the microbial population as well as an interface between the gas and liquid phases. The HFMBR was operated under anaerobic conditions at a temperature of 70 °C, with a continuous supply of gas (Praxair Canada Inc, Mississauga, ON, CA) whose CO content was adjusted using nitrogen. The variables were the CO partial pressure, temperature and the nutritional liquid velocity.

Analytical methods

The suspended solids (SS), volatile suspended solids (VSS), and chemical oxygen demand (COD) were determined according to Standard Methods (Eaton et al. 2005). The biomass concentration was quantified by measurements of the total COD of the suspension,

then converted into VSS using a factor of 1.37 g COD g^{-1} VSS according to the average elemental formula of $CH_{1.79}O_{0.5}N_{0.2}S_{0.005}$ for anaerobic bacteria (Roels 1983).

The gas composition (H_2, CO, CO_2) was measured by injecting 300 µL aliquot of gas (model 1750 gas-tight syringe, Hamilton, Reno, NV) into an HP 6890 gas chromatograph (Hewlett Packard, Palo Alto, CA) equipped with a thermal conductive detector (TCD) and a 11 m × 3.2 mm 60/80 mesh Chromosorb 102 packed column (Supelco, Bellafonte, PA). The column temperature was held at 60 °C for 7 min and increased to 225 °C at a rate of 60 °C per min. Argon was used as the carrier gas. The injector and detector were maintained at 125 °C and 150 °C respectively. The dissolved CO concentration (dCO) of liquid was estimated from the CO partial pressure in the headspace of the liquid sample-containing vial after equilibrium was reached at 90 °C (Henry's law), as described in the Supplementary content.

Volatile fatty acids (VFAs, i.e. acetic, propionic and butyric acids) were measured on an Agilent 6890 gas chromatograph (Wilmington, DE) equipped with a flame ionization detector (FID) on 0.2 µL samples diluted 1:1 (vol./vol.) with an internal standard of iso-butyric acid in 6% formic acid, directly injected on a glass column of 1 m × 2 mm Carbopack C (60–80 mesh) coated with 0.3% Carbowax 20 M and 0.1% H_3PO_4. The column was held at 130 °C for 4 min. Helium was the carrier gas fed at a rate of 20 mL min^{-1}. The injector and the detector were both maintained at 200 °C.

For measurement of solvents (methanol, ethanol, acetone, 2-propanol, tert-butanol, n-propanol, sec-butanol, n-butanol) 100 µL of liquid was transferred into a vial that had 20 mL of headspace and was closed with a crimped Teflon-coated septum. The vial was heated at 80 °C for 2 min, then 1000 µL of headspace gas were injected on a DB-ACL2 capillary column of 30 m × 530 mm × 2 µm using a Combipal autosampler (CTC Analytics AG, Zwingen, Switzerland). The column was held at 40 °C for 10 min. Helium was the carrier gas at a head pressure of 5 psi. The injector and the detector were maintained at 200 °C and 250 °C, respectively.

Pyruvate was monitored using a high-performance liquid chromatograph (HPLC) (pump model 600, autosampler model 717 plus, Waters Corp., Milford, MA) equipped with a

refractive index detector (Waters model 2414) connected to a photodiode array (PDA) detector (Waters model 2996). The separation was made on a Transgenomic ICSep IC ION-300 column (300 mm × 7.8 mm OD). The 0.01 NH_2SO_4 mobile phase had a flow rate of 0.4 ml min^{-1}. Analysis was carried out at 35 °C.

Pyruvate activity assessment

C. hydrogenoformans is able to grow on pyruvate as an alternative carbon and electron source to carbon monoxide (Svetlichny et al. 1991). Hence pyruvate can be used instead of CO, to evaluate the culture's bioactivity, without gas–liquid mass transfer of substrate can be limiting. The pyruvate-catabolizing activity of the cell suspension in the reactor circulating liquid was determined by measuring the rate of pyruvate depletion under substrate non-limiting conditions in a triplicate series of 120 mL serum bottles. Briefly after filled with reactor liquid, bottles were capped, sealed and flushed with N_2/CO_2 gas (80/20% vol./vol.) to establish anaerobic conditions, and placed in a rotary shaker (New Brunswick, Edison, NJ) in a dark, thermostatically controlled environment (70 ± 1 °C) and agitated at 100 rpm. The pyruvate solution was injected into all bottles to obtain an initial concentration of 3 g L^{-1}. Liquid samples were withdrawn from the bottles over time and their pyruvate concentration, measured. The specific activity was obtained by reporting the rate of substrate depletion to the VSS content measured in parallel in the reactor liquid.

The volumetric pyruvate activity of the reactor's attached biomass was measured on the entire HFMBR after the CO gas feeding was stopped and the liquid phase, drained out of the cartridge. The reactor was then operated in batch mode with a pyruvate-enriched medium (3 g L^{-1}) with mixing by internal liquid circulation. Liquid samples were withdrawn from cartridge's recirculation line over time and their pyruvate concentration, measured. The time course of substrate depletion allowed for the estimation of the reactor's pyruvate activity rate, using linear regression over the initial values following the lag time.

Scanning electron microscopy (SEM)

Pieces of biomass-immobilizing hollow fiber 1-cm long were rinsed twice in 1X PBS and then fixed in 2.5% glutaraldehyde in 0.1 M cacodylate buffer for 1 week. Samples were then dehydrated in increasing concentration of ethanol of 30, 50, 70, 80, 90, 95 and 100% for 15 min each. After dehydration with ethanol, further substitution to amyl acetate was carried out through graded baths of acetate:ethanol of 25:75, 50:50, 75:25, 100:0 for 15 min each. The samples were then dried using the critical point drying method in a CPD 030 (Leica Microsystems, Wetzlar, Germany) apparatus. Dried samples were then mounted on the SEM stubs with double side carbon tape and then sputter coated with a thin layer of Au–Pd. Sample examination was done using an S-4700 Hitachi FE-SEM (Tokyo, Japan) working under vacuum at an acceleration voltage of 2.0 kV. Elemental analysis of the hollow fiber membrane and the biofilm was carried out using a Hitachi S-3000N ESEM (Tokyo, Japan) operating at 15 kV and coupled to an Oxford INCA energy dispersive spectrometer (EDS) detector.

RESULTS

Volumetric CO removal performance of the HFMBR

Once inoculated with the *C. hydrogenoformans* pure culture 0.26 $g_{VSS}.Lrxr^{-1}$the HFMBR was operated under anaerobic conditions with a continuous supply of gas, and a constant liquid recirculation rate (Q_{liq}) of 150 mL min^{-1} corresponding to a liquid velocity (v_{liq}) of 13 m h^{-1}. The biofilm was gradually built up by increasing the volumetric rate of CO supply to the reactor (loading rate, Q_{CO}) continuously over 51 days (Phase I, Table 1). During this period, as Q_{CO} was increased from 0.02 to 2.64 mol d^{-1} and p_{CO}, from 0.2 to 2.5 atm, H_2 production rate followed the same pattern by increasing from 0.01 mol d^{-1} to 0.35 mol d^{-1}. From day 15, H_2 production yield ranged around 85 ± 13% whereas a maximum of 50% efficiency of CO consumption and metabolisation (E_{CO}) was obtained at a CO pressure (p_{CO}) of 1.0 atm. Augmenting CO loading resulted in a sharp decline in E_{CO} (14%) but in an increase of the volumetric removal activity. After 51 days of operation (last run of phase I, run 5),

volumetric bioactivity had reached 2.35 mol of CO consumed per liter of reactor and per day ($mol_{CO}.L_{rxr}^{-1}.d^{-1}$) for a Q_{CO} of 16.5 $mol.L_{rxr}^{-1}$. Although at this high Q_{CO}, E_{CO} was clearly limited by the volumetric bioactivity potential, we assumed that a biomass buildup was largely attained.

In the next phase (II), loading conditions were reset in the same range as before: p_{CO} of 2.0 atm and Q_{CO} of 4 $mol_{CO}.L_{rxr}^{-1}.d^{-1}$. This resulted in a volumetric rate of CO removal and consumption (R_{CO}) of 2 $mol_{CO}.L_{rxr}^{-1}.d^{-1}$ (E_{CO} 50%), which was lower than that of the previous step (run 5). This presumably indicates a transfer limitation likely due to the combined effect of reduced pressure and membrane aging. For the next run, a CO loading of 1.3 $mol_{CO}.L_{rxr}^{-1}.d^{-1}$ (p_{CO} 1.5 atm) was clearly limiting, resulting in an almost complete conversion of CO (E_{CO} 97.6 ± 1%). Then at a Q_{CO} of 7.2 $mol_{CO}.L_{rxr}^{-1}.d^{-1}$, gas–liquid transfer was still likely the limiting factor with an E_{CO} of 33%, although p_{CO} and R_{CO} were higher at 2.5 atm and 2.34 $mol_{CO}.L_{rxr}^{-1}.d^{-1}$, respectively. Another indication of limitation by mass transfer was the dCO concentrations which were quite literally zero (in comparison to higher values – 0.04 – 0.07 mM – at end of phase I – runs 3 – 5) (Table 1). Advantages and disadvantages of microporous membranes in a hollow fiber bioreactor for space applications.

Hence during phase III (runs 9 and 10), the liquid circulation rate has been increased from 150 to 750 then 1500 mL min^{-1} (corresponding to a v_{liq} of 65 and 130 m h^{-1}) in an attempt to improve the homogeneity of the gas distribution in the liquid phase and the CO availability to the biofilm and suspension microbes, since liquid flow velocity influences the boundary layer thickness and the diffusion rate at the biofilm liquid interface (Ruiz Careri 2005). This resulted in an improvement of R_{CO}, from 2.04 to 3.17 – 3.25 $mol_{CO}.L_{rxr}^{-1}.d^{-1}$ (as compared to run 6 with similar p_{CO} and Q_{CO}), with an E_{CO} at 68–69%. This means the gas–liquid transfer rate was improved and thus, the CO removal efficiency was limited by the reactor kinetics, i.e. the activity potential of the reactor's biomass. In the last runs (phase IV), the liquid flow was reset to 750 mL min^{-1}, since no significant difference was noticeable at a Q_{liq} of 1500 mL min^{-1} (run 10) as compared to the previous run (run 9). Yet in an attempt to further improve the CO availability to the microbes, the temperature was decreased from 70 to

60 °C to increase the solubility of CO, as *C. hydrogenoformans* is able to grow between 60 and 72 °C (Svetlichny et al. 1991). All other conditions were set at optima as obtained in previous phases. However E_{CO} rapidly dropped to 25%, with a R_{CO} of 0.9 $mol_{CO}.L_{rxr}^{-1}.d^{-1}$. It is thus obvious that the likely positive effect of higher CO dissolution and availability was offset by a significant decrease in the biological activity potential at lower temperature. A re-increase of temperature to 65 °C then 70 °C allowed for the biological removal potential to return to 2.5 $mol_{CO}.L_{rxr}^{-1}.d^{-1}$, with an E_{CO} at 67.5%.

Overall, these operation and performance changes had no impact on the hydrogen yield. The H_2 yield remained relatively constant from run 3 until the end at $92 \pm 4\%$ (mol mol^{-1}). Amongst the liquid metabolites, acetate and ethanol were the most significant; however their yields never exceeded 0.9 and 0.6% (mol mol^{-1} CO), respectively. Only traces of methanol, propionic acid and acetone were detected: maximum 23, 6.5 and 2.3 mg L^{-1}, respectively. Other potential metabolites (butyric acid, propanol, butanol) were never detected.

Biofilm development and growth

Conventional methods for biofilm measurement are usually based on invasive techniques (Joannis et al. 1998). Since no real-time sampling of the HFMR fiber was possible, a non-destructive method based on the volumetric and specific trophic activities was used. The volumetric activity of a culture is linearly proportional to the microorganism concentration in the culture when there are no growth limiting factors but the biomass itself. As *C. hydrogenoformans* is able to grow on pyruvate (Svetlichny et al. 1991), that substrate was used as the sole carbon and energy source to estimate the culture's activity rate, instead of CO, so the mass transfer could not be limiting. The pyruvate activity of the entire HFMBR's attached biomass was measured at the end of each experimental phase, at days 51, 77, 93, and 126 (Table 2), after the suspended biomass-containing liquid suspension was drained out of the cartridge and replaced with a pyruvate-containing medium. At the same time, the concentration of suspended biomass as well as its specific activity on pyruvate were measured on a representative sample of the liquid drained out of the HFMBR. Assuming that the activity

dependency of the attached cell to their density is similar to that of the cells in suspension, the amount of immobilized biomass was deduced from the volumetric pyruvate consumption rate of the reactor containing only the attached biomass, divided by the specific pyruvate activity of the suspended biomass. These estimates are then added to the direct measures of biomass in suspension in the liquid to give the total amount of biomass in the reactor at any given time. Results are summarized in Table 2. At the end of phase I the reactor contained a total of 7.61 $g_{VSS}.L_{rxr}^{-1}$. This therefore translates to an observed specific growth rate of 0.038 d^{-1} on average, considering a median biomass content of 3.8 $g_{VSS}.L_{rxr}^{-1}$and a cumulative biomass washout of 0.48 $g_{VSS}.L_{rxr}^{-1}$, over a time span of 51 d. Results also show that the immobilized biomass ratio remained constant at 84–86%, except at elevated liquid recirculation rates (Q_{liq} > 750 mL min^{-1}), where the biofilm proportion diminished to 57% at the benefit of the suspended biomass fraction. Hence v_{liq}, somewhere between 65 and 130 m h^{-1}, abraded the biofilm the detached cells of which simply remained in the liquid phase.

Scanning electron microscopy (SEM) was carried out on fiber samples from top, middle and bottom of the horizontally positioned cartridge after 4 months of operation. SEM images (Figure 2) showed a heterogeneous colonization of the membrane with higher populated areas at the top and bottom of the horizontal cartridge. Such heterogeneity of growth and distribution of *C. hydrogenoformans*, made it impossible to estimate a representative thickness of the biofilm formed on the HFMBR. In the most populated regions of the fibers, multilayer biofilms are clearly observed, with mushroom-shaped microcolonies, typical of laboratory biofilms grown under low laminar flow conditions (Sauer 2003; Karatan & Watnick 2009; Stoodley et al. 2002). The middle section was not as well colonized as the other parts and the shape of the colonies were more flattened compared to the colonies of the top and bottom of the horizontal cartridge. This is related to the fact that the linear flow of liquid and distribution of substrate and nutrient were likely uneven radially across the cartridge, considering the central fibers packing was a little denser and there was more void volume at the periphery than at the center of the cartridge (Figure S1, Supplementary content). In contrast, the longitudinal distribution of populations was relatively even (not shown).

Material balances processed on data cumulated over the entire experiment allowed for the estimation of the average rates of biomass true growth and decay, at 0.29 and 0.25 d^{-1}, respectively (Table 3). This relatively high microbial decay rate is linked to the extremely thermophilic conditions (70 °C), but also to the long solid retention time (SRT) typical of membrane bioreactors. Given an average amount of 7.3 $g_{VSS}.L_{rxr}^{-1}$ in the reactor and an average biomass washout rate of 0.054 $g_{VSS}.L_{rxr}^{-1}.d^{-1}$, the biomass SRT or age was in the range of 135 days. Endogenous respiration and microbial decay are exacerbated when the SRT is high, especially at high temperature. This is consistent with the reduction of the specific activity of the suspended biomass in the reactor (between 0.301 and 0.229 mol pyruvate $g^{-1}.VSS.d^{-1}$, Table 2) as compared with that of the fresh culture used as inoculum (0.447 ± 0.008 $mol_{pyruvate}.g^{-1}.VSS.d^{-1}$ at 70 °C). This activity difference would correspond to a suspended biomass content comprised of dead cells, cell debris, and other inert material, ranging between 33 and 49%. Other factors could also contribute to elevate the decay rate such as: the substrate limiting concentration (dissolved CO, most of the time measured between 0.01 and 0.07 mM); a potential deficiency in nutrients, related to the high HRT (ca. 16 days); and the toxicity potential of soluble microbial products (SMP, secondary metabolites and cell lysis products), the accumulation of which relates to both high HRT and SRT (Barker & Stuckey 1999).

The pyruvate-activity-based biofilm quantification was compared to the direct biomass-VSS measurement at the end of the experiment. The dismantled hollow fibers were sonicated during 24 h in distilled water to peel off the biofilm from the fibers, then total VSS, quantitated on the sonication liquid. The difference is slight, but significant (950 ± 44 mg VSS against 819 ± 17, i.e. 16%). This difference may be attributed to extracellular polymeric substances (EPS) likely less abundant in suspended biomass, and not accounted for in the indirect estimate of biofilm based on pyruvate activities, while the proportion of inactive or dead cells and cell debris would be similar in the attached and the suspended biomass. Therefore those EPS would amount to 130 mg/reactor, i.e. 14% of total attached biomass.

Results on biomass content of the reactor also allowed for estimating the actual specific rate of CO conversion in the reactor (Table 2). The highest value (0.44 $mol_{CO}.g^{-1}{}_{VSS}.d^{-1}$) occurred in phase III, where the gas–liquid transfer rate was improved at the highest liquid circulation flow rate, and biomass activity was the rate-limiting factor.

CO permeation and transfer rates

The highest volumetric CO transfer rate (k_La) measured on the abiotic reactor was 1.36 h^{-1} and observed at a p_{CO} of 2 atm and a v_{liq} of 130 m h^{-1} (details in the Supplementary content). This is comparable to data reported in the literature (Munasinghe & Khanal 2010). The immediate CO depletion by microorganisms present on the liquid side of the membrane maintained low dCO as measured (Table 1). This typically creates higher concentration gradients across the membrane, thereby accelerating gas diffusion at the liquid–membrane interface and CO transfer across the membrane or CO permeation (Ruiz Careri 2005). This was confirmed by the comparison of the CO permeance of the virgin membrane with that of the colonized fiber. The permeance reports the CO permeation rate to the total membrane surface area of the cartridge and the transmembrane pressure (TMP) i.e. the pressure difference on either side of the membrane. The permeance of the virgin membrane has been estimated at $1.59.10^{-12}$ $mol.m^{-2}.s^{-1}.Pa^{-1}$ (Supplementary content) or 0.0057 $mmol.m^{-2}.h^{-1}.kPa^{-1}$. The biotic membrane permeance to CO was assessed at each run of the experiment; the data were then plotted as a function of the actual TMP, in parallel to the operation time, i.e. the lifetime of the membrane (Figure 3). During phase I (lifetime < 51 d), the permeance ranged between 7.63 and 1.13 $mmol.m^{-2}.h^{-1}.kPa^{-1}$ (median value 3.35). This is an improvement by three orders of magnitude as compared to the abiotic membrane. However, during the subsequent phases, the permeance of the biotic membrane diminished with the operation time, ranging from 3.00 to 0.67 $mmol.m^{-2}.h^{-1}.kPa^{-1}$ (median value 1.95) between 72 and 111 days, to reach the lowest value at the end (day 126: 1.215 $mmol.m^{-2}.h^{-1}.kPa^{-1}$), albeit still quite higher than those of the abiotic membrane. As expected, this flux decline was caused by two factors, membrane fouling and aging.

DISCUSSION

Membrane biofouling is the main factor that typically explains the reduced membrane permeance over time. However in this case, the biofilm was not the key factor *per se*, since biofilm was likely mature between Phases I and II, and a decrease in membrane permeance was not observable at this time. Furthermore the membrane surface area was not colonized in totality. Nevertheless membrane fouling results also from complex interactions between the membrane material and various extracellular components associated with the medium and the culture, whether suspended or attached. The latter include extracellular polymeric substances (EPS) and other products produced in biofilms on the membrane surface. Other foulants include products of bacterial lysis, biocolloids, secondary metabolites and minerals from the growth medium. The deposition of these substances onto the membrane or their adsorption into the membrane pores reduce membrane porosity or clog the pores and lead to a decline in the filtration and permeation capacity and eventual inoperability of the membranes (Bouhabila 2001; Miura et al. 2007; Sombatsompop et al. 2006; Zhang et al. 2006; Liu et al. 2007). Therefore, facts that EPS accounted for a significant portion of the biofilm (at least 14%) and biomass decay rate was high are consistent with the permeance decrease observed and explained by biofouling. Another key factor contributing to permeance reduction is membrane aging, and is linked to the material's inherent lifetime, which is especially an issue when operating in extremely thermophilic conditions as in this study. In general, the lifetime of hollow fiber membranes varies from 30 days to 4 months, according to the literature (Bouhabila 2001; Zhang et al. 2006; Huang et al. 2008; Chang et al. 2002).

Regarding to the CO conversion, after the biofilm had sufficiently developed and matured, phase III conditions, with p_{CO} at or above 2 atm, and v_{liq} at 65 m h^{-1}, seemed to be optimal for maximizing the HFMBR performance. Higher v_{liq} (130 m h^{-1}) produced a higher

shearing stress, which detached a significant portion of the biofilm from the membrane, and/or prevented less sessile growth. This is also consistent with less colonization of the central fibers, where they seem tighter with less void volume, resulting in a greater shear. The flattened shape of the central colonies is consistent with previous observations that at high hydrodynamic shear, the biofilm, which acts as a viscoelastic liquid, shows an elongated shape in the liquid flow direction and forms filamentous streamers (Stoodley et al. 1999). Interestingly, once the liquid flow was set back to the initial velocity, the immobilized biomass ratio was restored to 84% regardless of other condition variations. This indicates that *C. hydrogenoformans* prefers sessile growth, as most bacterial strains which usually are gaining a higher resilience within biofilms (Stoodley et al. 2002).

These optimal conditions also yielded highest volumetric and specific CO conversion activities. However, this highest activity, at 0.44 $mol_{CO}.g^{-1}{}_{VSS}.d^{-1}$, is far from the maximal activity rate usually reported in the literature at optimal substrate concentration (Zhao et al. 2011) i.e. ca. 3 $mol_{CO}.g^{-1}{}_{VSS}.d^{-1}$. This is related to the low concentration of dissolved CO, as actually measured most of the time (0.01–0.07 mM) in the HFMBR liquid. Overall then, when the CO conversion performance of HFMBR is not limited by gas–liquid mass transfer, it is kinetically limited by the actual substrate concentration in the liquid.

CONCLUSION

In summary, considering that the highest amount of biomass retained in the reactor would be around 10 $g_{VSS}.L_{rxr}$-1, with a potential bioactivity rate limited at around 0.5 $mol_{CO}.g^{-1}{}_{VSS}.d^{-1}$, one may deduce from this work that the volumetric CO conversion performance of such a membrane bioreactor would be at the most in the range of 5 $mol_{CO}.L_{rxr}{}^{-1}.d^{-1}$. Furthermore although *C. hydrogenoformans* showed good performances (H_2 yield, bioactivity potential), membrane fouling and aging affected the membrane permeability and the CO transfer rate to such an extent that this could potentially become the most

detrimental limitation for higher and sustained syngas loading rates in the long run in an HFMBR system. Overall this experimental study demonstrated the feasibility of CO fermentation in an HFMBR and quantified key parameters which characterize the process, such as product yields, biomass growth and decay rates, biomass accumulation capacity, mass transfer and bioconversion specific rates. Such data would be instrumental, should a mathematical model be developed for process optimization and techno-economical feasibility assessment.

ACKNOWLEDGEMENTS

The authors wish to thank M.-F. Manuel, C. Beaulieu, A. Corriveau and S. Deschamps for their assistance and discussions. One of the authors (Y.Z.) was supported by the Canada NRC-China MOE Research and Post-doctoral Fellowship Program, and another (M.H.), by the Natural Sciences and Engineering Research Council of Canada (grant 185778-2009). NRCC paper No. 55026.

REFERENCES

Balat, H., & Kırtay, E. (2010). Hydrogen from biomass – Present scenario and future prospects. *International Journal of Hydrogen Energy*, *35*(14), 7416–7426. doi:10.1016/j.ijhydene.2010.04.137

Barker, D. J., & Stuckey, D. C. (1999). A review of soluble microbial products (SMP) in wastewater treatment systems. *Water Research*, *33*(14), 3063–3082. doi:10.1016/S0043-1354(99)00022-6

Bouhabila, E. (2001). Fouling characterisation in membrane bioreactors. *Separation and Purification Technology*, *22-23*(1-2), 123–132. doi:10.1016/S1383-5866(00)00156-8

Chang, I.-S., Le Clech, P., Jefferson, B., & Judd, S. (2002). Membrane Fouling in Membrane Bioreactors for Wastewater Treatment. *Journal of Environmental Engineering*, *128*(11), 1018–1029. doi:10.1061/(ASCE)0733-9372(2002)128:11(1018)

Das, D., & Veziroglu, T. N. (2001). Hydrogen production by biological processes: a survey of literature. *International Journal of Hydrogen Energy*, *26*(1), 13–28. doi:10.1016/S0360-3199(00)00058-6

Eaton, A., Clesceri, L., Rice, E., & Greenberg, A. (2005). *Standard methods for the examination of water and wastewater* (21st ed.). Washington, D.C.: American Public Health Association, American Water Works Association, Water Environment Federation.

Gerhardt, M., Svetlichny, V., Sokolova, T. G., Zavarzin, G. A., & Ringpfeil, M. (1991). Bacterial CO utilization with H_2 production by the strictly anaerobic lithoautotrophic thermophilic bacterium *Carboxydothermus hydrogenus* DSM 6008 isolated from a hot swamp. *FEMS Microbiology Letters*, *83*(3), 267–271.

Henstra, A. M., Sipma, J., Rinzema, A., & Stams, A. J. M. (2007). Microbiology of synthesis gas fermentation for biofuel production. *Current Opinion in Biotechnology*, *18*(3), 200–6. doi:10.1016/j.copbio.2007.03.008

Huang, L.-N., De Wever, H., & Diels, L. (2008). Diverse and Distinct Bacterial Communities Induced Biofilm Fouling in Membrane Bioreactors Operated under Different Conditions. *Environmental Science & Technology*, *42*(22), 8360–8366. doi:10.1021/es801283q

Joannis, C., Delia, M. L., & Riba, J. P. (1998). Comparison of four methods for quantification of biofilms in biphasic cultures. *Biotechnology Techniques*, *12*(10), 777–782. doi:10.1023/A:1008835811731

Karatan, E., & Watnick, P. (2009). Signals, regulatory networks, and materials that build and break bacterial biofilms. *Microbiology and Molecular Biology Reviews : MMBR*, *73*(2), 310–47. doi:10.1128/MMBR.00041-08

Karoor, S., & Sirkar, K. K. (1993). Gas absorption studies in microporous hollow fiber membrane modules. *Industrial & Engineering Chemistry Research*, *32*(4), 674–684. doi:10.1021/ie00016a014

Liu, H., Yang, F., Wang, T., Liu, Q., & Hu, S. (2007). Carbon membrane-aerated biofilm reactor for synthetic wastewater treatment. *Bioprocess and Biosystems Engineering*, *30*(4), 217–24. doi:10.1007/s00449-007-0116-1

Milliken, J. (2001). Alternative catalysts offer high activity , low cost Contacts, (April).

Miura, Y., Watanabe, Y., & Okabe, S. (2007). Membrane Biofouling in Pilot-Scale Membrane Bioreactors (MBRs) Treating Municipal Wastewater: Impact of Biofilm Formation. *Environmental Science & Technology*, *41*(2), 632–638. doi:10.1021/es0615371

Mohammadi, M., Najafpour, G. D., Younesi, H., Lahijani, P., Uzir, M. H., & Mohamed, A. R. (2011). Bioconversion of synthesis gas to second generation biofuels: A review. *Renewable and Sustainable Energy Reviews*, *15*(9), 4255–4273. doi:http://dx.doi.org/10.1016/j.rser.2011.07.124

Munasinghe, P. C., & Khanal, S. K. (2010). Syngas fermentation to biofuel: evaluation of carbon monoxide mass transfer coefficient (kLa) in different reactor configurations. *Biotechnology Progress*, *26*(6), 1616–21. doi:10.1002/btpr.473

Newsome, D. S. (1980). The Water-Gas Shift Reaction. *Catalysis Reviews*, *21*(2), 275–318. doi:10.1080/03602458008067535

Rezaiyan, J., & Cheremisinoff, N. P. (2005). *Gasification technologies: a primer for engineers and scientists*. Portland, OR: Boca Raton: Taylor & Francis.

Roels, J. A. (1983). *Energetics and kinetics in biotechnology*. Elsevier Biomedical Press.

Ruiz Careri, M. N. (2005). *Advantages and disadvantages of microporous membranes in a hollow fiber bioreactor for space applications*. Texas Tech University.

Sauer, K. (2003). The genomics and proteomics of biofilm formation. *Genome Biology*, *4*(6), 219. doi:10.1186/gb-2003-4-6-219

Sombatsompop, K., Visvanathan, C., & Ben Aim, R. (2006). Evaluation of biofouling phenomenon in suspended and attached growth membrane bioreactor systems. *Desalination*, *201*(1-3), 138–149. doi:10.1016/j.desal.2006.02.011

Song, C. (2009). Introduction to Hydrogen and Syngas Production and Purification Technologies. In *Hydrogen and Syngas Production and Purification Technologies* (pp. 1–13). John Wiley & Sons, Inc. doi:10.1002/9780470561256.ch1

Stams, A. J., Van Dijk, J. B., Dijkema, C., & Plugge, C. M. (1993). Growth of syntrophic propionate-oxidizing bacteria with fumarate in the absence of methanogenic bacteria. *Applied and Environmental Microbiology*, *59*(4), 1114–1119.

Stoodley, P., Lewandowski, Z., Boyle, J. D., & Lappin-Scott, H. M. (1999). Structural deformation of bacterial biofilms caused by short-term fluctuations in fluid shear: an in situ investigation of biofilm rheology. *Biotechnology and Bioengineering*, *65*(1), 83–92.

Stoodley, P., Sauer, K., Davies, D. G., & Costerton, J. W. (2002). Biofilms as complex differentiated communities. *Annual Review of Microbiology*, *56*, 187–209. doi:10.1146/annurev.micro.56.012302.160705

Sun, X., Meng, F., & Yang, F. (2008). Application of seawater to enhance SO2 removal from simulated flue gas through hollow fiber membrane contactor. *Journal of Membrane Science*, *312*(1-2), 6–14. doi:10.1016/j.memsci.2007.12.011

Svetlichny, V. A., Sokolova, T. G., Gerhardt, M., Kostrikina, N. A., & Zavarzin, G. A. (1991). Anaerobic Extremely Thermophilic Carboxydotrophic Bacteria in Hydrotherms of Kuril Islands Light Microscopy, 1–10.

Torres, W., Pansare, S. S., & Goodwin, J. G. (2007). Hot Gas Removal of Tars, Ammonia, and Hydrogen Sulfide from Biomass Gasification Gas. *Catalysis Reviews*, *49*(4), 407–456. doi:10.1080/01614940701375134

Wang, J., & Wan, W. (2009). Factors influencing fermentative hydrogen production: A review. *International Journal of Hydrogen Energy*, *34*(2), 799–811. doi:10.1016/j.ijhydene.2008.11.015

Zhang, J., Chua, H. C., Zhou, J., & Fane, A. G. (2006). Factors affecting the membrane performance in submerged membrane bioreactors. *Journal of Membrane Science*, *284*(1-2), 54–66. doi:10.1016/j.memsci.2006.06.022

Zhao, Y., Cimpoia, R., Liu, Z., & Guiot, S. (2011). Kinetics of CO conversion into H_2 by *Carboxydothermus hydrogenoformans*. *Applied Microbiology and Biotechnology*, *91*(6), 1677–1684. doi:10.1007/s00253-011-3509-7

FIGURES

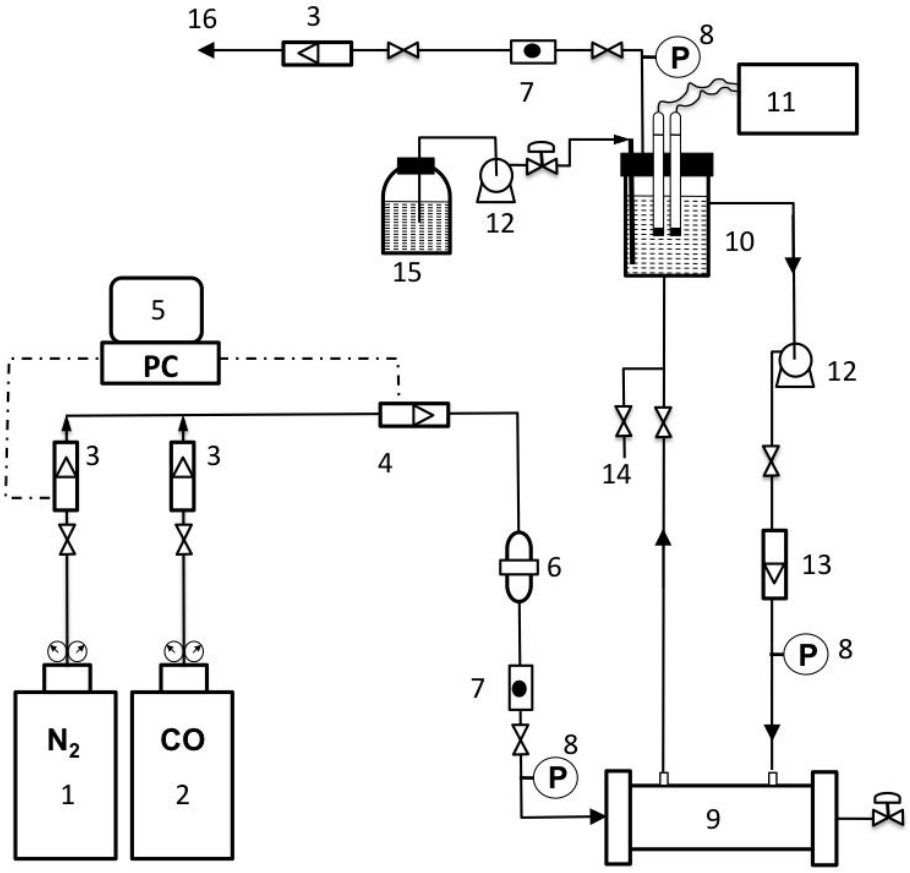

Figure 1: Schematic representation of the HFMBR set-up used for hydrogen production from CO. 1 – N_2 gas cylinder; 2 – CO gas cylinder; 3 – gas flow meter; 4 – pressure controller; 5 – gas composition controller; 6 – oxygen trap; 7 – gas sampling; 8 – pressure gauge; 9 – hollow fiber cartridge (Fig. S1, Supplementary content); 10 – liquid tank; 11 – pH and temperature sensors; 12 – peristaltic pump; 13 – liquid flow meter; 14 – liquid sampling; 15 – defined medium; 16 – venting.

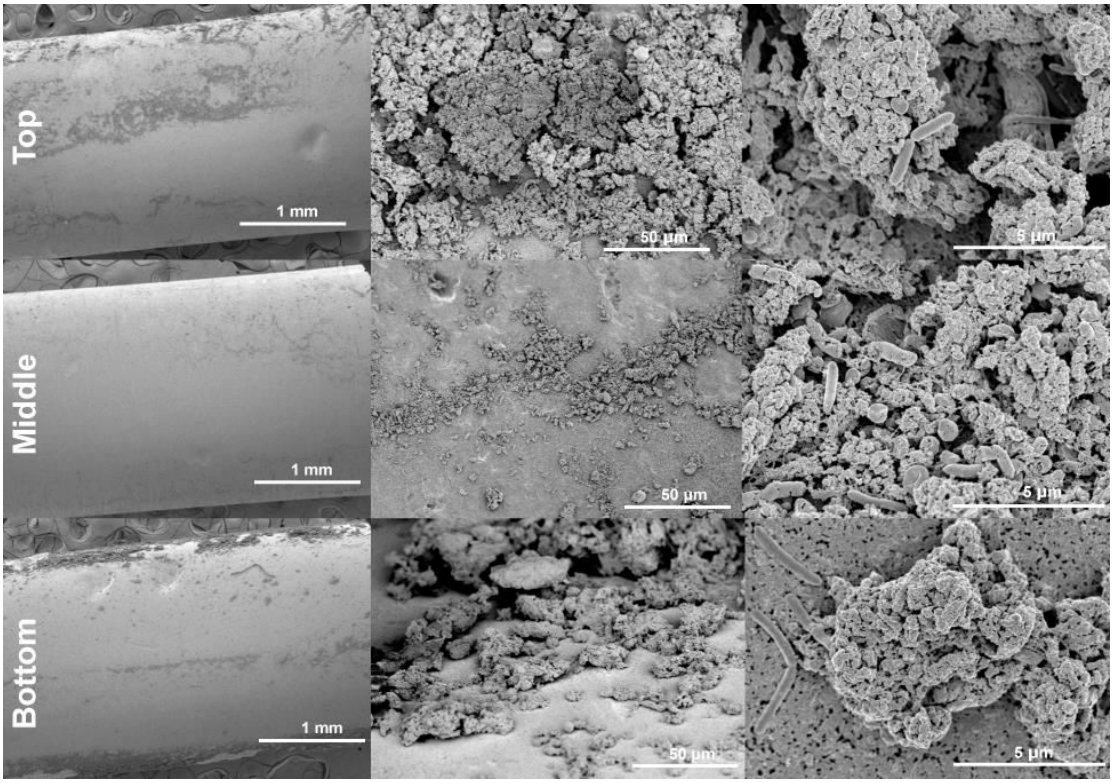

Figure 2: Scanning electron microscopy (SEM) images of *C. hydrogenoformans* biofilm grown on the hollow fiber membrane at various locations in the reactor, after 4 months of reactor continuous operation.

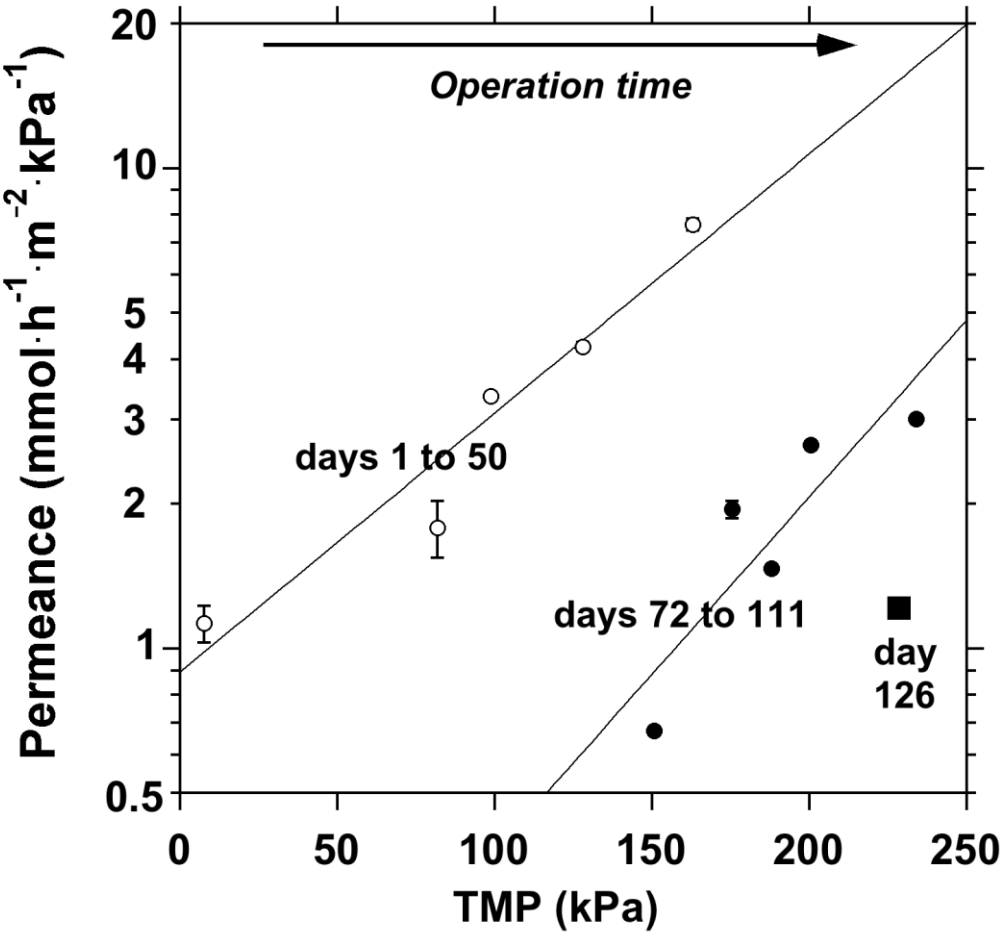

Figure 3: Effect of the transmembrane pressure (TMP) and membrane aging on CO permeance in the biotic hollow fiber membrane bioreactor (HFMBR).

Phase	Run		Temp.	v_{liq}	p_{CO}	Q_{CO} *	R_{CO} *	E_{CO} *	Y_{H2} *	dCO
	#	d	°C	$m \cdot h^{-1}$	atm	$mol \cdot L_{rxr}^{-1} \cdot d^{-1}$	mol $CO \cdot L_{rxr}^{-1} \cdot d^{-1}$	%	%	$mmol \cdot L^{-1}$
I biofilm build up	1	1-11	70	13	0.2	0.12 ±0.01	0.02 ±0	18.0 ±1.2	n.d.	0.12 ±0.01
	2	18-23	70	13	1.0	1.89 ±0.25	1.00 ±0.07	50.4 ±8.6	78.4 ±12.8	0.28 ±0.23
	3	29-33	70	13	1.5	4.39 ±0.10	1.13 ±0.02	25.4 ±0.4	86.0 ±6.7	0.04 ±0.03
	4	36-38	70	13	2.0	7.31 ±0.17	1.60 ±0.02	21.1 ±0.6	88.4 ±1.4	0.06 ±0.06
	5	47-51	70	13	2.5	16.53 ±0.76	2.35 ±0.1	13.7 ±0.3	88.9 ±2.2	0.07 ±0.05
II mature biofilm varying Q_{CO}	6	65-68	70	13	2.0	4.01 ±0.12	2.04 ±0.06	49.7 ±1.5	92.3 ±2.4	0.01 ±0.01
	7	71-72	70	13	1.5	1.31 ±0.07	1.33 ±0.01	97.6 ±1.2	85.7 ±1.5	0.00 ±0.00
	8	74-77	70	13	2.5	7.19 ±0.05	2.34 ±0.02	32.6 ±0.1	96.6 ±0.3	0.00 ±0.00
III varying v_{liq}	9	84-85	70	65	2.0	4.58 ±0.19	3.17 ±0.3	68.2 ±0.4	89.1 ±1.2	0.04 ±0.04
	10	86-93	70	130	2.0	4.69 ±0.04	3.25 ±0.17	69.3 ±3.3	92.3 ±4.3	0.05 ±0.01
IV varying temperature	11	108-111	60	65	2.5	3.72 ±0.02	0.91 ±0.02	24.5 ±0.5	93.3 ±5.4	0.42 ±0.53
	12	112-117	65	65	2.5	3.77 ±0.02	2.34 ±0.02	62.2 ±0.6	93.1 ±2.1	n.d.
	13	122-126	70	65	2.5	3.72 ±0.05	2.49 ±0.03	67.5 ±0.8	92.1 ±2.0	n.d.

Table 1: Performance of the hollow fiber membrane bioreactor (HFMBR) as a function of the operational time and conditions. v_{liq}, liquid velocity; Q_{CO}, volumetric CO loading rate; E_{CO}, CO conversion efficiency; R_{CO}, volumetric CO removal rate; Y_{H2}, hydrogen yield from CO ($mol\ mol^{-1}$); dCO, dissolved CO concentration; n.d., not determined. [a] Averages ± standard deviation

Phase	Time (phase end)	v_{liq}	Pyruvate activity		Suspended biomass[a]	Attached biomass[b]		Total biomass	Biofilm/ total biomass	In-reactor specific activity
			Overall reactor attached biomass	Biomass in suspension in the reactor liquid						
	d	$L \cdot h^{-1}$	$mol \cdot d^{-1}$	$mol \cdot g^{-1}$ VSS$\cdot d^{-1}$	mg VSS	mg VSS	g VSS$\cdot m^{-2}$	g VSS$\cdot L_{rxr}^{-1}$	%	mol CO$\cdot g^{-1}$ VSS$\cdot d^{-1}$
I	51	13	0.234	0.229 ±0.010	195 ±10	1021 ±51	11.4 ±0.6	7.61	84	0.31
II	77	13	0.345	0.301 ±0.001	180 ±9	1119 ±56	12.4 ±0.6	8.12	86	0.29
III	93	130	0.191	0.284 ±0.02	515 ±26	672 ±47	7.5 ±0.5	7.42	57	0.44
IV	126	65	0.245	0.3 ±0.02	159 ±8	819 ±41	9.1 ±0.5	6.1	84	0.41
	133			Direct biomass quantification		950 ±44	10.6 ±0.5			

Table 2: Biomass content of reactor and biomass profile and specific activity at the end of each operational phase of the HFMBR. [a] directly measured in the drained liquid; ± standard deviation. [b] indirectly estimated, by dividing the reactor pyruvate activity by the suspension pyruvate specific activity; ± standard deviation

Parameter	Average or cumulative value[a]
Y_{H2} (%, mol $H_2 \cdot mol^{-1}$ CO consumed)	90.5 ±3.4
$Y_{acetate}$ (%, mol acetate$\cdot mol^{-1}$ CO consumed)	0.11 ±0.21
$Y_{ethanol}$ (%, mol ethanol$\cdot mol^{-1}$ CO consumed)	0.03 ±0.04
$Y_{X/CO}$ (g VSS$\cdot mol^{-1}$ CO consumed) [b]	1.19
Cumulative CO consumed (mol$\cdot L_{rxr}^{-1}$)	204
Cumulative biomass formed (g VSS$\cdot L_{rxr}^{-1}$) [c]	243
Cumulative biomass washout (g VSS$\cdot L_{rxr}^{-1}$)	6.8
Reactor content in biomass (at end of experiment) (g VSS$\cdot L_{rxr}^{-1}$)	6.1
Observed growth rate (averaged over phase I) (d^{-1}) [d]	0.038
Decay rate (d^{-1}) [e]	0.25
True growth rate (d^{-1}) [f]	0.29

Table 3: CO conversion yield and kinetics data of the HFMBR, based on averages or cumulative balances.

[a] over 126 days, unless otherwise indicated; ± standard deviation.

[b] $Y_{X/CO} = 0.5 \cdot (1 - Y_{H2}/100 - Y_{acetate}/100) \cdot 12/0.47$ with 0.5 C-mol fixed into biomass per mol CO assimilated (i.e. not consumed for H_2/acetate production) (Zhao et al. 2011), 12, the molecular weight of carbon (g$\cdot mol^{-1}$ C), and 0.47, the carbon fraction of biomass (g C$\cdot g^{-1}$ VSS) (Roels 1983).

[c] cumulated CO consumed multiplied by $Y_{X/CO.}$ [d] estimated from total VSS accumulated in reactor and cumulative VSS washout, over a time span of 56 days, and considering a median biomass content of 3.8 g VSS$\cdot L_{rxr}^{-1}$

[e] cumulative biomass formed, substracted by the final biomass content of the reactor and the cumulated biomass washout, and divided by the average biomass content of the reactor and the time span (126 d)

[f] observed growth plus decay rate

Annexe 2: Performance of a *Carboxydothermus hydrogenoformans*-immobilizing membrane reactor for syngas upgrading into hydrogen - Supplementary content

Ya Zhao[a,b], Mathieu Haddad[b,c], Ruxandra Cimpoia[b], Zhijun Liu[a], Serge R. Guiot[b,c]

[a] Faculty of Chemical, Environmental and Biological Engineering, Dalian University of Technology, Dalian 116012, P.R. China

[b] Bioengineering Group, Energy, Mining and Environment, National Research Council of Canada, 6100 Royalmount Avenue, Montreal, Quebec, Canada H4P 2R2

[c] Department of Microbiology, Infectiology and Immunology, Université de Montréal, Montreal, Canada H3C 3J7

Author contribution: RC and YZ designed the experiment; YZ and MH carried out the experimental work; RC, MH and SRG interpreted the results; MH and SRG wrote the manuscript.

Article status: This article was submitted for publication to International Journal of Hydrogen Energy on 13 June 2012, accepted on 6 November 2012 and published online 24 December 2012.

Zhao, Y., Haddad, M., Cimpoia, R., Liu, Z., & Guiot, S. R. (2013). Performance of a Carboxydothermus hydrogenoformans-immobilizing membrane reactor for syngas upgrading into hydrogen. International Journal of Hydrogen Energy, 38(5), 2167 – 2175. doi:http://dx.doi.org/10.1016/j.ijhydene.2012.11.038

BIOREACTOR DESCRIPTION

The hollow fiber membrane bioreactor (HFMBR) consisted of a cartridge (UMP-1047R, Pall, Ann Arbor, MI) where 100 hollow fibers in polyvinyldenedifluoride (PVDF) (Asahi Kasei, Tokyo, JP) were bundled and potted within a housing as shown in Figure S1. Two inlet and outlet ports allowed fluid feeding to the lumen side of all the hollow fibers which were manifolded at both ends of the fiber bundle, as well as two lateral ports, for fluid feeding to the shell side. The working volume on the shell side amounted to 160 mL. Each hollow fiber had a nominal pore size of 0.2 µm, an inner and outer diameter of 0.8 and 1.4 mm, respectively, a useful length of 210 mm, and an outer surface area of 9 cm^2.

Figure S1: Hollow fiber cartridge. A. Lateral external view. B. Cross-sectional view of an end.

METHOD FOR DISSOLVED CARBON MONOXIDE ANALYSIS IN CULTURE MEDIUM

The method that was developed to measure the dissolved CO concentration (dCO) is based on the principle that the amount of CO dissolved in the liquid at equilibrium is proportional to the partial pressure of the gas above the surface of the solution (Henry's law). The CO displacement from the sample liquid to the headspace gas phase of a sealed vial is

facilitated by elevated temperature such as 90ºC. Ten minutes were required to make sure that gas-liquid equilibrium was reached at 90ºC. The vials were pre-tared, both empty and fully filled with water, including stopper and cap. An approximate 4.5 mL volume of liquid culture medium to be tested was transferred with a gas-tight syringe into a 6 mL gas-tight glass vial. The vial was then sealed promptly with a gray rubber stopper and an aluminum cap and weighted. The difference between this weight and empty tare and filled tare determined accurately the liquid sample volume (V_{SL}, mL) and the headspace volume (V_{HS}, mL), respectively. The vials were then placed in a 90°C thermostatic water bath during 10 min. Afterwards the CO content in the headspace gas was determined by GC either as $p_{CO/HS}$ (atm), or as $C_{CO/HS}$ (mg CO.L^{-1} headspace). The residual dCO concentration in the vial's liquid sample was calculated from $p_{CO/HS}$ using the Henry's law constant of CO at 90°C for the culture medium, i.e. 2511 atm.L.mol^{-1}, as estimated by the methodology detailed in the next paragraphs, and the molecular weight of CO (MW_{CO} = 28 g.mol^{-1}). The sum of the CO contents in both liquid and gas volumes of the vial yields thus the original dCO in the medium, which is summarized as follows:

$$dCO_{medium}[mol \times L^{-1}] = \frac{p_{CO/HS}\ [atm]}{2521\ [atm \times L \times mol^{-1}]} + \frac{V_{HS}[mL] \times C_{CO/HS}[mg \times L^{-1}]}{V_{SL}[mL] \times MW_{CO}[g \times mol^{-1}] \times 1000\ [mg \times g^{-1}]}$$

Values of the Henry's law constant are easily available from classical handbooks (Lide Frederikse, H.P.R., 1995; Perry , Green, Don W., Maloney, James O., 1984), however those data only apply to pure water or solvent or very dilute solutions. For the above-developed headspace method to be accurate, the actual value of the Henry's law constant for the buffer solution or the defined medium in which dCO has to be assessed is needed. To do so defined medium was saturated by 100% CO at 35ºC. Nine mL samples of saturated medium were transferred into 12 mL vials according to the above protocol, except that the vials were heated at 100ºC. At this temperature, it is assumed that CO is almost completely stripped out from the liquid phase to the headspace gas phase, because of the low CO solubility at 100ºC (0.0025 g.L^{-1} or 0.09 mM i.e. 10% of solubility product at 35ºC) and the strong stripping effect of

water vapors. The vial's headspace gas is analyzed by GC, and the resulting CO content of gas, multiplied by V_{HS} and divided by V_{SL}, yields the dCO concentration of medium at 35ºC, from which is derived the actual Henry's constant for the defined medium.

Values of the Henry's constant at other temperatures can be calculated using the following equation:

$$H = H_S \, e^{-K \left(\frac{1}{T} - \frac{1}{T_S} \right)}$$

where: H is the Henry's constant at a given temperature (T, in K), H_S, the Henry's constant (996.9 atm.L.mol^{-1}) at standard temperature (T_S, 298 K i.e. 25°C), and K, the temperature dependence constant (K_{CO} = 1300) (Lide Frederikse, H.P.R., 1995).

Validation of the Henry's constant evaluation methodology was performed on demineralized water saturated by 100% CO at 35ºC. The data found experimentally is close-fitting the literature value (1112 ±41 as compared to 1148 atm.L.mol^{-1}). Twin validation of the headspace method for dCO analaysis was achieved on demineralized water saturated by serial CO gas dilutions and on serial dilutions of water saturated by 100% CO, at 35ºC. The results are shown in Figure S2. There was a tight linear correlation between the measured values, using the method as described above, with a Henry's constant of 2176 atm.L.mol^{-1} for pure water at 90ºC (Lide Frederikse, H.P.R., 1995), and the nominal values, based on the Henry's constant of 1148 atm.L.mol^{-1} at 35ºC. The regression coefficients (slope) were 0.92 and 0.98, with a coefficient of determination (R^2) of 0.988 and 0.916, respectively. The detection limit was observed at 0.06 mmol.L^{-1}.

Therefore the approach proposed constitutes a simple, straightforward and practical alternative to the CO-bound myoglobin/spectrophotometry method (Kapic 2005; Riggs 2004), which in comparison appears laborious and prone to error, and offers a limit of detection which is higher (0.1 mmol.L^{-1}) (Riggs & Heindel 2006; Jones 2007; Bonam et al. 1984), or to

other headspace methods valid only for detection of trace amounts of CO (up to 12 nmol.L^{-1}) (Xie et al. 2002).

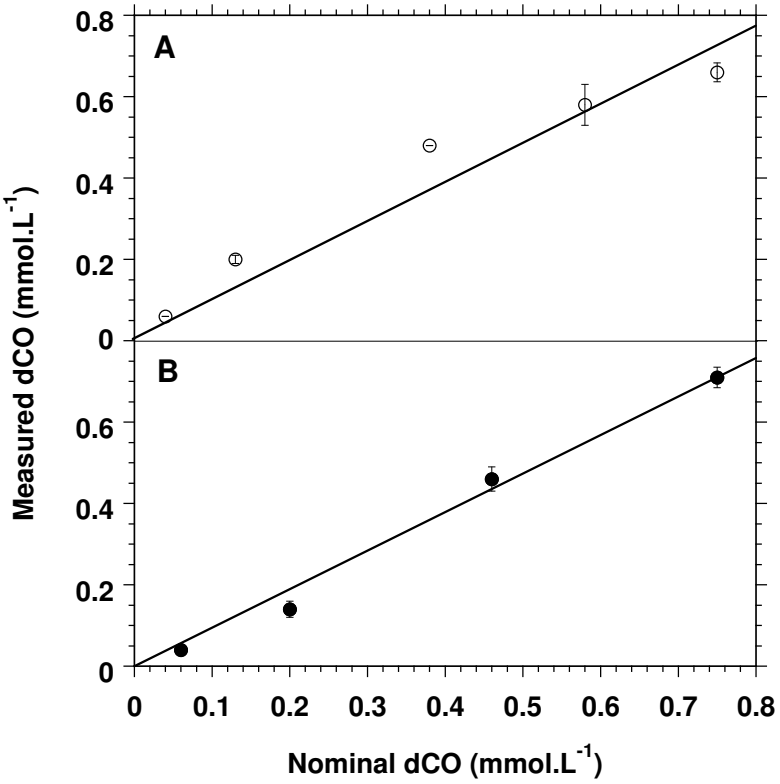

Figure S2: Comparison of dissolved CO concentrations (dCO) measured by the headspace method with nominal dCO on serial dilutions of water saturated by 100% CO (A) and on demineralized water saturated by serial CO gas dilutions (B), at 35ºC. Linear regressions: (A) $y = 0.98x$ ($R^2 = 0.916$); (B) $y = 0.92x$ ($R^2 = 0.988$)

PERMEANCE OF THE HOLLOW FIBER SYSTEM (ABIOTIC)

The mass transfer of CO from gas in the fiber lumen to the liquid on the shell side involves three steps: diffusion of CO into the gas stream, diffusion of CO through the membrane, transfer of CO in water. Although hollow fiber membranes may improve the gas-liquid mass transfer rate due to the absence of dispersion phenomena (absence of bubbles) and

the large specific surface area between the two phases, both material and structure of fibers cause additional resistance to gas transfer. Hence three resistances in series determine the mass transfer of gas across the membrane and include a resistance in the gas phase, the membrane resistance and a resistance in the liquid phase. As the mass transfer resistance in the gas phase is negligible, the overall resistance for gas transfer in a membrane system corresponds to the sum of the two latter resistances.

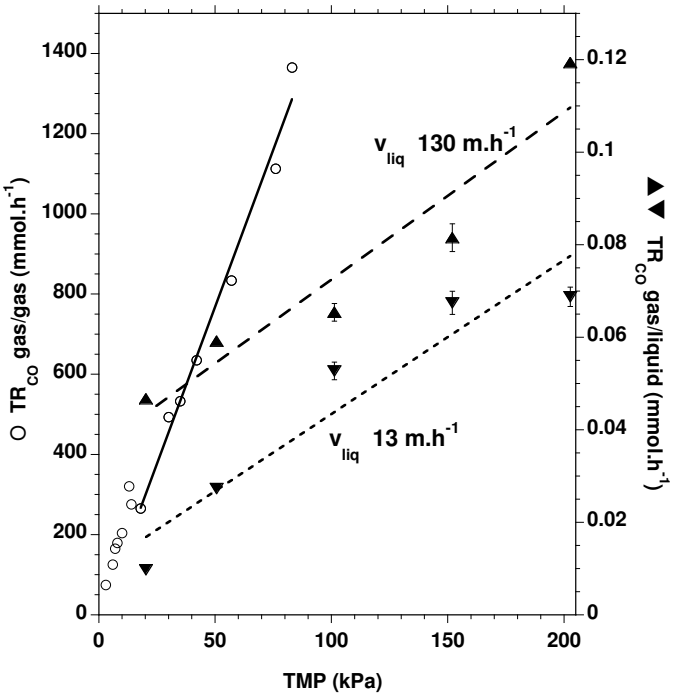

Figure S3: Effect of transmembrane pressure (TMP) on the CO transfer rate (TR_{CO}) through the PVDF membrane in abiotic conditions

In order to characterize the membrane resistance to CO, the CO transfer rate (TR_{CO}) across the membrane was measured at 70º C for a variety of transmembrane pressures (TMP) in abiotic conditions for gas/gas and gas/liquid systems, i.e. without and with liquid in the shell side, respectively. The tests were performed in a virgin HFMBR cartridge with a working

volume on the sell side of 40 mL and a total membrane surface area of 0.02 m^2 for the gas/gas system, and 0.09 m^2 for the gas/liquid system. The TR_{CO} through the PVDF membrane for gas/gas system was estimated by measuring in batch (closed system) the mass change between the CO applied to the HFMBR cartridge inlet (diluted with nitrogen as needed) and the CO in the shell side, initially filled with air at atmospheric pressure, as a function of time (ISO 2007). The CO transfer rate through the PVDF membrane for gas/liquid system was measured in the HFMBR cartridge filled with defined media, for various liquid linear velocities. The reactor was feed with CO at constant pressures of 20, 51,101, 152 and 203 kPa. Liquid was sampled each hour from the shell side of the HFMBR until saturation was reached, and analyzed for its dissolved CO content using the method presented above. The permeance of the PVDF membrane was then estimated, by reporting TR_{CO} to the total membrane surface area of the cartridge and the TMP differential. The SI unit of permeance is moles per square meter per second per Pascal ($mol.m^{-2}.s^{-1}.Pa^{-1}$).

The membrane permeance to CO decreased rapidly with TMP increase up to 18 kPa and stabilized at around 2 10^{-7} $mol.m^{-2}.s^{-1}.Pa^{-1}$ above 18 kPa. The linear relationship between transfer rate and TMP shows that each kPa of TMP increased TR_{CO} of 15.58 mmol per hour or 4.3 µmol per second (R^2 0.98). This yields an average permeance of $2.15 \cdot 10^{-7} \pm 0.11 \cdot 10^{-7}$ $mol.m^{-2}.s^{-1}.Pa^{-1}$ for the gas/gas system (Figure S3). This result is comparable with data reported in the literature (Okubo et al. 1991; Basile et al. 1996). Therefore in our HFMBR, even if the CO permeance is one order of magnitude lower as compared to hydrogen (Okubo et al. 1991), the use of a PVDF membrane offers a permeance that is orders of magnitude higher than what would be obtained with a silicone membrane (Montoya 2010).

The permeance measured in the gas/liquid system aggregates effect of both resistances of membrane and liquid phases. The presence of liquid in the reactor shell side decreased significantly the transfer rate. For a similar range of TMPs the transfer rate decreased from a median 635 $mmol.h^{-1}$ (gas to gas transfer) to 0.06 $mmol.h^{-1}$ (Figure S3), i.e. four orders of magnitude lower than in the gas/gas system. This is essentially due to the liquid resistance, since membrane pores represent essentially a gas phase because of the hydrophobic nature of the PVDF membrane. This difference is typically of the same order of magnitude as the

difference between diffusivities of gases in the air and water, as shown in Table S1. The linear relationship between transfer rate and TMP in the gas/liquid system yields an average permeance of $1.59 \cdot 10^{-12}$ mol.m^{-2}.s^{-1}.Pa^{-1} (R^2 0.91) and $3.28 \cdot 10^{-12}$ mol.m^{-2}.s^{-1}.Pa^{-1} (R^2 0.89), at a liquid linear velocity (v_{liq}) of 13 and 130 m.h^{-1}, respectively (Figure S3).

Temp. (K)	293	303	343
System		*D* (cm^2.s^{-1})	
CH_4 / air	0.106	–	0.301
CO / air	0.208	–	0.257
H_2 / air	0.627	–	0.666
CH_4 / H_2O	$0.16 \cdot 10^{-4}$	$0.21 \cdot 10^{-4}$	$0.70 \cdot 10^{-4}$
CO / H_2O	$0.20 \cdot 10^{-4}$	$0.24 \cdot 10^{-4}$	$0.63 \cdot 10^{-4}$
H_2 / H_2O	$0.46 \cdot 10^{-4}$	$0.57 \cdot 10^{-4}$	$1.37 \cdot 10^{-4}$

Table S1: Gas diffusivity (*D)* for partial pressure of 101.3 kPa (1 atm) and temperature as specified, in gas/air and gas/water systems (Gilliland et al. 1974; Coward & Georgeson 1937; Guillory 2010; Wise & Houghton 1968)

GAS-LIQUID MASS TRANSFER RATE OF THE ABIOTIC HFMBR

The volumetric gas-liquid mass transfer coefficient (k_La) of the HFMBR was determined by dynamic method at 70° C under abiotic conditions, as described elsewhere (Amir Kapic, Jones, & Heindel, 2006; Munasinghe & Khanal, 2010). The reactor was fed with CO at partial pressure (p_{CO}) ranging from 0.2 to 2 atm. Liquid was recirculated on the shell side at flow rates (Q_l) of 150 and 1500 mL·min^{-1}. Those rates corresponded to liquid linear velocities (v_l) of 13 and 130 m·h^{-1} and to Reynolds numbers of 127 and 1270; the flow hence was laminar in both cases. Therefore presuming that the liquid CO concentration at the interface is in equilibrium with the CO concentration in the gaseous phase, k_La can be

calculated from the following equation:

$$\ln \frac{C_s - C_0}{C_s - C} = k_L a \times t$$

where C, C_o and C_s are the CO concentration in the liquid phase ($mg.L^{-1}$) at time t, at time 0 and at saturation, respectively. The dissolved CO content of liquid sampled each hour from the shell side of the HFMBR was measured until saturation was reached, as explained above. Data were fitted to the above equation to estimate the k_La by linear regression.

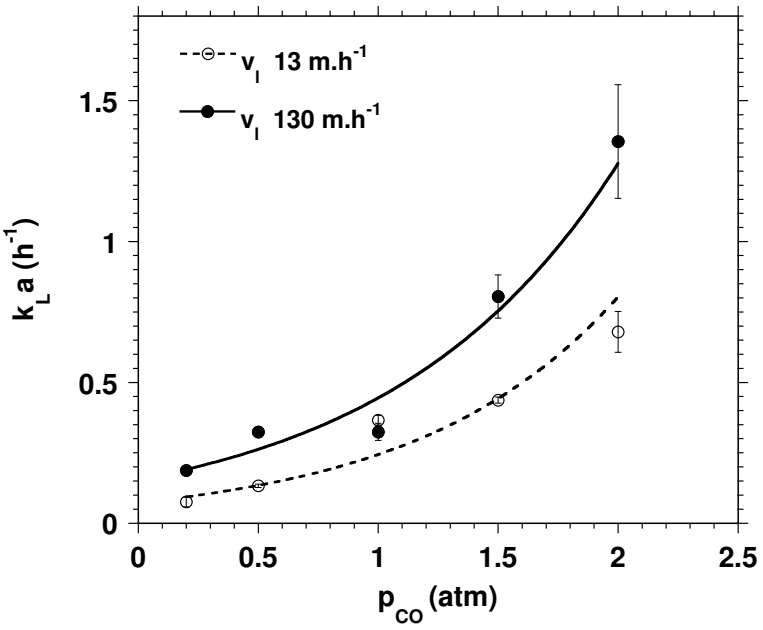

Figure S4: Volumetric mass transfer coefficient (k_La) for CO in the HMFR as a function of CO partial pressure (p_{CO}) and liquid linear velocity (v_l)

The k_La values obtained varied exponentially with p_{CO}, from 0.08 to 1.36 h^{-1} (Figure S4). The increase of both liquid velocity and p_{CO} had a positive impact on the k_La value. Nevertheless, the increase of p_{CO} had a higher impact than that of liquid velocity, probably because the flow remained laminar. Accordingly the dissolved CO concentration reached at equilibrium was not dependent on the velocity and varied linearly with p_{CO} from 0.11 to 1.13 $mmol.L^{-1}$ (Figure

S5). The k_La values were significantly smaller than those obtained for other gases in similar operational conditions (Karoor & Sirkar 1993; Gabelman & Hwang 1999). This is likely inherent to the nature of the CO gas at the actually elevated temperature conditions, since the CO diffusivity in water changes less from 293 to 343 K than that of H_2 or CH_4 (Table S1).

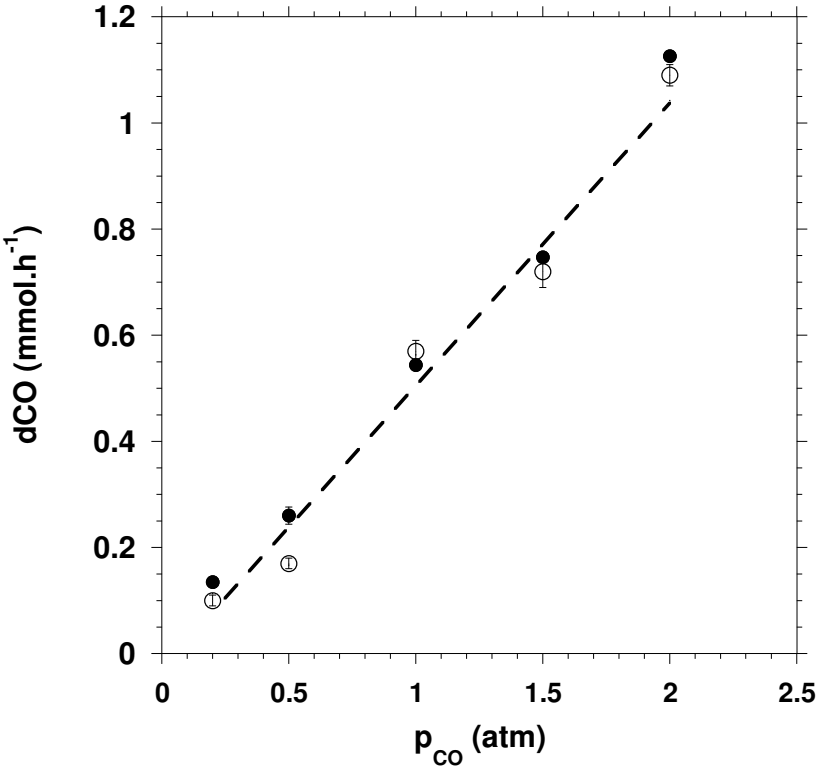

Figure S5: Dissolved CO concentration (dCO) at equilibrium as a function of the CO partial pressure (p_{CO}) at the gas inlet (O v_l = 13 m.h^{-1}; ● v_l = 130 m.h^{-1}; --- nominal)

REFERENCES

Basile, A., Criscuoli, A., Santella, F., & Drioli, E. (1996). Membrane reactor for water gas shift reaction. *Gas Separation & Purification*, *10*(4), 243–254. doi:10.1016/S0950-4214(96)00024-2

Bonam, D., Murrell, S. A., & Ludden, P. W. (1984). Carbon monoxide dehydrogenase from Rhodospirillum rubrum. *J. Bacteriol.*, *159*(2), 693–699.

Coward, H. F., & Georgeson, E. H. M. (1937). 226. The diffusion coefficient of methane and air. *Journal of the Chemical Society (Resumed)*, 1085. doi:10.1039/jr9370001085

Gabelman, A., & Hwang, S.-T. (1999). Hollow fiber membrane contactors. *Journal of Membrane Science*, *159*(1-2), 61–106. doi:10.1016/S0376-7388(99)00040-X

Gilliland, E. R., Baddour, R. F., Perkinson, G. P., & Sladek, K. J. (1974). Diffusion on Surfaces. I. Effect of Concentration on the Diffusivity of Physically Adsorbed Gases. *Industrial & Engineering Chemistry Fundamentals*, *13*(2), 95–100. doi:10.1021/i160050a001

Guillory, J. K. (2010). Book Review of CRC Handbook of Chemistry and Physics. 91st Edition CRC Handbook of Chemistry and Physics. 91st Edition . Edited by W. M. Haynes CRC Press (Taylor and Francis Group) , Boca Raton, FL . 2010 . xi +2610 pp. 22 × 29 cm. ISBN 978-1-4398-2077-3. *Journal of Medicinal Chemistry*, *53*(24), 8780–8780. doi:10.1021/jm101422n

ISO. (2007). *ISO. Rigid cellular plastics — Determination of water vapour transmission properties* (p. 14).

Jones, S. T. (2007). *Gas liquid mass transfer in an external airlift loop reactor for syngas fermentation*. Iowa State, Ames, IOWA.

Kapic, A. (2005). *Mass Transfer Measurements for Syngas Fermentation*. Iowa State University, Ames, IA.

Kapic, Amir, Jones, S. T., & Heindel, T. J. (2006). Carbon Monoxide Mass Transfer in a Syngas Mixture. *Industrial & Engineering Chemistry Research*, *45*(26), 9150–9155. doi:10.1021/ie060655u

Karoor, S., & Sirkar, K. K. (1993). Gas absorption studies in microporous hollow fiber membrane modules. *Industrial & Engineering Chemistry Research*, *32*(4), 674–684. doi:10.1021/ie00016a014

Lide Frederikse, H.P.R.,, D. R. (1995). *CRC handbook of chemistry and physics, 1995-1996 : a ready-reference book of chemical and physical data*. Boca Raton (Florida): CRC Press.

Montoya, J. P. (2010). Membrane gas exchange: Using hollow fiber membranes to separate gases from liquid and gaseous streams. *Ann Arbor; MI: MedArray; Inc.* Retrieved July 18, 2010, from www.permselect.com/files/Using_Membranes_for_Gas_Exchange.pdf

Munasinghe, P. C., & Khanal, S. K. (2010). Syngas fermentation to biofuel: evaluation of carbon monoxide mass transfer coefficient (kLa) in different reactor configurations. *Biotechnology Progress*, *26*(6), 1616–21. doi:10.1002/btpr.473

Okubo, T., Haruta, K., Kusakabe, K., Morooka, S., Anzai, H., & Akiyama, S. (1991). Equilibrium shift of dehydrogenation at short space-time with hollow fiber ceramic membrane. *Industrial & Engineering Chemistry Research*, *30*(4), 614–616. doi:10.1021/ie00052a002

Perry , Green, Don W., Maloney, James O.,, R. H. (1984). *Perry's Chemical engineers' handbook.* New York: McGraw-Hill.

Riggs, S.S. (2004). *Carbon Monoxide and Hydrogen Mass Transfer in a Stirred Tank Reactor*. Iowa State University, Ames, IA.

Riggs, Seth S, & Heindel, T. J. (2006). Measuring carbon monoxide gas-liquid mass transfer in a stirred tank reactor for syngas fermentation. *Biotechnology Progress*, *22*(3), 903–6. doi:10.1021/bp050352f

Wise, D. L., & Houghton, G. (1968). Diffusion coefficients of neon, krypton, xenon, carbon monoxide and nitric oxide in water at 10–60°C. *Chemical Engineering Science*, *23*(10), 1211–1216. doi:10.1016/0009-2509(68)89029-3

Xie, H., Andrews, S. S., Martin, W. R., Miller, J., Ziolkowski, L., Taylor, C. D., & Zafiriou, O. C. (2002). Validated methods for sampling and headspace analysis of carbon monoxide in seawater. *Marine Chemistry*, *77*(2-3), 93–108. doi:10.1016/S0304-4203(01)00065-2